Contract Report

Thermocatalytic CO_2-Free Production of Hydrogen from Hydrocarbon Fuels

Prepared for:
United States Department of Energy
Under Cooperative Agreement:
No. DE-FC36-99GO10456

FINAL REPORT

08/01/1999 - 08/31/2003

Florida Solar Energy Center
1679 Clearlake Road, Cocoa, FL 32922

Technical Point of Contact:
Nazim Muradov, Ph.D.
Principal Research Scientist
Telephone: 321-638-1448
Facsimile: 321-638-1010
E-mail: muradov@fsec.ucf.edu

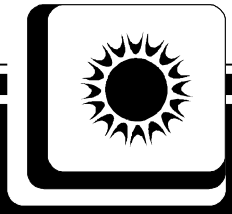

THERMOCATALYTIC CO_2-FREE PRODUCTION OF HYDROGEN FROM HYDROCARBON FUELS

PREPARED FOR THE UNITED STATES DEPARTMENT OF ENERGY
Under Cooperative Agreement
No. DE-FC3699GO10456

Final Report

08/01/1999 - 08/31/2003

FLORIDA SOLAR ENERGY CENTER
UNIVERSITY OF CENTRAL FLORIDA
1679 Clearlake Road, Cocoa, FL 32922

Technical Point of Contact:
Nazim Muradov, Ph.D.
Principal Research Scientist
Telephone: 321-638-1448
Facsimile: 321-638-1010
E-mail: muradov@fsec.ucf.edu

CONTENT

LIST OF FIGURES

LIST OF TABLES

EXECUTIVE SUMMARY

The main objective of this project is the development of an economically viable thermocatalytic process for production of hydrogen and carbon from natural gas or other hydrocarbon fuels with minimal environmental impact. The three major technical goals of this project are:

1) to accomplish efficient production of hydrogen and carbon via sustainable catalytic decomposition of methane or other hydrocarbons using inexpensive and durable carbon catalysts,
2) to obviate the concurrent production of CO/CO_2 byproducts and drastically reduce CO_2 emissions from the process, and
3) to produce valuable carbon products in order to reduce the cost of hydrogen production

The important feature of the process is that the reaction is catalyzed by carbon particulates produced in the process, so no external catalyst is required (except for the start-up operation). This results in the following advantages:

- no CO/CO_2 byproducts are generated during hydrocarbon decomposition stage,
- no expensive catalysts are used in the process,
- several valuable forms of carbon can be produced in the process depending on the process conditions (e.g., turbostratic carbon, pyrolytic graphite, spherical carbon particles, carbon filaments etc.),
- CO_2 emissions could be drastically reduced (compared to conventional processes).

The following is a brief description of major findings:

- The technical feasibility of CO_2-free production of hydrogen via thermocatalytic decomposition (TCD) (or pyrolysis) of different hydrocarbons was demonstrated. Methane, propane and gasoline were efficiently converted into hydrogen-rich gas and carbon using selected carbon catalysts.
- The catalytic activity and stability of more than 30 different forms and modifications of carbon were examined, and most promising carbon catalysts were selected for further evaluation.
- The effect of the operational parameters and hydrocarbon nature on the hydrogen yield was determined. Depending on the above factors, hydrogen concentration in the effluent gas varied in the range of 30-90 v.%, balance- CH_4 and small amount of C_2+ hydrocarbons. No CO or CO_2 was detected among the reaction products.
- The factors controlling carbon catalyst activity and long-term stability were studied. It was found that the surface area and crystallographic structure mostly determined the catalytic activity of carbon catalysts. This was confirmed by XRD, BET, XPS and SEM studies of carbon catalysts.
- A kinetic model for methane decomposition reaction over carbon catalysts was developed. Major kinetic parameters of methane decomposition reaction (rate constants, activation energies, etc.) over selected carbon catalysts were determined. Intermediate and final products of methane and propane pyrolysis were identified and quantified.
- Various conceptual designs for the hydrocarbon pyrolysis reactor, including packed bed, tubular, free volume, fluid wall and fluidized bed reactors, were evaluated; the experimental

reactors for decomposition of methane were fabricated and tested. Advantages and disadvantages of each type of the reactor were assessed. Fluidized bed reactor was selected as a baseline reactor for the process.

- The means for improving the catalyst long-term stability and process sustainability were determined. It was found that the process sustainability could be improved using two approaches: (i) the in-situ generation of catalytically active carbon species produced by co-decomposition of methane and unsaturated and/or aromatic hydrocarbons, and (ii) reactivation of carbon catalysts via surface treatment with activating agents, e.g., steam and/or CO_2. **U.S. Patent No. 6,670,058 B2** was granted for the development of the process.
- The effect of moisture present in commercial hydrocarbon fuels on the process efficiency and the catalyst activity and stability was determined. It was demonstrated that the presence of small amounts of moisture (<2 v%) in the feedstock slightly improved the process efficiency. However moisture resulted in contamination of hydrogen with CO (which could be removed from the product gas via methanation reaction)
- It was determined that sulfur compounds (most importantly, H_2S) did not adversely affect the process efficiency. Significant portion of H_2S was catalytically decomposed into hydrogen and elemental sulfur. In the presence of CO_2, hydrogen sulfide was converted into mixture of H_2, CO, S_2 and minor amounts of COS with the yield of 95%.
- A bench-scale 1 kW_{th} thermocatalytic reactor (TCR) for CO/CO_2-free production of hydrogen-rich gas was designed, fabricated and operated using methane or propane as feedstocks. TCR produced gases with H_2 concentration up to 80 v.%, balance- CH_4.
- TCR was tested in combination with PEM fuel cell. It was demonstrated that the TCR-produced hydrogen gas could be directly fed to PEM fuel cell with no need for gas conditioning (e.g., water gas shift, preferential oxidation) and gas separation stages required by conventional technologies (e.g., steam reforming, partial oxidation). **U.S. Patent No.6,653,005 B1** was granted for the development of TCR-PEM FC apparatus.
- A 3kW TCR was designed, fabricated and operated using pipeline natural gas and commercial propane as feedstocks.
- Carbon products of the process were analyzed by a number of material characterization techniques, including XRD, SEM, AES, XPS, EDS, DR- FTIR. The market value of the carbon products were evaluated.
- Techno-economic analysis of hydrogen and carbon production by thermocatalytic decomposition of natural gas was conducted in cooperation with NREL. It was determined that hydrogen could be produced at a selling price of $7-21/GJ depending on the cost of natural gas and carbon selling price.
- Carbon products of the process were tested for the number of applications, e.g., Li-ion batteries, direct carbon fuel cells, etc. The market value of the carbon products was evaluated.
- Studies on the modeling and scaling up of the fluidized bed reactor for thermocatalytic decomposition of natural gas were conducted

1. INTRODUCTION

Given the advantages inherent in fossil fuels, such as their availability, cost-competitiveness, convenience of storage and transportation, they are likely to play a major role in hydrogen production for the 21st century. In principle, hydrogen can be produced from hydrocarbon fuels (e.g. natural gas, NG) by reaction with water, oxygen, water/oxygen, and decomposition:

1. Reaction with water (steam methane reforming, SMR):

$$CH_4 + 2H_2O \rightarrow 4H_2 + CO_2 \quad (1\text{-}1)$$

2. Reaction with oxygen (air) (partial oxidation, POx):

$$CH_4 + O_2 \rightarrow 2H_2 + CO_2 \quad (1\text{-}2)$$

3. Reaction with water and oxygen (air) (autothermal reforming, ATR):

$$CH_4 + H_2O + 1/2O_2 \rightarrow 3H_2 + CO_2 \quad (1\text{-}3)$$

4. Methane decomposition reaction:

$$CH_4 \rightarrow 2H_2 + C \quad (1\text{-}4)$$

First three approaches produce large amounts of CO_2: up to 0.25-0.33 m^3 CO_2 per m^3 of H_2 produced. For example, a typical hydrogen plant with the capacity of approximately one million m^3 of hydrogen per day produces about 0.25 million standard cubic meters of CO_2 per day (exclusive of stack gases), which is normally vented into the atmosphere.

There are several possible ways to mitigate CO_2 emission problem. Among them are traditional (e.g. more efficient use of fossil fuel energy resources; increase in usage of non-fossil fuels, etc.) as well as the approaches which include sequestration of CO_2 produced by the conventional processes. The perspectives of CO_2 sequestration is actively discussed in the literature. The main objective of carbon sequestration is to prevent anthropogenic CO_2 emissions from reaching the atmosphere by capturing and securely storing CO_2 underground or under the ocean. However, there are some environmental uncertainties associated with CO_2 sequestration.

A novel approach to hydrogen production without CO_2 emissions is related to decomposition of NG (or other hydrocarbon fuels) into hydrogen and carbon. This process is much less developed comparing to the conventional processes of SMR and POx. Thus, the main objective of this work is to develop the thermocatalytic process for CO_2-free production of hydrogen and carbon from methane and other hydrocarbon fuels. Another objective is to compare the thermocatalytic process with methane steam reforming process coupled with CO_2 sequestration.

If cost effective CO_2-free hydrogen production technologies are developed and implemented, there would be practically no environmental constraints on using fossil fuels on a large scale for the foreseeable future.

2. TECHNICAL BACKGROUND

2.1. Conventional Processes of Hydrogen Production

Steam Reforming of Methane

For decades, steam reforming of methane (or NG) has been the most efficient and widely used process for the production of hydrogen. Typical capacities of SMR plants are in the range of hundreds of thousands of cubic meters per hour of hydrogen, which makes them most economical among all hydrogen producing technologies. The process basically represents a catalytic conversion of methane (a major component of the hydrocarbon feedstock) and water (steam) to hydrogen and carbon oxides, and consists of three main steps:

a) steam reforming: $CH_4 + H_2O \rightarrow CO + 3H_2$ $\Delta H^o = 214.5$ kJ/mol (2-1)
b) water-gas shift reaction: $CO + H_2O \rightarrow CO_2 + H_2$ $\Delta H^o = -41.5$ kJ/mol (2-2)
c) gas purification (CO_2 removal)

Overall: $CH_4 + 2H_2O \rightarrow CO_2 + 4H_2$ $\Delta H^o = 173.0$ kJ/mol (2-3)

Four moles of hydrogen are produced in the reaction with half of it coming from the methane and another half from water. The theoretical energy requirement per mole of hydrogen produced for the overall process is equal to 173/4= 43.3 kJ/mole H_2. To ensure a maximum conversion of CH_4 into the products, the process generally employs a steam/carbon ratio of 3÷5, the process temperature of 800-900^{o}C and pressure of 35 atm [1]. The SR process thermal efficiency is seldom greater than 50% [1]. A steam reformer fuel usage is a significant part (up to 30-40%) of the total NG usage of a typical hydrogen plant. The typical composition of a synthesis gas after the reformer is (expressed in v.%): H_2- 74, CO- 18, CO_2- 6, CH_4- 2. After two stages (high and low temperature) of water gas shift conversion the concentration of CO usually drops to 0.4 v.%. Finally, the raw gas passes a series of gas purification units, first, to remove bulk of CO_2 and then to remove the residual CO and CO_2. The average purity of H_2 after these stages is 97-98 v.%. Hydrogen at 99.99 v.% purity can be obtained after additional purification using a pressure swing adsorption (PSA) unit. There is no by-product credit for the process and, in the final analysis, it does not look environmentally benign due to large CO_2 emissions The total CO_2 emission from SR process reaches up to 0.35-0.42 m^3 per each m^3 of hydrogen produced.

Partial Oxidation

Partial oxidation (POx) of NG (catalytic and non-catalytic) can be described by the following equations:

$CH_4 + 1/2O_2 \rightarrow CO + 2H_2$ $\Delta H^o = -35.6$ kJ/mol (2-4)

$CH_4 + O_2 \rightarrow CO_2 + 2H_2$ $\Delta H^o = -319.3$ kJ/mol (2-5)

$CO + H_2O \rightarrow CO_2 + H_2$ $\Delta H^o = -41.5$ kJ/mol (2-6)

2--3 moles of hydrogen are produced per one mole of methane. Both reactions are exothermic which implies that the reactor does not need an external heat source. If pure oxygen is used in the process, it has to be produced (or purchased) and stored which significantly adds to the cost of the system. On the other hand, if POx process uses air as an oxidizer, the effluent gas is heavily diluted by nitrogen which results in larger water gas shift reaction (WGSR) and gas purification units. The maximum theoretical concentration of hydrogen in the effluent gas using pure oxygen is 66.7 v.%, however, the concentration drops to 40.9 v.% if air is used as an oxidizer.

$$CH_4 + 1/2(O_2 + 79/21)N_2 \rightarrow 2H_2 + CO + 79/42N_2 \qquad \Delta H^o = -35.6 \text{ kJ/mol} \qquad (2\text{-}7)$$

POx process has a number of important advantages over SR:

- it provides a simplified system due to absence of external water and heat supply, therefore, it is potentially less expensive,
- POx reactor potentially has the capability to process a variety of gaseous and liquid hydrocarbon fuels including methane, LPG, gasoline, diesel fuel, methanol, etc.,

However, POx process also suffers from the following disadvantages:

- POx reformate, which is heavily diluted with nitrogen, has lower calorific value,
- since POx process is exothermic and involve significantly higher temperatures, it might have greater thermal loses,

Autothermal Reforming

In autothermal reforming (AR) process hydrocarbon fuel reacts with a mixture of water and oxygen:

$$2C_nH_{2n+2} + n/2O_2 + nH_2O \rightarrow 2nCO + (3n+2)H_2 \qquad (2\text{-}8)$$

$$C_nH_{n+2} + n/2O_2 + nH_2O \rightarrow nCO_2 + (2n+1)H_2 \qquad (2\text{-}9)$$

The energy released by hydrocarbon oxidation reaction drives steam reforming process. The overall process is exothermic and it features almost the same advantages and disadvantages of POx process, although, AR produces somewhat more hydrogen per unit of hydrocarbon fuel consumed relative to POx. Rolls-Royce/Johnson-Mathey and International Fuel Cell/ONSI have been working on the development of the autothermal reformer units [2].

Steam-Iron Process

There have been attempts to produce high-purity hydrogen from hydrocarbons by modification of well known steam-iron process. For example, in a process developed by H Power Corp. (U.S.A.) sponge iron is oxidized in multiple bed reactor to provide high-purity hydrogen to a

fuel cell, while already depleted beds are regenerated (reduced) using synthesis gas delivered from a methane-fueled steam reformer (or POx unit):

$3Fe + 4H_2O \rightarrow Fe_3O_4 + 4H_2$ $\Delta H^o = -151.3$ kJ/mol (Fe_3O_4) (2-10)

$Fe_3O_4 + 4CO \rightarrow 3Fe + 4CO_2$ $\Delta H^o = -14.7$ kJ/mol (Fe_3O_4) (2-11)

$Fe_3O_4 + 4H_2 \rightarrow 3Fe + 4H_2O$ $\Delta H^o = 151.3$ kJ/mol (Fe_3O_4) (2-12)

The advantage of this process is that it produces very pure hydrogen without energy- and material-intensive stages of hydrogen purification (e.g. WGSR and CO_2 removal). However the process is multistage, requires high temperatures (for the reduction of magnetite, Fe_3O_4, to sponge iron) and additional step of NG steam reforming (or POx). In a vehicle application, authors suggest that a 113 kg bed of sponge iron granules placed in a car which will react with a steam to produce hydrogen for fuel cell or internal combustion engine [3]. The spent iron oxide will be blown out of the bed with air pressure and sent off for the regeneration (reduction) in a stationary unit, and a replacement dose of fresh sponge iron will be pumped in. According to the stoichiometry of the iron-steam reaction, the production of 1 m^3 of hydrogen requires 2.1 kg of sponge iron and 0.75 kg of H_2O. Considering that at least a two- or tree-fold surplus of water will be required to enhance the kinetics of the reaction and bring it to completion, the total weight of the reagents on board would be 3.6-4.4 kg per 1 m^3 of hydrogen produced (not accounting the fuel required for start-up). Calculations show that in order to supply 20 kW fuel cell with pure hydrogen obtained from 113 kg of sponge iron one needs to regenerate iron oxide bed every 2 hours of driving, thus, almost every day. The theoretical yield of hydrogen is 3 moles H_2 per mole of CH_4, which in real systems will be significantly less due to heat losses and consumption of methane as a heat source.

2.2. Production of Hydrogen by Methane Decomposition

Thermal Decomposition of Methane

Thermal decomposition (TD) of methane produces hydrogen and carbon as expressed by the following chemical equation:

$CH_4 \rightarrow C + 2H_2$ $\Delta H^o = 75.6$ kJ/mol (2-13)

The energy requirement per mole of hydrogen produced (37.8 kJ/mole H_2) is somewhat less than that for the SR process. The process is slightly endothermic so that less than 10% of the heat of methane combustion is needed to drive the process. In addition to hydrogen as a major product, the process produces a very important by-product: clean carbon. The process is environmentally compatible, as it produces relatively small amounts of CO_2 (approximately 0.05 m^3 per m^3 of H_2 produced, if CH_4 is used as a fuel). It should be noted, however, that the process could potentially be completely CO_2-free if a relatively small part of hydrogen produced (approximately 14%) is used as a process fuel.

TD of NG is a technologically simple one-step process and, unlike SMR and POx, it does not require several expensive technological steps such as WGSR, CO_2 removal, oxygen production, steam generation and excess steam removal (drying). A preliminary process design for a continuous methane decomposition process and its economics have been conducted [9]. The techno-economic assessment showed that the cost of hydrogen produced by TD of NG ($58/1000 m^3 H_2, with carbon credit), was somewhat lower than that for the SR process ($67/1000 m^3 H_2) [4]. It should be noted that the capital cost component of the production cost for TD process (before carbon credit) is equal to 12.8% comparing that to 29.1 and 47.9% for SMR and POx, respectively [4].

Plasma Decomposition

Plasma-assisted decomposition of hydrocarbons with the production of hydrogen and carbon has become an active area of research recently. Kvaerner company of Norway has developed a methane decomposition process which produces hydrogen and carbon black by using high temperature plasma (CB&H process) [5]. The advantages of thermal plasma process are: high thermal efficiency (>90%), high fuel flexibility, purity of hydrogen (98 v.%) and production of valuable byproduct- carbon. The authors claim very low CO_2 emissions associated with the plasma process.

In the paper [6], the authors advocated a plasma-assisted decomposition of methane into hydrogen and carbon. It was estimated that 1-1.9 kWh of electrical energy is consumed per one normal cubic meter of hydrogen produced. The authors stated that plasma production of hydrogen is free of CO_2 emissions. However, since most of the electric energy supply in the world comes from fossil fuels, the electricity-driven hydrogen production processes, including plasma and electrochemical processes, are among CO_2 producers.

Thermocatalytic Decomposition

There has been attempts to use catalysts in order to reduce the maximum temperature of thermal decomposition of methane. Thus, in 60-s, Universal Oil Products Co. has developed the HYPRO process for continuous production of hydrogen by catalytic decomposition of a gaseous hydrocarbon streams [7]. Methane decomposition was carried out in a fluidized bed catalytic reactor in the range of temperatures from 815 to 1093^{o}C. Supported Ni, Fe and Co catalysts (preferably, Ni/Al_2O_3) were used in the process. The coked catalyst was continuously removed from the reactor to the regeneration section where carbon was burned off by air, and the regenerated catalyst returned to the reactor. Unfortunately, the system with two fluidized beds and the solids-circulation system was too complex and expensive and could not compete with the SR process.

NASA has conducted studies on the development of catalysts for methane decomposition process for space life support systems [8]. A special catalytic reactor with a rotating magnetic field to support Co-catalyst at 850^{o}C was designed. In 70s, a group of U.S. Army researchers has been developing a fuel processor (conditioner) to catalytically convert different hydrocarbon fuels to hydrogen which was used to feed a 1.5 kW fuel cell [9]. A stream of gaseous fuel entered one of two reactor beds, where hydrocarbon decomposition to hydrogen took place at

870-980^{o}C and carbon was deposited on the Ni-catalyst. Simultaneously, air entered the second reactor where the catalyst regeneration by burning coke off the catalyst surface occurred. The streams of fuel and air to the reactors then were reversed for another cycle of decomposition-regeneration. The reported fuel processor did not require WGS and gas separation stages, which was a significant advantage. However, the thermal efficiency of this type processors, in general, is relatively low (<60%) and they produce CO_2 in quantities comparable with SR and PO processes. Recently, several groups of researchers have reported on the development of hydrocarbon fuel processors for the fuel cells applications using similar concept [10,11].

It was found that almost all transition metals (d-metals) to some extent exhibited catalytic activity toward methane decomposition reaction, and some of them demonstrated remarkably high activity. It should be noted, however, that there is no universal agreement among different groups of researchers regarding the choice of the most efficient metal catalyst for methane decomposition. For example, it was demonstrated [12] that the rate of methane activation in the presence of transition metals followed the order: Co, Ru, Ni, Rh > Pt, Re, Ir > Pd, Cu, W, Fe, Mo. The authors [10,13] have found Pd to be the most active catalyst for methane decomposition, whereas, Ni was the catalyst of choice in the publication [14], and Fe and Ni in publications [15,16]. According to the data presented in [17], Co catalyst demonstrated highest activity in methane decomposition reaction.

Of particular interest are catalytic methane decomposition reactions producing special (e.g. filamentous) form of carbon. For example, the authors [18] have reported catalytic decomposition of methane over Ni catalyst at 500^{o}C with the production of hydrogen and whisker carbon. Concentrated solar radiation was used to thermally decompose methane into hydrogen and filamentous carbon [19]. The advantages of this system include the efficient heat transfer due to direct irradiation of the catalyst and CO_2-free operation.

The nature of methane-metal interaction during decomposition reaction is still debated in the literature. For example, according to [20], the activation energy for methane decomposition is lower for the metals with stronger metal-carbon bonds, which correlates with the following order of activity: Fe > Co > Ni. Our experimental data on methane decomposition over alumina-supported Fe, Ni and Co catalysts at 850^{o}C are in a good agreement with the theory. However at lower temperatures (<700^{o}C) the order of catalytic activity toward methane decomposition changed to Ni > Fe > Co. Apparently, other factors, including hydrogen-metal interaction, also play significant role in methane activation over transition metal catalysts.

No conclusive study is presented in the literature on the mechanism of methane decomposition over metal catalysts. Most likely, a general Langmuir-type mechanism, similar to that suggested for CH_4-D_2 exchange over metal films [21] may be applied to metal-catalyzed methane decomposition reaction:

$$CH_4 + 2^* \rightarrow CH_3^* + H^* \qquad (2\text{-}14)$$

$$CH_3 + ^* \rightarrow CH_2^* + H^* \qquad (2\text{-}15)$$

$$CH_2 + ^* \rightarrow CH^* + H^* \qquad (2\text{-}16)$$

$$CH + * \rightarrow C + H* \quad (2\text{-}17)$$

where, * is an active site.

In this report we present an account of work on the development of novel carbon-based catalysts for methane decomposition process. Carbon catalysts offer the following advantages over metal catalysts: (i) no catalyst regeneration is required, (ii) no sulfur poisoning, (iii) high fuel flexibility, (iv) production of a valuable byproduct carbon, and (v) significant reduction in CO_2 emissions.

3. EXPERIMENTAL

3.1. Reagents.

Methane (99.99%v.) (Air Products and Chemicals, Inc.) was used without further purification. Samples of activated carbons, graphites, glassy carbon, synthetic diamond powder, fullerenes, carbon nanotubes and acethylene black were obtained from Alfa Aesar and used without further purification. Barneby Sutcliffe Corp. and Cabot Corp. supplied different CB and AC (coconut) samples, respectively. All carbon samples were used in the form of fine powder (<100μm). Activated alumina samples (Fisher Scientific and Alfa Aesar) were used without further purification.

Table 3-1. Carbon Catalysts Tested for Catalytic Activity in Methane Decomposition Reaction

Manufacturer (brand name) of carbon catalyst	Origin of carbon	Surface area, m^2/g	Method of activation of AC
NORIT Americas (Darco KB-B)	hardwood	1500	steam/chemical
NORIT Americas (Darco 20-40)	lignite coal	650	steam
NORIT Americas (Norit RO 0.8)	peat	900	steam
NORIT Americas (G-60)	proprietary	900	steam
Barnebey Sutcliff Corp. (CL-20)	coconut shell	1500	steam
Barnebey Sutcliff Corp. (KE)	coconut shell	1150	steam
Barnebey Sutcliff Corp. (GI)	coconut shell	1300	steam
Kanzai Coke & Chemicals (KCC) (MAXSORB MSP-15)	carbonized phenol resin	1980	KOH
KCC (MAXSORB MSP-20)	phenol resin	2260	KOH
KCC (MAXSORB MSC-25)	petroleum coke	2570	KOH
KCC (MAXSORB MSC-30)	petroleum coke	3370	KOH
Cabot (CB Black Pearls 2000)	petroleum	1500	
Cabot (CB Black Pearls 120)	petroleum	25	
Cabot (Vulcan XC72)	petroleum	254	
Cabot (Regal 330)	petroleum	94	
Acetylene Black	acetylene	80	
Diamond powder synthetic		7.9	
Graphite crystalline	petroleum coke	3-10	
Graphite microcrystalline	coke	10-12	
Graphite natural	graphite	4-6	
Glassy carbon			

3.2. Apparatus.

The schematics of the experimental set-up used for hydrogen production via thermocatalytic decomposition hydrocarbons is presented on Figure 3-1. The set-up consisted of 3 main subsystems: (1) a thermocatalytic reactor (with temperature-controlled electric heater and pre-

heater), (2) a feedstock metering and delivery sub-system for gaseous and liquid hydrocarbons, and (3) analytical sub-system.

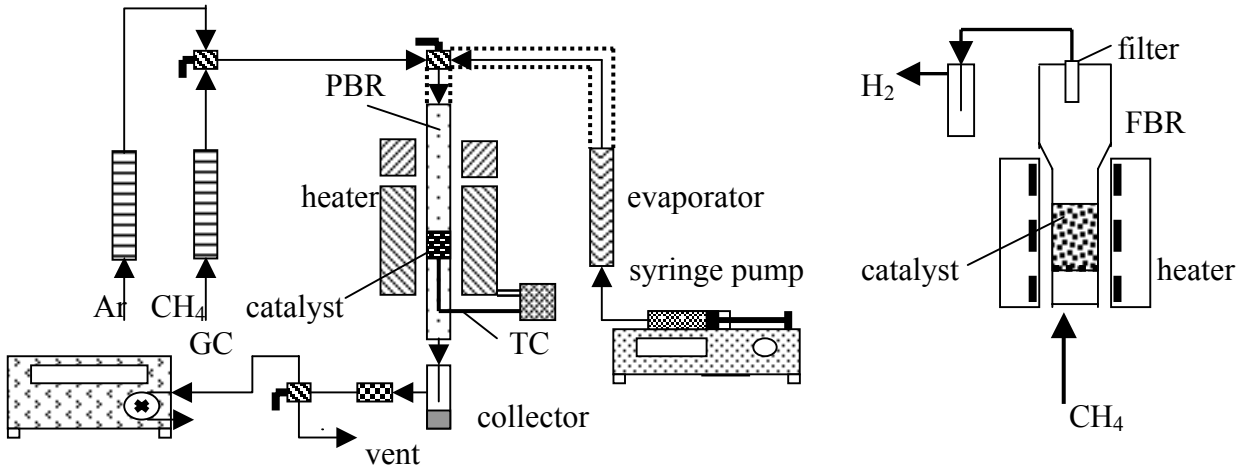

GC- gas chromatograph, TC- thermocouple, PBR- packed bed reactor

Figure 3-1. Schematic Diagram of the Experimental Set-up with Packed Bed (left) and Fluidized Bed (right) Reactors

The catalytic reactors were made out of a fused quartz or ceramic (alumina) in order to reduce the effect of the reactor material on the rate of hydrocarbon decomposition. The reactor temperature was maintained at a constant temperature via a type K thermocouple and Love Controls microprocessor. Amount of carbon catalyst used in the experiments varied in the range of 0.03-5.0 g. Gaseous hydrocarbons flow rates varied from 5 ml/min to 2 l/min. Gaseous hydrocarbons (methane, propane) were metered by flow meters, and liquid hydrocarbons were metered and delivered to the reactor by a syringe pump via a temperature-controlled evaporator. Gaseous products of hydrocarbon decomposition passed through a condenser (for separation of liquid byproducts), a filter (for separation of airborne carbon particles and aerosols) and were analyzed gas-chromatographically).

3.3. Analysis

The analysis of the products of methane decomposition was performed gas chromatographically: SRI- 8610A (a thermal conductivity detector, Ar carrier gas, a silica gel column, temperature programming from 27 to 180^{o}C) and Varian-3400, FID, He-carrier gas, Hysep D_b. SEM studies were performed using Amray 1810 scanning electron microscope. XRD studies were conducted using Rigaku diffractometer with D/MAX 2200T/PC ULTIMA accessory. Polynuclear aromatic byproducts were analyzed spectrophotometrically (Shimadzu UV-2401PC). Carbon particle size and distribution measurements were performed using Model 770 ACCUSIZER (Particle Sizing Systems, Inc.).

4. METHANE DECOMPOSITION OVER CARBON CATALYSTS

4.1. Catalytic Activity of Carbons in Methane Decomposition Reaction

We determined the catalytic activity of the variety of carbon-based materials of different structure and origin toward methane decomposition. Table 4-1 summarizes the experimental results of methane decomposition reaction in the presence of different modifications of elemental carbon including wide range of activated carbons (AC), carbon blacks (CB), carbon fiber, glassy carbon, and crystalline graphites, and others, at 850°C and residence time of approximately 1 s. Each carbon sample was characterized by two important parameters: initial activity presented as an initial methane conversion rate, in mmole/min-g (K_m^o) and sustainability displayed in the Table 4-1 as the ratio of methane conversion rate after one hour to the initial methane conversion rate (K_m^1/K_m^o). The available data on the surface area (SA) of carbon samples tested are also presented in the Table 4-1.

It is understood that higher are both K_m^o and K_m^1/K_m^o parameters, better is the carbon catalyst. The experiments indicated that, in general, activated carbons exhibited highest initial activity (per unit of catalyst weight), but relatively low sustainability (K_m^1/K_m^o). It is noteworthy that AC samples of different origin and surface area displayed relatively close initial activity (K_m^o) in the range of 1.6-2.0 mmole/min-g.

Table 4-1. Comparative Assessment of Different Carbon Catalysts in Methane Decomposition Reaction

Carbon Catalyst	SA, m^2/g	K_m^o, mmole/ min-g	K_m^1/K_m^o	Carbon Catalyst	SA, m^2/g	K_m^o, mmole /min-g	K_m^1/K_m^o
AC, Coconut KE	1150	1.76	0.05	Acetylene Black	80	0.22	0.98
AC, Coconut CL	1650	1.67	0.18	CB, Black Pearls	25	0.22	0.48
AC, Coconut GI	1300	1.90	0.07	CB, Regal 330	94	0.42	0.40
AC, Hardwood	1500	2.04	0.32	CB, Vulcan XC72	254	0.48	0.41
AC, G-60	900	1.63	0.28	CB, Black Pearls	1500	1.15	0.60
AC, Lignite	650	1.77	0.31	Glassy Carbon	-	0.95	0.06
AC, Peat RO	900	1.63	0.19	Diamond Powder	-	0.16	0.48
AC, petrol. coke	-	1.29	0.47	Carbon FibersPAN	-	0.05	0.50
Graphite, natural	4-6	0.02	2.87	Carbon Nanotubes	-	0.08	0.92
Graphite, crystal.	3-10	0.10	0.63	Soot (Fullerene)	-	1.90	0.63
Graphite, crystal.	10-12	0.07	0.82	Fullerenes $C_{60/70}$	-	1.34	0.11

Carbon black catalysts (including acetylene black) exhibited somewhat lower initial activity than AC, but better sustainability. Carbons with the ordered structure (graphite, diamond, carbon fiber) demonstrated the lowest initial activity toward methane decomposition reaction.

Fullerenes $C_{60/70}$ and fullerene soot displayed relatively high initial activity, whereas, multi-walled carbon nanotubes showed very low catalytic activity in methane decomposition.

It was found that besides the nature of carbon material, its relative catalytic activity in methane decomposition reaction was proportional to the surface area of carbon. Figure 4-1 depicts the methane conversion rate (in mmole/min-g) as a linear function of the surface area of carbon catalysts in semi-log coordinates. The plot includes data for all the modifications of carbon tested, including AC, CB, graphites and others. It should be noted that only limited number of carbon catalysts could be compared based on the unit of surface area. For example, activated carbon (KBB) produced from hardwood (with SA=1500 m^2/g) demonstrated the initial methane conversion rate of 1.36 μmole/min-m^2, comparing to 0.77 μmole/min-m^2 for carbon black (BP-2000) with the same surface area.

Figure 4-2 (a) demonstrates the kinetic curves of methane decomposition over different types of AC, CB and graphite at 850°C and different residence times. It can be seen that at comparable conditions AC catalysts have higher initial activity than CB catalysts, although, CB-catalyzed decomposition of methane is more sustainable than AC-catalyzed. At relatively high residence times AC catalysts produced H_2/CH_4 mixtures with the initial hydrogen concentrations reaching up to 90 v.% and higher, which is an indication of the high catalytic activity. This, however, was followed by the rapid drop in the catalytic activity and the decrease in methane decomposition rate. CB-catalyzed methane decomposition reached quasi-steady state rate over 20-30 min and remained practically stable for several hours, followed by the gradual decline in the reaction rate.

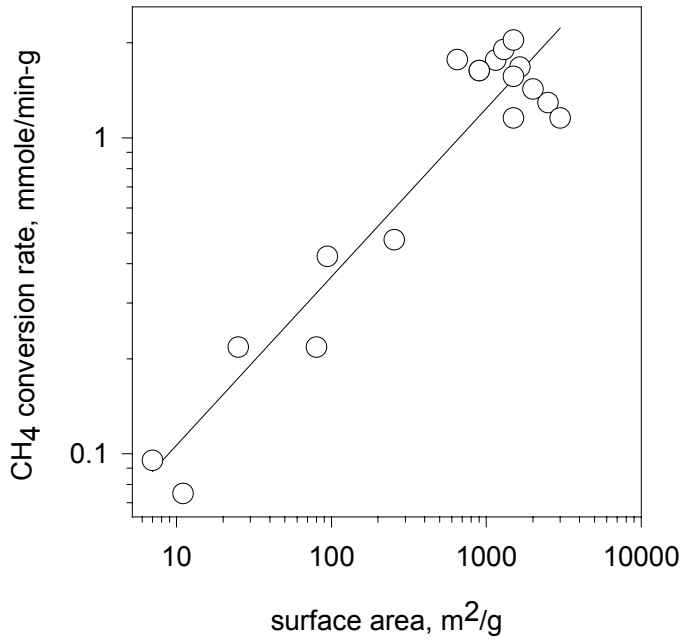

Figure 4-1. Methane Conversion Rate as a Function of Catalyst Surface Area

The initial rate of methane decomposition over amorphous carbons (e.g. acetylene black and carbon blacks) was relatively low, but the process demonstrated good sustainability over long period of time. Figure 4-2 (left) demonstrates the kinetic curves of methane decomposition over acetylene black which was conducted at 850°C and residence time of 12 s for almost 24 hours.

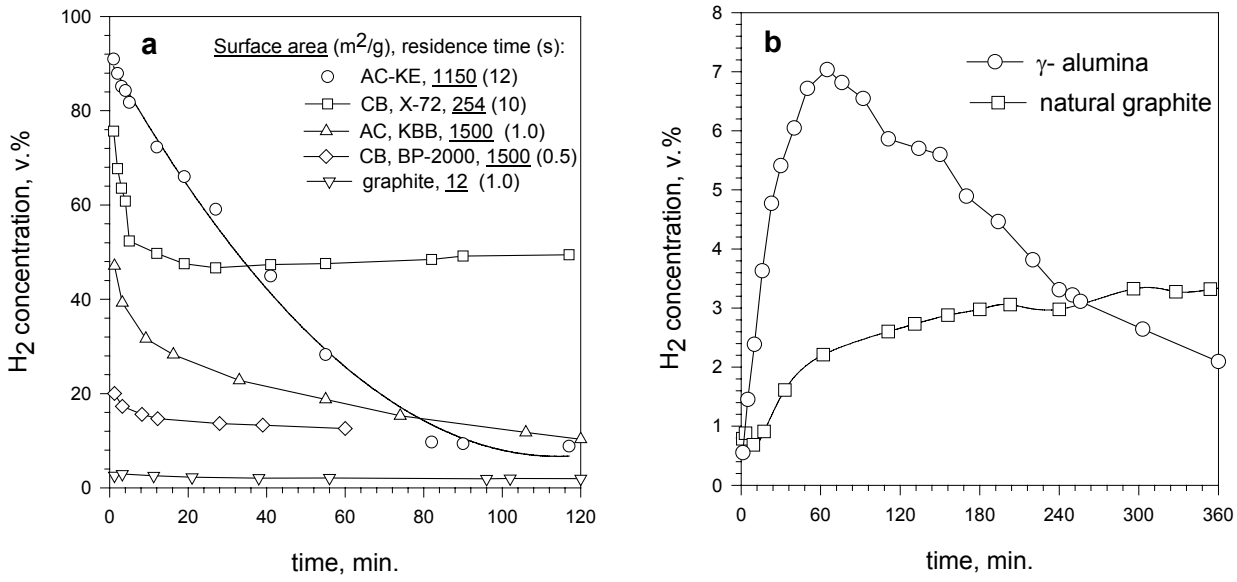

Figure 4-2. Methane Decomposition over Different Carbon Catalysts at 850°C

Over period of 6 hours the process reached quasi-state regime which lasted for 9 hours, after which the methane decomposition rate slowly declined. No methane decomposition products other than hydrogen and carbon and small amounts of C_2 hydrocarbons ($\Sigma(C_2H_4+C_2H_6)< 0.3$ v.%) were detected in the effluent gas during the entire process. The amount of carbon produced corresponded to the volume of H_2 within the experimental margin of error (5%).

Figure 4-3 (right) shows the kinetic curves of methane decomposition over different forms of carbon blacks at relatively high space velocities (or low residence times, approx. 1 s), which explains low methane decomposition yields.

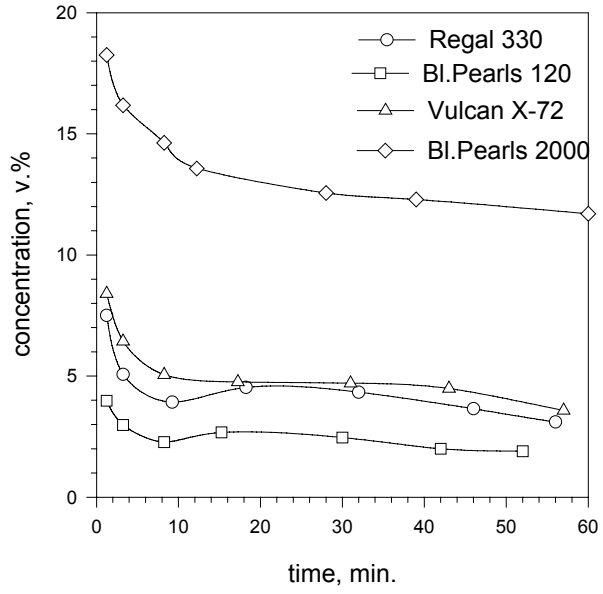

Figure 4-3. Methane Decomposition over Different Carbon Blacks at 850°C

Figure 4-4 demonstrates the results of methane decomposition over different samples of activated carbon at 850°C. These experiments were purposely conducted at low residence times (approx. 1 s) in order to differentiate the kinetic curves, which otherwise would be very close to each other. This resulted in some drop of hydrogen concentration in the effluent gas. However, the trend is apparent: all samples of activated carbon, regardless their origin, showed very close initial activity in methane decomposition, but rapidly deactivated over the period of one hour.

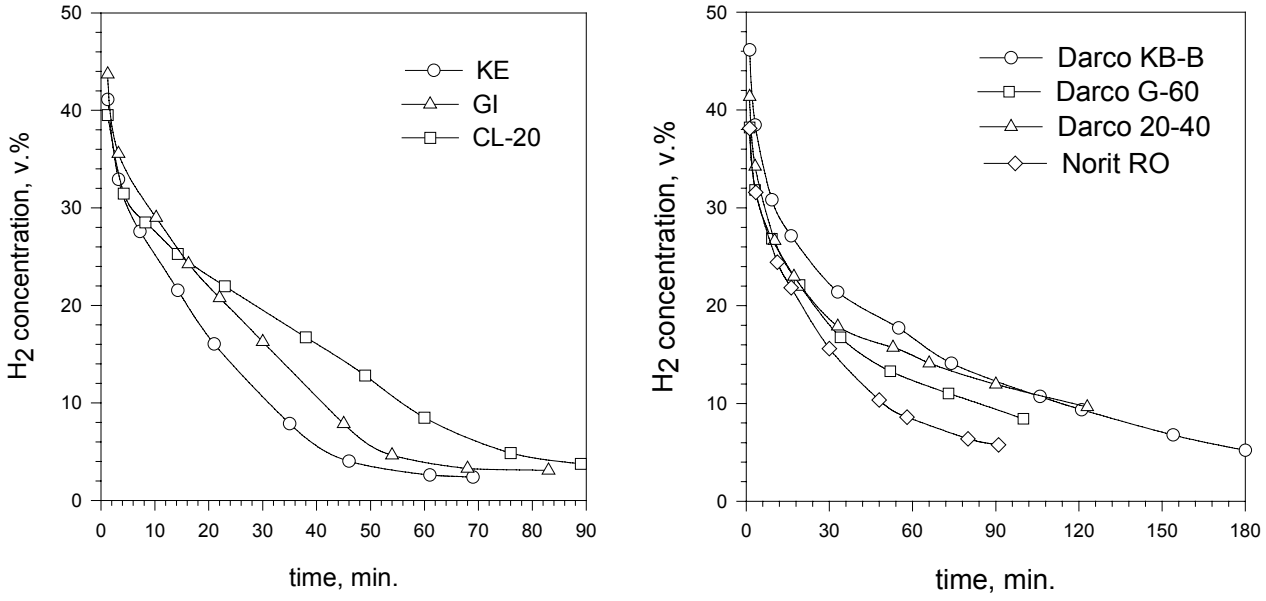

Figure 4-4. Methane Decomposition over Different Activated Carbons at 850oC

Figure 4-5 depicts the kinetic curves of methane decomposition over some "exotic" forms of carbon, including fullerenes and carbon nanotubes. It is apparent that glassy carbon and fullerenes C_{60} demonstrated relatively high initial activity, but very low stability toward methane decomposition reaction.

According to the Table 4-1 and Figure 4-2 graphites have the lowest initial catalytic activity (per unit of weight) in methane decomposition reaction. Among other factors, this could be attributed to the low surface area of graphites. However, the following experimental observation proves that graphites are indeed catalytically inert toward methane decomposition.

It was found that the initial methane conversion rates in the presence of synthetic and natural graphites (with SA from 3 to12 m^2/g) and three different modifications of Al_2O_3 (including α- and γ-forms) with the surface area from 6 to 275 m^2/g were in the same range of 0.2-1.0 mmol/min-g (at the same temperature and residence time). This experiment indicates that methane decomposition over graphites is most likely due to the thermal rather than catalytic processes. Inertness of graphite toward methane decomposition was earlier reported in [22].

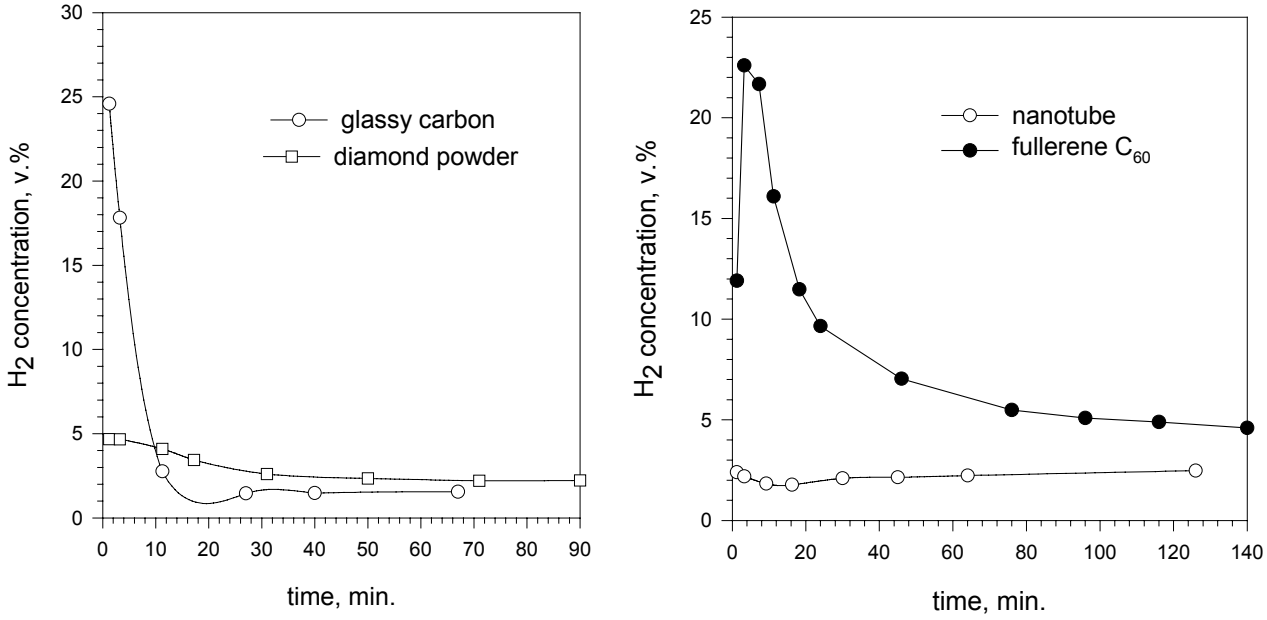

Figure 4-5. Methane Decomposition over Glassy Carbon, Diamond Powder, Fullerene C_{60} and Carbon Nanotubes

It is noteworthy that the sustainability factor (K_m^1/K_m^o) for natural graphite is more than unity, which indicates that the catalytic activity of carbon produced from methane is higher than that of the graphite. The same kinetic behavior was observed with both α- and γ- modifications of alumina. Figure 4-2 (b) depicts the kinetic curves of hydrogen production over natural graphite (SA=4-6 m^2/g) and γ-alumina (SA= 275 m^2/g) at 850°C and residence time of approximately 1 s. These experiments clearly point toward certain catalytic properties of carbon produced from methane. However the catalytic activity of this form of carbon is quite low and, obviously, much less than that of AC and CB-type catalysts.

These experimental results can be explained as follows. It is known that the initial rate of hydrocarbon decomposition depends on the nature of a support (substrate). As the substrate surface is covered with carbon species, the rate of methane decomposition may increase or decrease, depending on the relative catalytic activity of the substrate and the carbon produced. The total rate of the methane decomposition process is the sum of the rates of carbon nuclei formation and carbon crystallites growth. It was determined that the activation energy of the carbon nuclei formation during methane decomposition (316.8 kJ/mole) is much higher than the activation energy of the carbon crystallites growth (227.1 kJ/mole) [23]. Thus, in general, the rate of carbon crystallites growth tends to be higher than the rate of carbon nuclei production. The carbon particles produced during methane decomposition over AC catalysts, most likely, tend to have an ordered graphite-like structure and the rate of carbon crystallite growth exceeds that of nuclei formation. The catalyst surface is rapidly covered with relatively large graphite-like crystallites, which occupy active sites and result in inhibition of the catalytic activity toward methane decomposition. In the case of CB-type catalysts, the rates of crystallites growth and

nuclei formation become comparable, resulting in the quasi-steady state methane decomposition. Low initial hydrogen production rate over alumina and natural graphite surface is due to high activation energy of nuclei formation over these materials. The increase in hydrogen production rate after the short induction period can be explained by the increase in the concentration of carbon nuclei on the surface and the methane decomposition rate over relatively small carbon crystallites. This is followed by the growth of the existing carbon crystallites and, as a result, the reduction of the active surface area and gradual decrease in methane decomposition rate. It case of graphite, methane decomposition rate slowly reached the steady state conversion rate controlled by the catalytic activity of carbon produced from methane. The nature of active sites responsible for the efficient decomposition of methane over the fresh surface of AC and CB catalysts is yet to be understood.

4.2. Effect of Temperature and Space Velocity on Methane Decomposition Yield

We studied the effect of temperature and methane space velocity on the yield of methane decomposition using different carbon catalysts. Figure 4-6 (a) depicts the temperature dependence of the initial H_2 concentration in the effluent gas in the presence of carbon black and activated carbon catalysts at different residence times (τ). It is clear that the initial activity of AC catalysts is higher than that of CB catalysts over the entire range of temperatures 600-1000^{o}C.

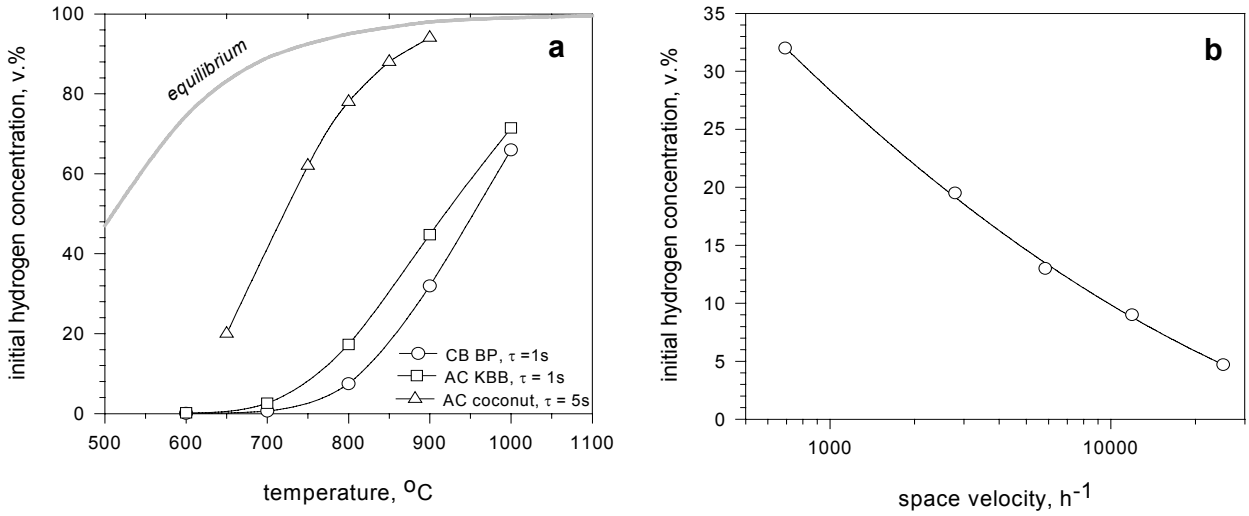

Figure 4-6. Effect of Temperature (a) and Methane Space Velocity (b) on Methane Decomposition Yield.

At sufficiently high temperatures (e.g. 900^{o}C and higher) and residence times (e.g. 5 s and higher) the initial concentration of hydrogen in the effluent gas approaches the thermodynamic equilibrium concentration, which is an indication of high catalytic activity at these conditions. At 650^{o}C and below the methane conversion rate was negligible.

Figure 4-6 (b) demonstrates the effect of methane space velocity on the initial concentration of hydrogen in the effluent gas produced by methane decomposition over carbon black (BP-2000)

at 850°C presented in semi-log coordinates. Ten fold increase in space velocity of methane results in 3-4 fold decrease in methane decomposition yield. It should be noted that in this paper, for the sake of comparability, both the residence time and the space velocity relate to the volume of the carbon catalyst within the reactor.

The initial catalytic activity of AC is much higher than that of carbon produced from methane, therefore, the second component of the kinetic equation could be neglected, which results in a typical exponential drop shape of the kinetic curve. In contrast to AC, graphite catalysts (particularly, natural graphite) have very low initial catalytic activity toward methane decomposition reaction, therefore the first component of the kinetic equation is negligible, and the resulting kinetic curve is either flat, or is described by the exponential rise to maximum law. The same is true for the methane decomposition over alumina surface.

We determined the kinetic parameters of methane decomposition reaction over different carbon catalysts. Table 4-2 summarizes the major kinetic parameters (apparent reaction rate constants, frequency factors and activation energies) for CB and AC catalysts at the range of temperatures 700-900°C.

Table 4-2. Apparent Reaction Rate Constants and Activation Energies for CH_4 Decomposition over CB and AC Catalysts

Catalyst	T°C	k, s^{-1}	E_a, kJ/mol	α, s^{-1}
Carbon black, BP-2000 SA= 1500 m^2/g	750	0.035	235.9	4.3×10^9
	850	0.480		
	950	2.125		
Activated carbon, KBB SA= 1500 m^2/g	600	0.0015	200.7	4.9×10^8
	700	0.026		
	800	0.178		
	900	0.602		

Thus, the apparent rate constants for methane decomposition in the presence of carbon black BP-2000 (k_{CB}) and activated carbon KBB (k_{AC}) catalysts could be expressed as follows:

$$k_{CB} = 4.3\times10^9 \exp(-235.9/RT) \qquad 750\text{-}950^oC \qquad (4\text{-}1)$$

$$k_{AC} = 4.9\times10^8 \exp(-200.7/RT) \qquad 600\text{-}900^oC \qquad (4\text{-}2)$$

Figure 4-7 depicts the Arrhenius plot for methane decomposition over AC (KBB) catalyst. The activation energies of methane decomposition reactions over carbon catalysts are characteristic of surface reaction rate controlled processes.

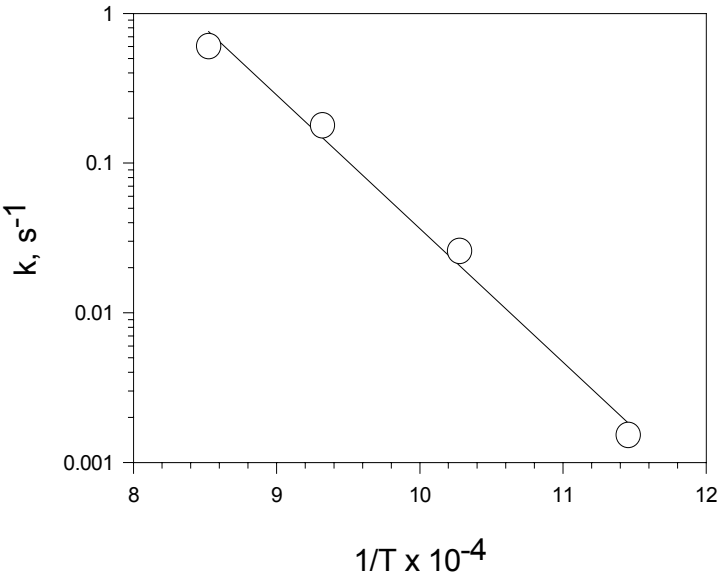

Figure 4-7. Arrhenius Plot for CH_4 Decomposition

4.3. Catalytic Pyrolysis of Propane over Carbon Catalysts

Due to a relatively weak C – H bond in propane molecule (402.2 kJ/mol) it is somewhat easier to split propane than methane molecule (methane C – H bond energy is 440.0 kJ/mol). 26.0 kJ is required to produce one mole H_2 from propane, comparing that to 8.9 kcal for methane:

$$C_3H_8 \rightarrow 3C + 4H_2 \qquad \Delta H^o = 103.9 \text{ kJ/mol} \qquad (4\text{-}3)$$

However thermal cracking of propane at high temperatures proceeds via a thermodynamically more favorable formation of methane and ethylene:

$$C_3H_8 \rightarrow CH_4 + C_2H_4 \qquad \Delta H^o = 81.3 \text{ kJ/mol} \qquad (4\text{-}4)$$

Therefore, during pyrolysis of propane, in most cases, we observed the production of gaseous mixture containing hydrogen, methane, ethylene and small amounts of ethane and propylene. Figure 4-8 depicts the experimental results of propane catalytic pyrolysis over CB (a) and AC (b) type catalysts at 800°C in a packed bed reactor. Similar to methane decomposition, activated carbon demonstrated high initial activity followed by the rapid drop in catalytic activity. At the onset of the process hydrogen and methane were the only products of propane pyrolysis. Practically no C_2^+ byproducts were found in the effluent gas during first 10 min.

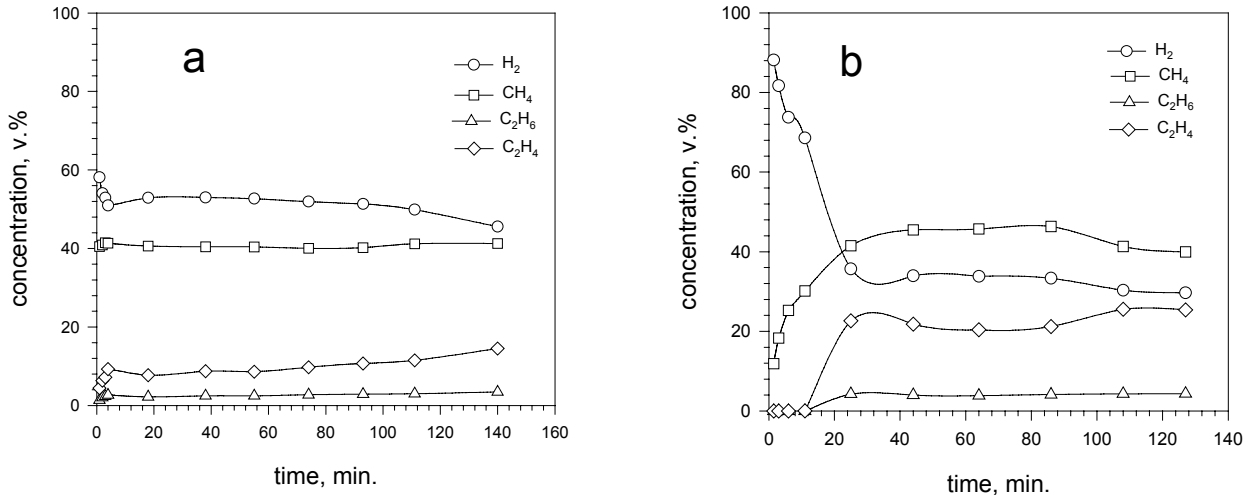

Figure 4-8. Propane Pyrolysis over CB (XC-72) (a) and AC (KE) (b) at 800°C

Quasi-steady state pyrolysis of propane was established after 30-40 min with methane being the major product of pyrolysis and significant concentration of ethylene in the effluent gas.

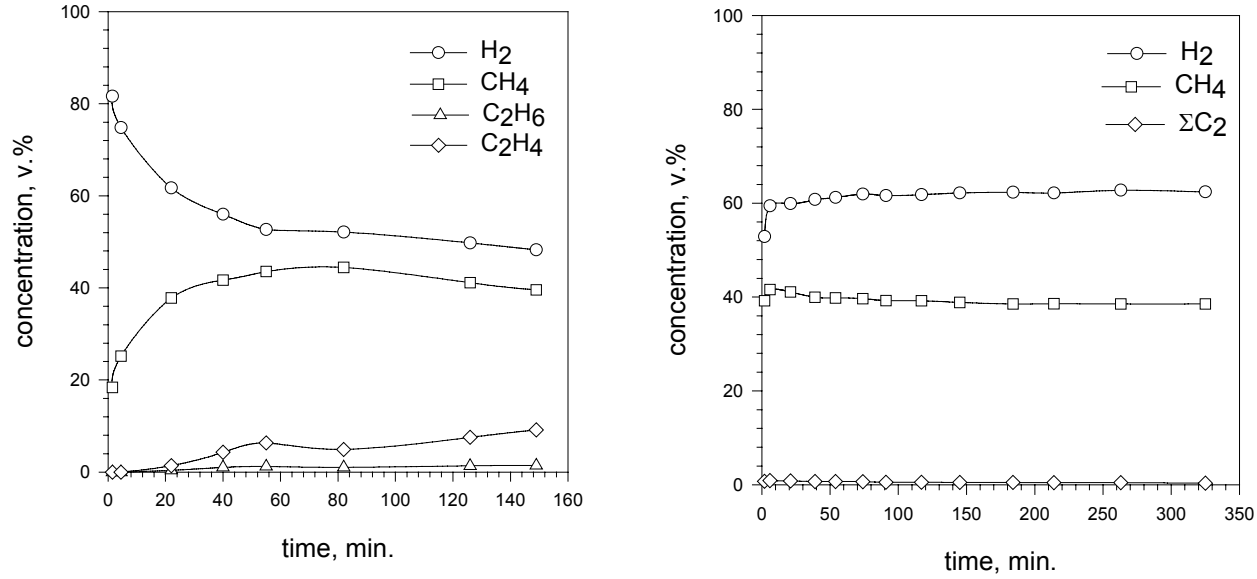

Figure 4-9. Propane Pyrolysis over Activated Carbon (Phenol Resin) (800°C) (left) and Acetylene Black (850°C) (right)

The composition of the effluent gas of propane pyrolysis over AC catalyst approximately corresponded to the following chemical equation:

$$C_3H_8 \rightarrow 0.8\ H_2 + CH_4 + 0.6C_2H_4 + 0.8C \qquad \Delta H^o = 60.3\ kJ/mol \qquad (4\text{-}5)$$

Propane pyrolysis over carbon black was characterized by lower initial rate, but was more sustainable comparing to AC catalyst, as shown on Figure 4-8 (a). Quasi-steady state rate of propane pyrolysis was reached in approximately 5 min and the process remained stable for approximately 2 hours. Hydrogen was a major component of the effluent gas during CB-catalyzed pyrolysis of propane.

Figure 4-9 depicts the results of propane pyrolysis over activated carbon produced from phenol resin (left) and acetylene black (right). As in previous cases, AC-type catalyst demonstrates higher initial activity and lower stability, comparing to CB-type catalysts.

4.4. Catalytic Pyrolysis of Liquid Hydrocarbons

From the thermodynamic point of view the decomposition (pyrolysis) of liquid hydrocarbons is more favorable than the decomposition of methane, as almost 1.5-2 times less energy is required to produce a unit volume of hydrogen. We conducted a series of experiments on the catalytic pyrolysis of a wide range of liquid hydrocarbons (hexane, octane, gasoline and diesel fuel) using different carbon-based catalysts.

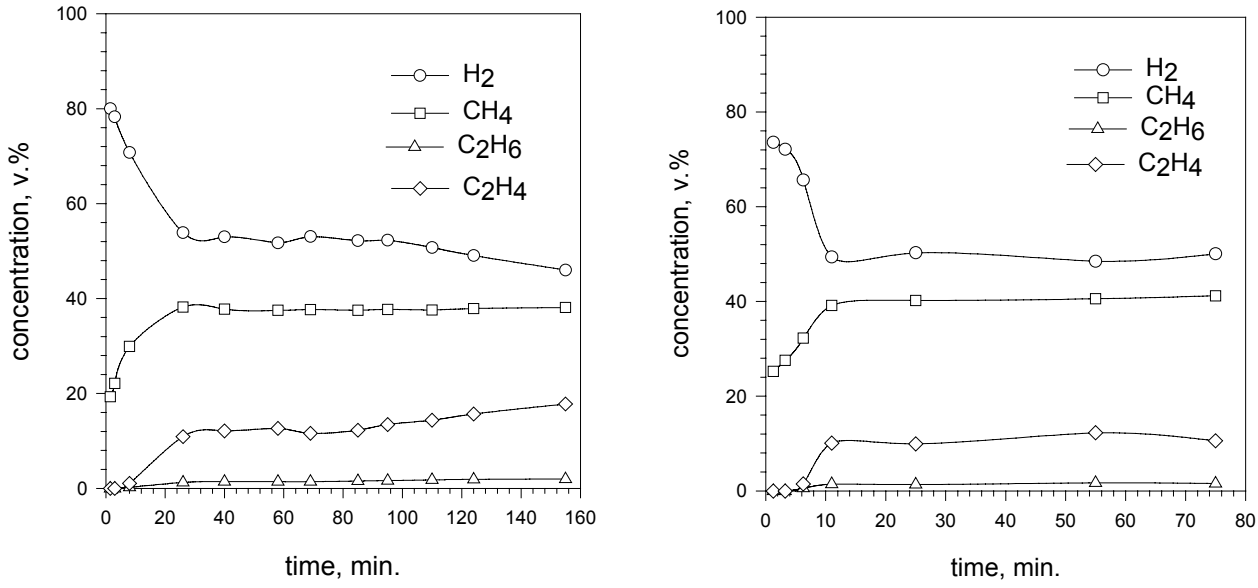

Figure 4-10. Pyrolysis of Hexane (left) and Gasoline (right) over Activated Carbon (Phenol Resin) at 800°C Gasoline

Figure 4-10 depicts the experimental results of the catalytic pyrolysis of hexane and gasoline over carbon catalysts at 800°C. In both cases, the quasi-steady state production of the pyrolysis products was achieved over period of 10-20 min. After 1-1.5 hours we observed the production of small amounts of the dark liquid products. The gas production rate reached 700 mL/min per mL/min of gasoline. In the case of diesel fuel the concentration of hydrogen in the effluent gas with one reactor arrangement was in average 30-40%v.

4.5. Studies on the Improvement of Catalyst Stability and Process Sustainability

4.5.1. Carbon Catalyst Stability Issues

The development of carbon catalysts featuring long term stability is one of the major aspects of this work. The experimental results indicated that catalyst deactivation during methane decomposition is common for all types of carbon-based catalysts (although, CB is deactivated much slower than AC). It was determined that three chief factors contribute to carbon catalyst deactivation:

1) blocking of catalytically active sites by carbon deposits,
2) surface deposition of catalytically inactive carbon particulates, and
3) reduction in catalytic surface area

Our approach to solving catalyst deactivation problem is based on an in-situ generation of carbon species catalytically active in methane decomposition reaction. It is known that the catalytic activity of carbons in methane decomposition is determined by the size of carbon crystallite and its structure [23]. Potentially, the size of carbon crystallites can be affected by the reaction temperature and the presence of other hydrocarbons. The size of the carbon crystallite produced during thermal decomposition of methane is an inverse function of the reaction temperature: higher is the temperature, smaller is the carbon crystallite [23]. Figure 4-11 depicts the correlation between the size of carbon crystallite produced by methane decomposition and the reaction temperature. It is clear that increase in temperature from 800 to 1100°C would result in only three-fold reduction in carbon crystallite size. Thus, improvement in catalytic activity of carbon particles via temperature-induced reduction of their crystallite size would require significant increase in methane decomposition temperature (several hundred degrees), which may not be desirable.

We explored the accelerating effect of certain hydrocarbons on the methane decomposition rate as the means of improving long-term stability of carbon catalysts and the sustainability of the process as a whole. It was found that the improvement in the process sustainability can be achieved via in-situ generation of catalytically active carbon particles produced by co-decomposition of hydrocarbons other than methane. We determined the relative catalytic activity of carbons produced by decomposition of hydrocarbons of different classes, e.g. alkanes, unsaturated and aromatic hydrocarbons. Particularly, it was found that carbon produced by decomposition of unsaturated and aromatic hydrocarbons are catalytically more active than one produced from methane, or other alkanes. Figure 4-12 demonstrates the accelerating effect of ethylene on methane decomposition rate.

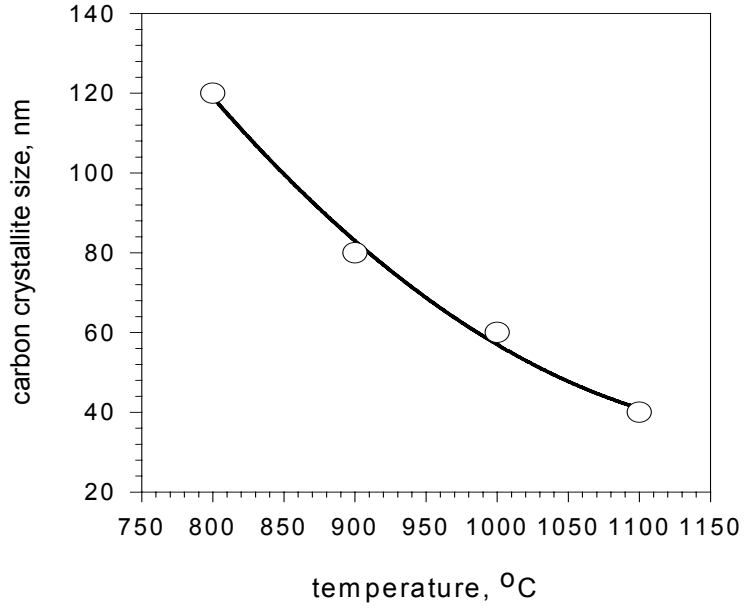

Figure 4-11. Carbon Crystallite Size as a Function of Temperature

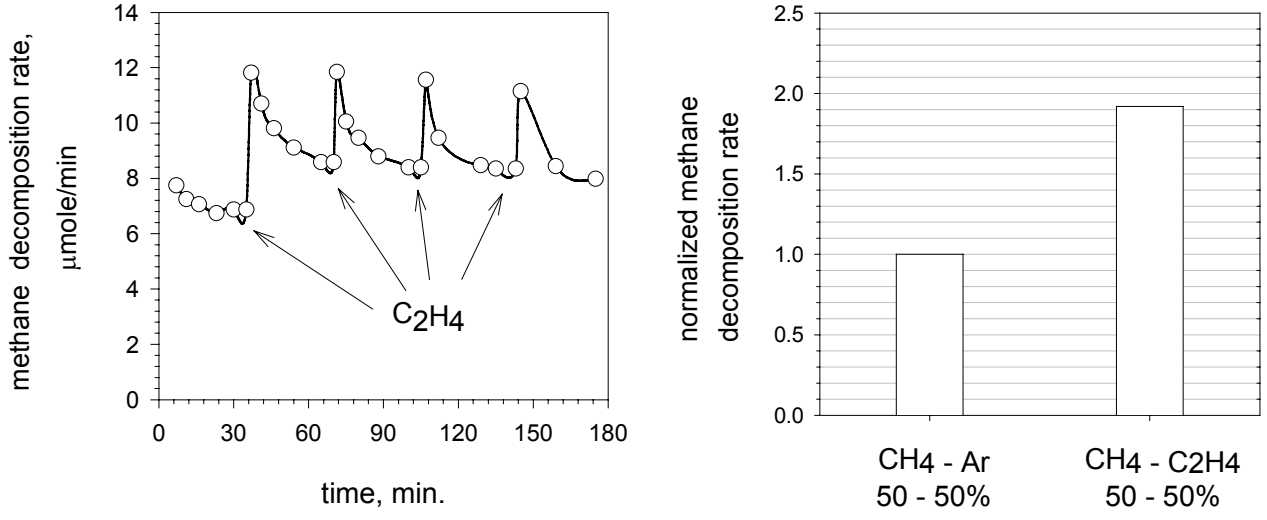

Figure 4-12. Effect of Ethylene on Methane Decomposition Rate at 850°C

The experiment started with thermal decomposition (850°C) of methane over the surface of activated alumina until quasi-steady state was established (approx. 0.5 h). A pulse of ethylene was introduced into the reactor, followed by rapid purging the reactor with an inert gas (to remove products of ethylene decomposition), and the introduction of methane into the reactor. We observed a sharp increase (spike) in methane decomposition rate during first seconds after methane introduction, followed by its gradual decline to a steady state level. This procedure was repeated several times, and every time we observed a surge in methane decomposition rate after ethylene pulse (see Figure 4-12, left). Thus, this experiment proved that carbon produced from ethylene is catalytically more active in methane decomposition than one produced from methane. The accelerating effect of ethylene on methane decomposition reaction was also demonstrated in a continuous flow experiment using binary CH_4-C_2H_4 (50-50 v.%) mixtures. Particularly, we observed that the rate of methane decomposition over the surface of silica gel at 850°C almost doubles in the presence of ethylene (Figure 4-12, right). Thus, decomposition of hydrocarbon with low activation energy (ethylene) induces the decomposition of hydrocarbon with high activation energy (methane).

Similar, even more pronounced effect, was observed when benzene pulses were introduced into the reactor where methane decomposition took place (see Figure 4-13, left). It was found that the yield of hydrogen produced by the decomposition of methane in a binary mixture with benzene vapor (5 v.%) at 850°C increased almost 8 fold compared to pure methane (after adjusting for the amount of hydrogen produced by benzene) (Figure 4-13, right).

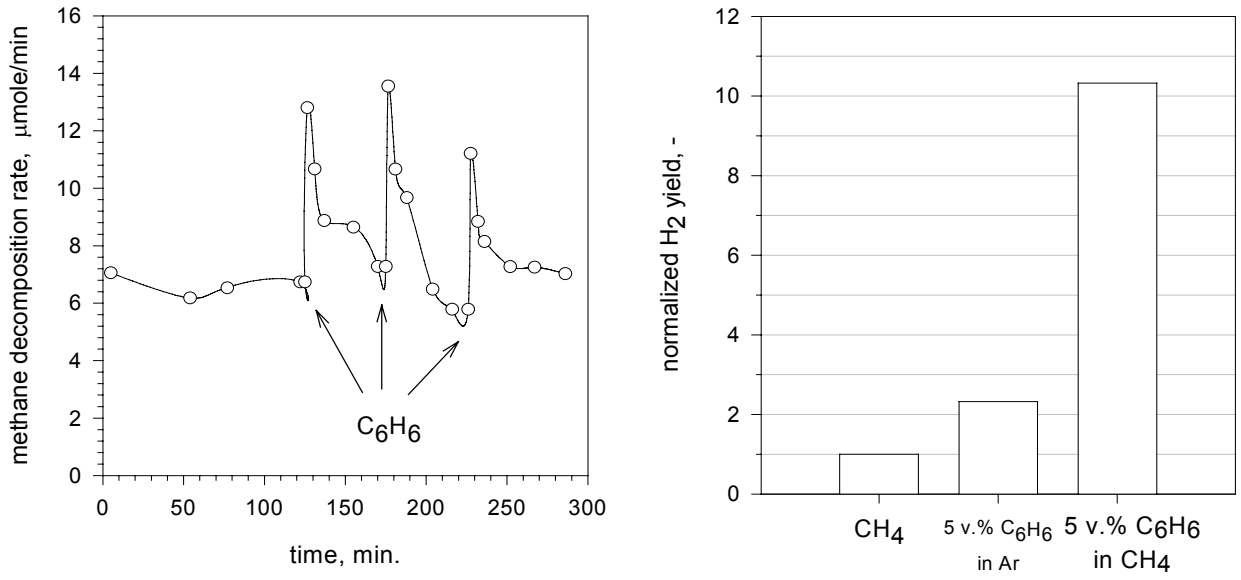

Figure 4-13. Effect of Benzene Vapors on Methane Decomposition at 850°C

Figure 4-14 summarizes the relative activity of carbons produced by decomposition of different hydrocarbons in methane decomposition reaction (normalized against catalytic activity of carbon produced from methane). It was concluded that among all the hydrocarbons tested, carbon produced from aromatics (benzene and naphthalene) exhibited highest catalytic activity toward methane decomposition.

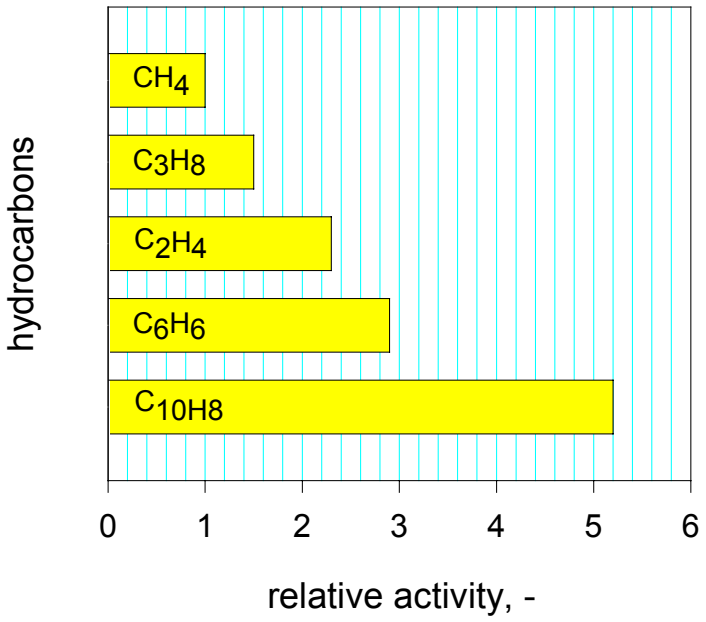

Figure 4-14. Relative Activity of Carbons Produced from Different Hydrocarbons in Methane Decomposition Reaction at 850°C

The relative activity of carbons produced from methane, ethylene and benzene is a linear function of carbon crystallite size in semi-log coordinates (Figure 4-15).

These data have important implications on the improvement of the process sustainability of hydrocarbon decomposition process. At relatively high space velocities noticeable amounts of ethylene and aromatics are present in the gases of propane and methane-propane pyrolysis. Thus, recycling pyrolysis gas (with olefins and aromatics) back to the reactor after separation of hydrogen could significantly improve the long term stability of carbon catalyst and the process sustainability.

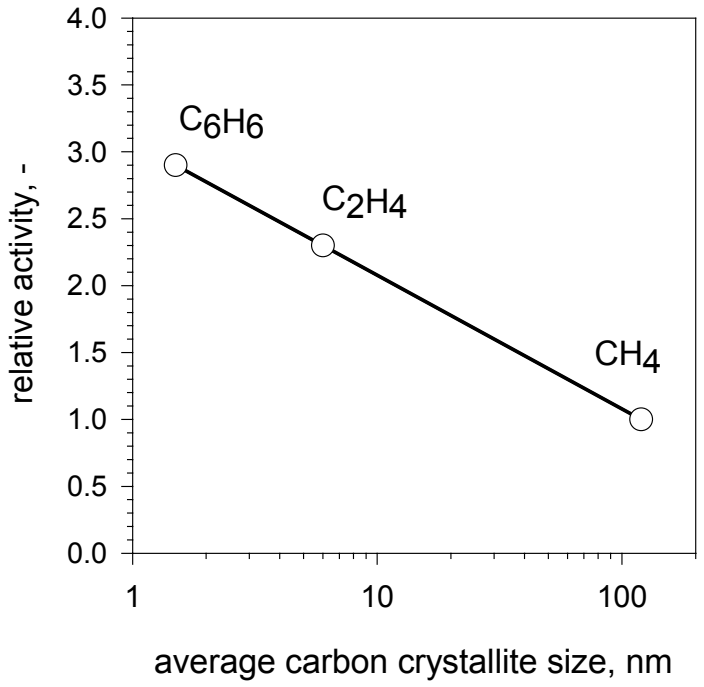

Figure 4-15. Relative Activity of Carbons Produced from Methane, Ethylene and Benzene as a Function of Carbon Crystallite Size

It was previously determined that major factors contributing to carbon catalyst deactivation were: blocking of active sites by catalytically inactive carbon particulates, and the reduction in catalytic surface area. It was found that the rate of catalyst deactivation depends on the nature of carbon catalyst and hydrocarbon and the operational parameters (e.g., temperature). Particularly, at higher temperatures (e.g., >850^{o}C) the pace of catalyst deactivation in methane decomposition reaction noticeably decreases compared to moderate temperatures (750-850^{o}C). Activated carbon (AC) catalysts demonstrated both the highest initial activity and the highest rate of deactivation among all the carbon samples tested. In contrast, the initial rate of methane decomposition over amorphous carbons (e.g. carbon blacks, CB, and acetylene black), was somewhat lower than that of AC samples, but the rate of deactivation was also slower. CB-catalyzed methane decomposition reached a quasi-steady state rate (over 10-20 min) and remained practically stable for several hours, followed by the gradual decline in the reaction rate.

A typical empirical correlation for the decay of catalytic activity by coking is given by:

$$C_c = A\, t^n \qquad (4\text{-}6)$$

where C_c is the concentration of carbon on the surface of the catalyst, t is time, and both A and n are fouling parameters which are dependent on reactor conditions such as the temperature and feed flow rate. If it is assumed that the carbon concentration is directly proportional to the surface area of the catalyst, then equation (2) may be written as:

$$S = A\, t^{n} \tag{4-7}$$

Where in Equation (2), S is the surface area per unit mass of the catalyst. Therefore, if the log of the surface area is plotted against the log of time, the plot should be a straight line of slope n and intercept of log A.

Figure 4-16 shows a plot of the log of the surface area against the log of time for both carbon black and activated carbon catalysts. Both catalysts were subjected to the same reactor conditions of a feed of pure methane at 10 ml/min, and a reactor temperature of 800^{0}C. The empirical decay law for carbon black is given as:

$$S = 1821\, t^{-0.0566} \tag{4-8}$$

Also, the decay law for activated carbon is given as:

$$S = 1037\, t^{-0.2483} \tag{4-9}$$

The value of n is an order of magnitude larger for activated carbon than for carbon black. This shows that the surface area of activated carbon will decrease significantly faster than that of carbon black.

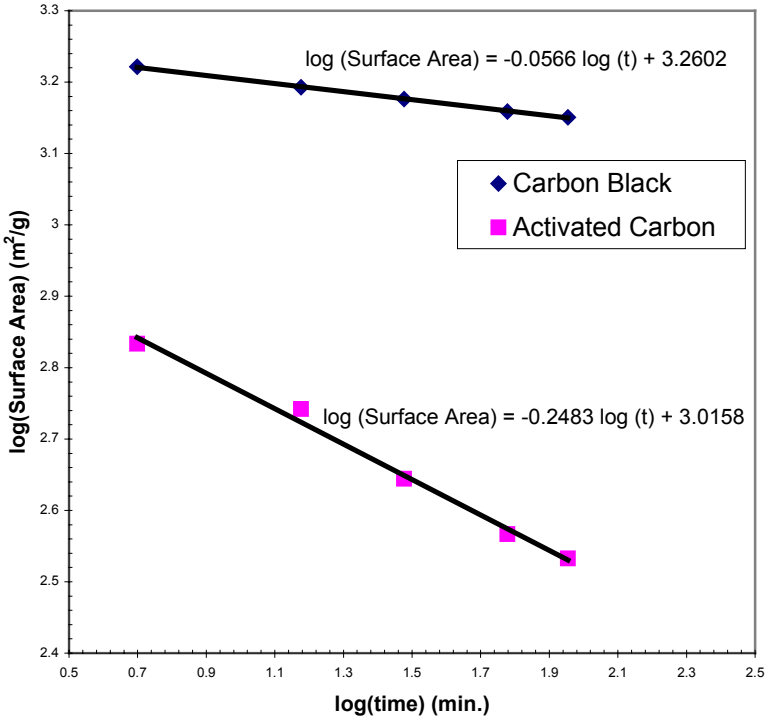

Figure 4-16. An Empirical Correlation for Catalyst Deactivation by Carbon Deposition for the Thermocatalytic Decomposition of Methane.

The above experimental results can be explained as follows. The catalytic activity of carbons in hydrocarbon decomposition is determined by the size of carbon crystallite and its structure, which in turn are governed by the temperature and the nature of hydrocarbon. Particularly, the size of the carbon crystallite produced during thermal decomposition of methane is an inverse function of the reaction temperature: higher is the temperature, smaller are the carbon crystallites. The total rate of the methane decomposition reaction is the sum of the rates of carbon nuclei formation and carbon crystallites growth. The rate of carbon nuclei formation is proportional to the substrate surface area: carbons with high surface area (e.g. ACs and some CBs) tend to have high initial catalytic activity. It was determined that the activation energy of the carbon nuclei formation during methane thermal decomposition (316.8 kJ/mole) is much higher than the activation energy of the carbon crystallites growth (227.1 kJ/mole) [23]. Thus, in general, the rate of carbon crystallites growth tends to be higher than the rate of carbon nuclei generation. With the rise in the temperature the mean size of carbon crystallites tends to decrease resulting in the increase in methane decomposition rate. This explains the experimental fact that at high temperatures (e.g., >850^{o}C) carbon catalysts tend to deactivate at slower rate compared to lower temperatures.

Rapid deactivation of AC catalysts can be explained by blocking of AC pores by growing carbon crystallites which hinder the internal diffusion of methane molecules. Pore diffusion controlled reaction could also be responsible for the insensitivity of methane decomposition rate to the origin and surface area of ACs. In contrast, the most of CB surface is relatively easily accessible to methane molecules during decomposition reaction. CBs differ in particle size, average aggregate mass, morphology, etc. (e.g. the oil furnace process produces CBs with particle diameters in the range of 10-250 nm, and surface area of 25-1500 m^2/g). CBs with high external surface area (e.g. BP-2000) result in relatively high steady state methane decomposition rate. The process could go on for several hours until most of the surface is covered with carbon crystallites produced from methane. It was estimated that it would take almost three hours to cover the surface of CB (BP-2000) with carbon species produced from methane (which is in acceptable agreement with the experiment). After 3-4 hours we observed gradual decrease in methane decomposition rate, due to rapid carbon crystallite growth and reduction in the catalytic surface area.

It was determined that carbons produced by thermal decomposition of different hydrocarbons exhibit dissimilar catalytic activities in methane decomposition reaction. In particular, the catalytic activity of carbons produced from different hydrocarbons can be arranged in the following order:

naphthalene > benzene > ethylene > propane > methane

The accelerating effect of ethylene and benzene on the methane decomposition rate is shown in Figure 4-17. In this series of experiments methane and methane-hydrocarbon mixtures were thermally decomposed over the surface of an inert support (SiO_2) at 850^{o}C. It is clear that in the presence of ethylene and benzene methane decomposition rate increases two and seven fold, respectively.

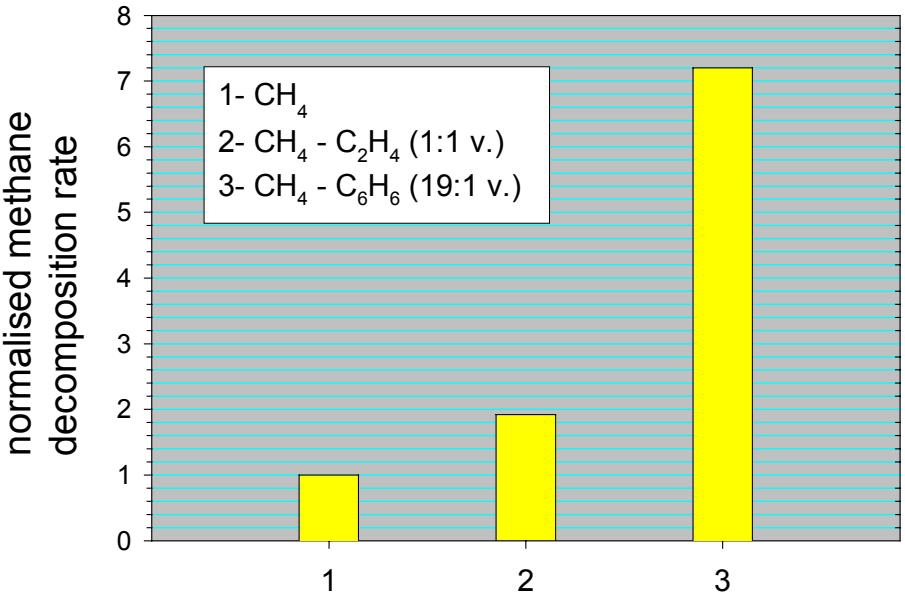

Figure 4-17. Effect of Ethylene and Benzene on Methane Decomposition Rate at 850°C

It was shown that the activity of carbon crystallites in methane decomposition reaction is a reverse function of their size: smaller crystallites are catalytically more active than larger ones. Thus, the rate of methane decomposition over relatively small crystallites (2-3 nm) produced from ethylene or benzene is higher compared to that of relatively large crystallites (approx. 100 nm) produced from methane.

The following theoretical considerations explain the effect of hydrocarbons (e.g., ethylene) on methane decomposition rate. The mean size of carbon crystallite (L_n) and the surface density (N_n) of crystallites in the n^{th} layer of carbon can be found from the following expressions [23]:

$$L_n = 2W\tau_n \quad (4\text{-}10)$$

$$N_n = P_{n-1}\tau_n U \quad (4\text{-}11)$$

where, W is the rate of crystallite growth, τ_n - time required for the formation of n^{th} layer, P-perimeter of the carbon crystallite, U- the rate of nuclei formation

Considering that

$$N = 1/L_a^2 \quad (4\text{-}12)$$

$$P = 4L_aN/2 \quad (4\text{-}13)$$

$$P = 2L_a \quad (4\text{-}14)$$

and

$$L_n=(L_{n-1}\frac{W}{U})^{1/3} \tag{4-15}$$

$$V=2d(UW)^{1/2} \tag{4-16}$$

$$L_a=\left(\frac{W}{U}\right)^{1/2} \tag{4-17}$$

(where L_a is a mean carbon crystallite size on the plane; V is rate of carbon growth in the direction normal to the plane; d is distance between graphitic layers)

the following expressions can be obtained for the growth of carbon crystallites from methane decomposition on the surface of carbon crystallites produced from ethylene:

$$\frac{L_n}{L_{CH_4}}=\left(\frac{L_{n-1}}{L_{CH_4}}\right)^{1/3} \tag{4-18}$$

$$L_n = L_{CH_4}\left(\frac{L_{C_2H_4}}{L_{CH_4}}\right)^{1/3^n} \tag{4-19}$$

Multiplying equation (8) by (9)

$$V_n L_n = V_{CH_4} L_{CH_4} = 2Wd \tag{4-20}$$

and comparing (11) and (12)

$$V_n = V_{CH_4}\left(\frac{L_{CH_4}}{L_{C_2H_4}}\right)^{1/3^n} \tag{4-21}$$

The equations (11) and (13) allow to determine the mean size and growth rate of carbon crystallites for n-th carbon layer. Evidently,

at $n \to \infty$ $V_n \to V_{CH4}$ and $L_n \to L_{CH4}$

These considerations explain the experimental fact that the rate of methane decomposition over small carbon crystallites obtained from ethylene is higher than a stationary rate; however, after reaching the steady state regime ($n\to\infty$)the kinetics of the process is governed by the rate of growth of carbon crystallites produced from methane.

The accelerating effect of olefins and aromatics on methane decomposition rate could advantageously be used to improve the process sustainability of hydrogen production from natural gas. This can be accomplished by recycling the gaseous stream containing methane-C_2+ mixture back to the reactor after hydrogen separation (see Figure 4-18).

The experiments with the simulated NG feedstock (e.g., gaseous mixtures comprising 90 v.% CH_4 and 10 v.% C_3H_8) demonstrated that the effluent gas after the catalytic reactor contains noticeable amounts of ethylene, benzene, naphthalene vapors and other C_2+ compounds (up to 10 v.% and higher, depending on the operational conditions). After the separation of hydrogen, these heavy components of NG pyrolysis gas are recycled to the reactor where they are decomposed with the production of catalytically active carbon species resulting in the acceleration of methane decomposition reaction. We call this mode of increase in the catalytic activity of carbon catalysts the "in-situ" activation, since it takes place in the reactor during methane decomposition stage.

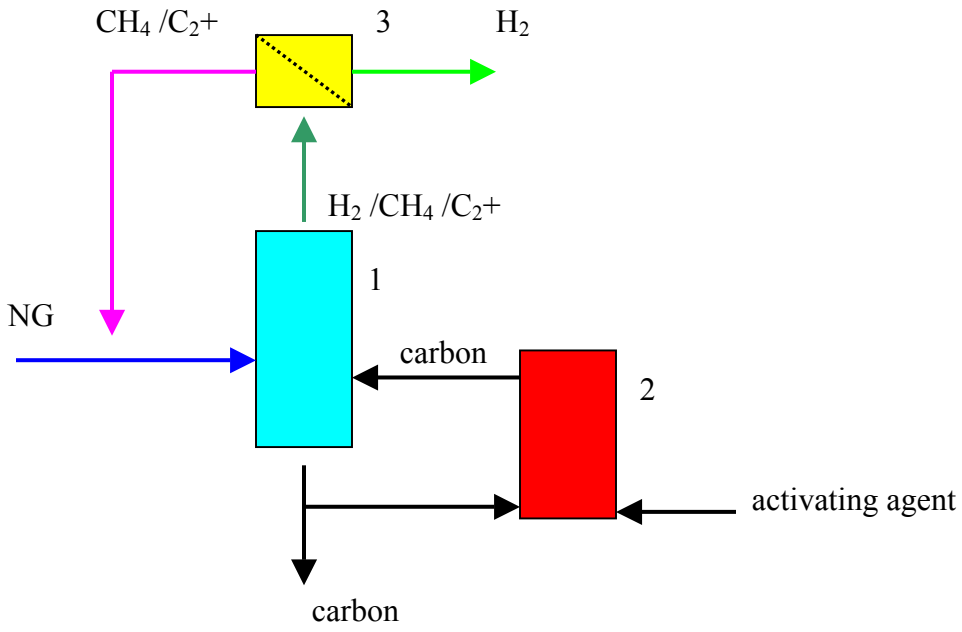

Figure 4-18. Simplified Block-diagram of TCD of NG
1- fluidized bed reactor, 2- fluidized bed heater, 3- gas separation unit

4.5.2. Reactivation of Carbon Catalysts Using Activating Agents

Earlier, we reported on catalytic activity of a variety of carbon materials of different origin and structure, including a wide range of activated carbons (AC), carbon blacks (CB), graphites, nanostructured carbons, etc., toward methane decomposition reaction. In this study we explore some aspects of carbon catalyst deactivation and regeneration of catalytic activity toward TCD

of methane using AC and CB catalysts. As a general comment, practically no methane decomposition products other than hydrogen and carbon were detected in the effluent gas during the experiments. At the very beginning of the experiments (first 5-10 min.) very small amounts of CO (corresponding to CO selectivity of <1 mol.%) were detected in the pyrolysis gas. Apparently, CO originates from the adsorbed and/or pore-entrained oxygen and water molecules. The control experiments with hydrogen pretreatment of carbon samples at 800^{o}C for 0.5 hr demonstrated 5-fold decrease in initial CO concentration. Considering the enormous surface area of carbon samples tested (500-1500 m^2/g) it would probably take much longer time to get rid of all the adsorbed and entrained oxidants from the carbon samples. After partial deactivation of carbon catalysts (usually, 2-3 hrs) trace amounts of C_2 hydrocarbons could also be detected in the effluent gas. The control experiments using an inert contact (silica gel with surface area of 600 m^2/g) demonstrated that no appreciable thermal decomposition of methane occurred at temperatures up to 900^{o}C (thus, all the reactions discussed are of a heterogeneous nature). All references to the catalytic activity of carbon samples relate to the methane decomposition rate (MDR) per unit of carbon weight per minute (mmole/min-g).

Figure 4-19 depicts the kinetic curve of hydrogen production via methane decomposition over AC (Lignite) at 800^{o}C along with the data on the surface area of carbon samples. There was a rapid drop in catalytic activity of carbon catalyst over first 0.5 hr followed by a quasi-steady methane decomposition rate (controlled by the catalytic activity of carbon particulates produced from methane). It is evident that carbon surface area also dropped almost synchronously with the methane decomposition rate. This experiment illustrates that carbon catalyst deactivation could be mainly attributed to the loss in catalytic surface area. It should be noted that although there exists a general dependence of MDR on the carbon surface area, the latter is not the only factor determining the catalytic activity of carbon samples. For example, the experimental data showed no apparent correlation between surface area and the catalytic activity within the family of activated carbons. Furthermore, AC produced from hardwood (AC-KBB with surface area of 1500 m^2/g) demonstrated an initial MDR almost twice of that for carbon black (BP-2000) with the same surface area.

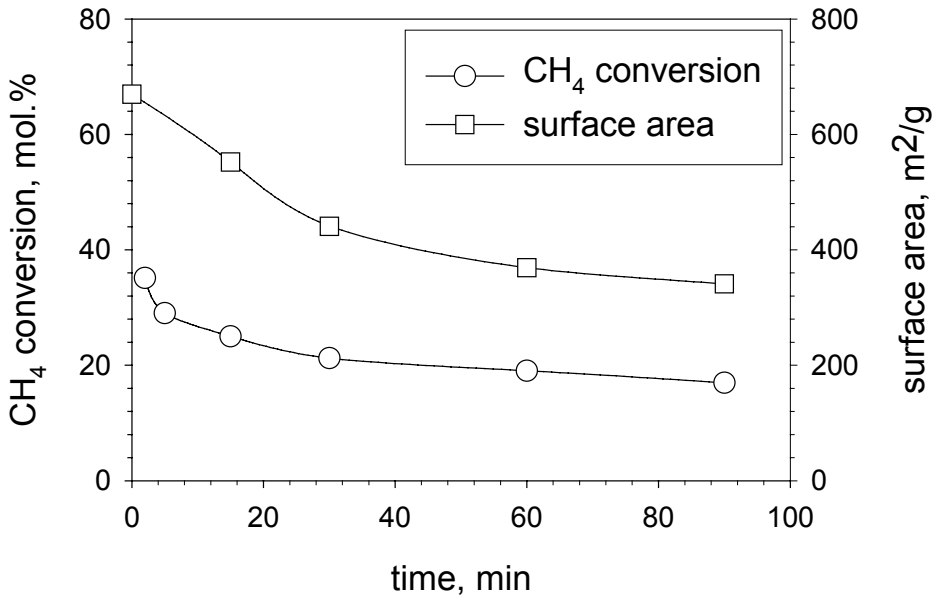

Figure 4-19. Correlation Between Methane Conversion Yield and Carbon Catalyst Surface Area. Temperature 800°C.

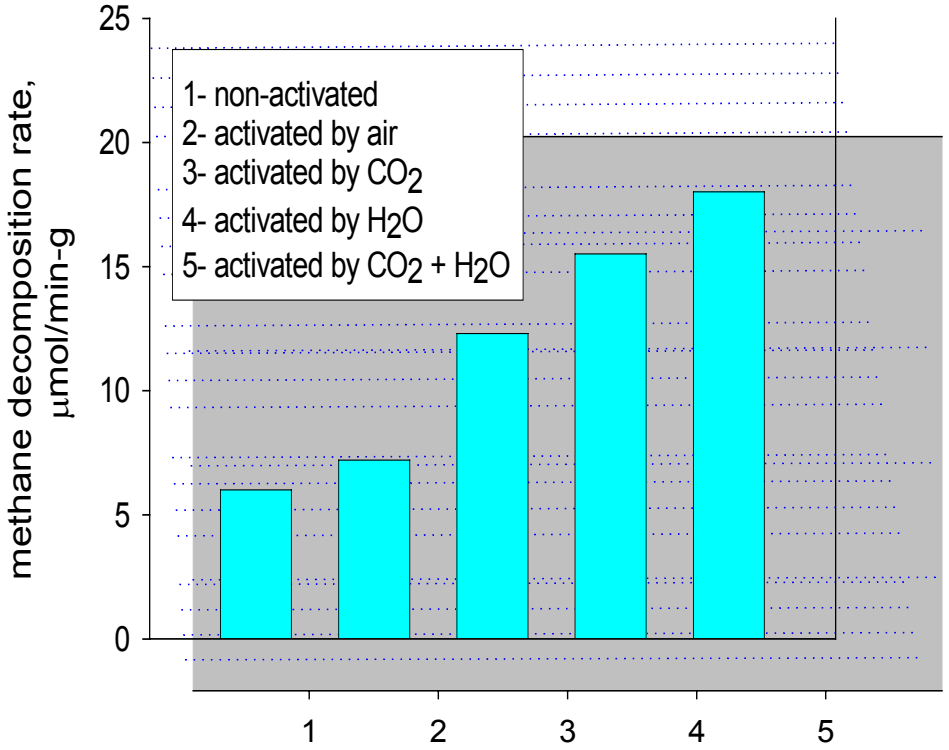

Figure 4-20. Effect of Carbon Catalyst Activation by Different Activating Agents on the Methane Decomposition Rate at 850°C. Activation Temperature 950°C

It is well known that the surface area of carbon particulates can be increased in the presence of activating agents at elevated temperatures. High temperature steam, CO_2 or their mixtures are the most common activating agents in the production of activating carbons from a variety of carbonaceous materials (hardwood, lignite, coconut shell, petroleum coke, etc.). In our work we attempted to apply this approach to increase the surface area and, consequently, catalytic activity of carbon particulates in the methane decomposition reaction. In particular, we studied the effect of carbon catalyst activation on the rate of methane decomposition using several activating agents: air, steam, CO_2 and steam-CO_2 mixtures. In this series of experiments the deactivated CB carbon catalyst (after exposure to methane at 850^{o}C for 6 hr) were subjected to the treatment with equimolar amounts of steam, CO_2 and air at 950^{o}C. The effect of carbon activation on the methane decomposition rate is shown in Figure 4-20. It is evident that the treatment of carbon particles with steam and steam-CO_2 (1:1 by volume) mixtures resulted in significant increase in methane decomposition rate. Air exhibited a relatively low carbon activating efficiency.

In principle, the activation of carbon particles with activating agents can be accomplished in the heater (see Figure 4-18) where temperature conditions (900-1000^{o}C) are suitable for the activation process. Since the catalyst activation occurs outside the catalytic reactor we call this operation the "external" activation (to distinguish it from "in-situ" activation taking place within the reactor). Thus, both "in-situ" and "external" catalyst activation mechanisms can contribute to the improvement in the process sustainability. It is important to note that these two modes of catalyst activation act independently and potentially can complement each other.

4.5.3. Verification of Process Sustainability

Earlier we found that one of the main factors leading to deactivation of carbon catalysts relates to the drastic reduction in catalytic surface area during methane decomposition. In principle, the surface area of carbon particulates can be increased via their surface treatment with activating agents at elevated temperatures. High temperature steam, CO_2 or their mixtures are the most common activating agents in the production of activating carbons from a variety of carbonaceous materials. In our work we attempted to apply this approach to increase the surface area and, consequently, catalytic activity of carbon particulates in methane decomposition reaction. In particular, we studied the effect of carbon catalyst activation on the rate of methane decomposition using several oxidizing agents: air, steam, CO_2 and steam-CO_2 mixtures. Figure 4-21 depicts the effect of steam treatment on the improvement of catalytic activity of carbon samples. In this series of experiments the deactivated carbon samples (after exposure of a carbon catalyst to methane at 850^{o}C) were subjected to the treatment by steam at 950^{o}C. It was demonstrated that the treatment of carbon particles with steam resulted in the increase in surface area and simultaneously in the increase in methane decomposition rate. The process was repeated several times and in each case we observed the same pattern of behavior. The average concentration of hydrogen in the effluent gas was estimated at 45-50 v.%. This experiment proves that the process could be arranged for the continuous production of hydrogen-rich gas using two apparatuses: a pyrolyzer and a heater/activator.

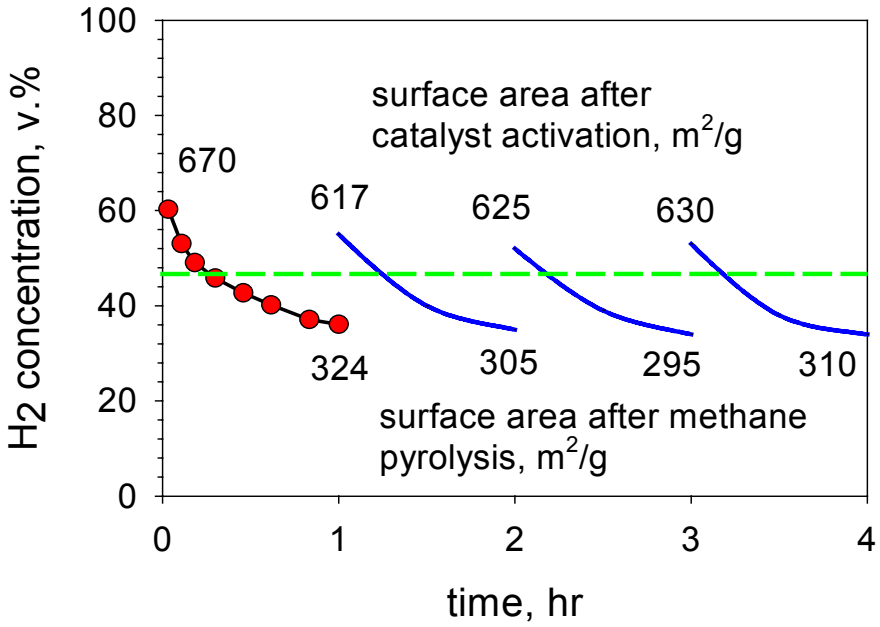

Figure 4-21. Methane Decomposition over Carbon Catalyst in Cyclic Mode: Pyrolysis-Activation. Temperature of Pyrolysis 850°C, Temperature of Steam Treatment 900°C.
X-axis shows pyrolysis time only.

We also found also that the rate of deactivation depends on the nature of carbon catalyst and hydrocarbon and the operational parameters (e.g., temperature). Particularly, it was found at higher temperatures (e.g., >850°C) the pace of catalyst deactivation in methane decomposition reaction noticeably decreases. As previously reported, activated carbon (AC) catalysts demonstrated highest initial activity among all the carbon samples tested, but also a highest rate of deactivation. In contrast, the initial rate of methane decomposition over amorphous carbons, e.g. carbon blacks (CB) and acetylene black (AB), was somewhat lower than that of AC samples, but the rate of deactivation was also slower. This phenomenon could be explained in terms of the size of carbon crystallites and their structure, which in turn are governed by the temperature and the nature of hydrocarbon.

Other factors can also contribute to the accelerating effect of water vapor on methane decomposition rate. For example, it is conceivable that active radicals can be generated on the carbon catalyst surface in the presence of such an oxidizing agent as water. These radicals are capable of attacking methane molecules at elevated temperatures with the formation of methyl radicals which initiate the chain of consecutive reactions leading to production of carbon, as shown in following chemical equations:

$$R - O^{\bullet} + CH_4 \rightarrow R - O - H + CH_3^{\bullet} \qquad (4\text{-}22)$$

$CH_3^{\bullet} \rightarrow$ olefins $\rightarrow$ aromatics $\rightarrow$ carbon (4-23)

where, R-O is, for example, carboxyl radical

This is in agreement with the results of surface analysis of carbon samples. In particular, XPS analysis of carbon samples surface before the methane pyrolysis reaction showed the presence of oxygen that disappeared after the pyrolysis.

4.6. Effect of Moisture and Sulfur on Methane Decomposition Rate

The objective of this task is to determine the effect of moisture, sulfur and other impurities present in commercial hydrocarbon fuels on the process efficiency. Potentially, these compounds can affect the catalyst activity and stability and contaminate hydrogen with reactive impurities, e.g., CO, H_2S, etc.

4.6.1. Effect of Moisture and Adsorbed Oxygen

Moisture is likely to be present in various quantities in the industrial grade (commercial) hydrocarbon fuels. We studied the effect of small amounts of water vapor on the rate of methane decomposition over the carbon catalyst (CB, BP2000). It was found that the introduction of small amounts (2.4 v.%) of water in the methane feedstock at the operational conditions of the thermocatalytic reactor (800-900^{o}C) resulted in the formation of carbon oxides (CO and CO_2). The control experiments revealed that carbon oxides are produced via reaction of steam with carbon rather than with methane (thus, the contribution of methane steam reforming into the overall process is negligible). The important observation was that the presence of small amounts of water vapor in methane noticeably reduced the rate of catalyst deactivation.

We also looked at the effect of small amounts of water and adsorbed air (oxygen) present on the surface of carbon samples on the methane decomposition rate. Activated carbon typically contains approximately 12 wt.% water, most of which was removed from the catalyst by heating to 500^{o}C. However, a heat pretreatment of carbon samples by purging with Ar at 800^{0}C for 30 minutes did not remove all oxidants (water and oxygen) from the carbon catalyst. Figure 4-22 shows the amounts of carbon monoxide (CO), hydrogen (H_2), and methane (CH_4) produced from passing pure CH_4 over AC (lignite) at 850^{0}C. It can be seen that the initial CO content is approximately 0.75 vol. %, but after 20 minutes drops to nearly 0.05 vol. %. BET surface area analysis showed that the surface area of the catalyst decreased from an initial value of 650 m^2/g to 189 m^2/g after 100 minutes. This experiment indicates that curtain amount of oxidants exist on the surface of carbon either in the form of strongly adsorbed (chemisorbed) species or oxygenated surface groups (hydroxyl, carboxyl, etc.).

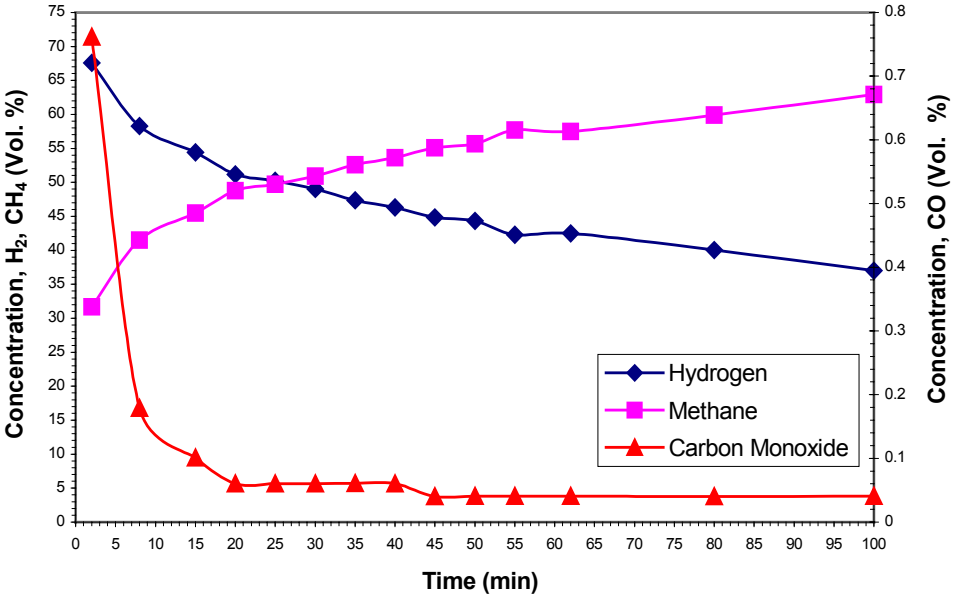

Figure 4-22. H_2, CH_4, and CO Concentrations in the CH_4 pyrolysis Gas over granulated AC (Lignite)

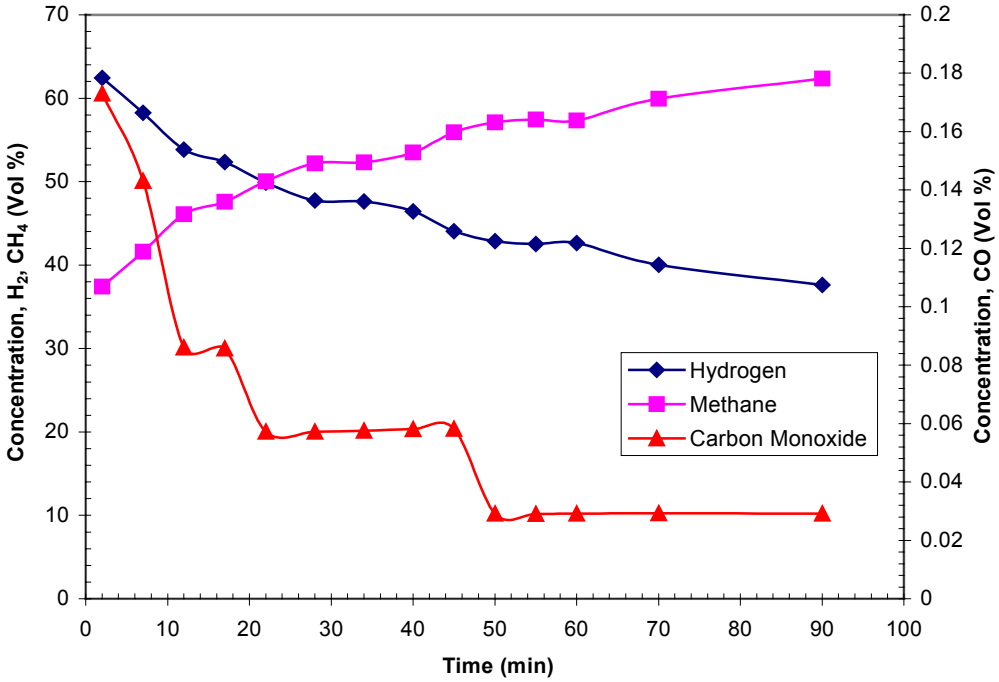

Figure 4-23. H_2, CH_4, and CO Concentrations in the CH_4 pyrolysis Gas over granulated AC (Lignite) Pretreated with Hydrogen at 900°C

In the following experiment we tried to remove strongly adsorbed oxidants in the reduced atmosphere. The fresh AC (lignite) catalyst was first treated with Ar at 800^0C for 30 minutes, followed by passing 99.99 vol. % H_2 over the sample at 900^0C for 40 minutes. Figure 4-23 shows that initial CO productions reduced from to 0.18 vol. %. After 20 minutes, CO accounted for less than 0.06 vol. % of the effluent gas. It was demonstrated that the pretreatment with H_2 did not affect the methane decomposition rate. BET surface area analysis showed that the surface area of the catalyst decreased from an initial value of 650 m^2/g to 254 m^2/g after 90 minutes.

The positive effect of water vapor on methane decomposition rate can be attributed to the increase in catalytic surface area of carbon particulates via surface steam gasification. From this point of view, the effect might be similar to that discussed in the previous section. However, other factors can also contribute to the accelerating effect of water vapor on methane decomposition reaction rate. For example, it is conceivable that active radicals can be generated on the carbon catalyst surface in the presence of such an oxidizing agent as water. These radicals are capable of attacking methane molecules at elevated temperatures with the formation of methyl radicals which initiate the chain of consecutive reactions leading to production of carbon, as shown in Figure 4-24.

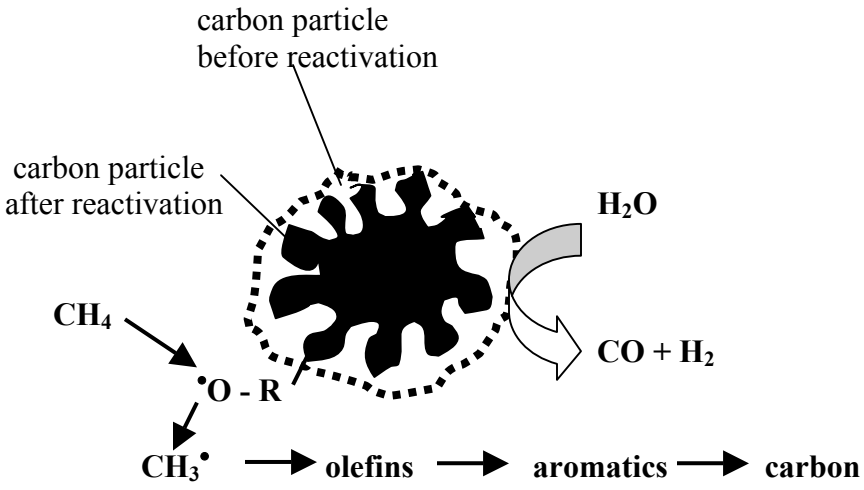

Figure 4-24. Reaction Scheme Explaining Effect of Water Vapor on Methane Decomposition Rate over Carbon Particles

The presence of CO/CO_2 impurities in hydrogen gas in many cases might be undesirable (e.g., CO even in trace quantities deactivates PEM fuel cell). Fortunately, in small quantities, carbon oxides can be efficiently removed from hydrogen via methanation reactions:

$$CO + 3H_2 \rightarrow CH_4 + H_2O \qquad \Delta H^o = -251 \text{ kJ/mole} \qquad (4\text{-}24)$$

$$CO_2 + 4H_2 \rightarrow CH_4 + 2H_2O \qquad \Delta H^o = -253 \text{ kJ/mole} \qquad (4\text{-}25)$$

These reactions occur at relatively low temperatures (300-400°C) and require the presence of Ni- or Ru-based catalysts. The experiments indicated (see Figure 4-25) that carbon oxides could be practically removed from the hydrogen-methane stream with the aid of a methanator using an alumina-supported Ru-catalyst and operating at 350°C. It can be seen that CO concentration dropped from 2500 ppmv (before) to approx. 3 ppmv (after methanator).

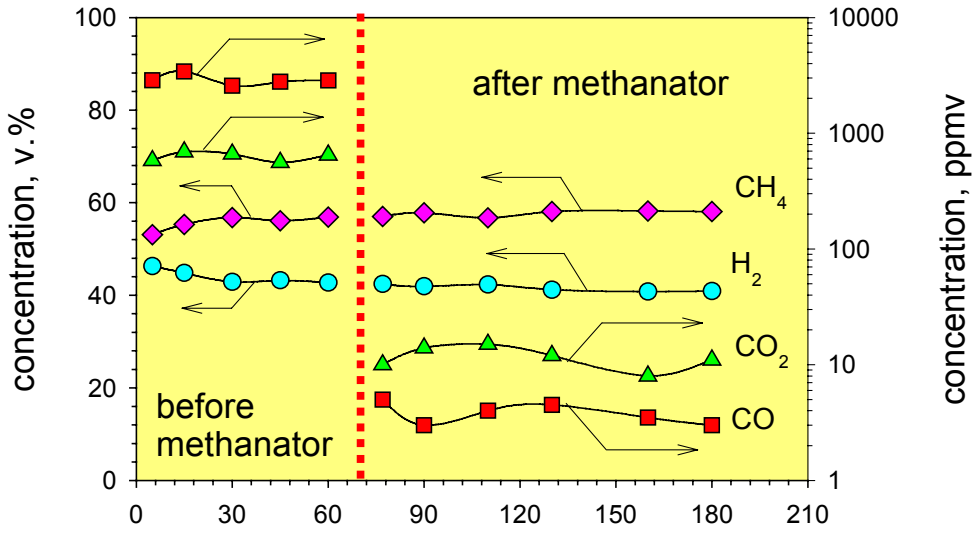

Figure 4-25. Removal of Carbon Oxides from H_2-CH_4 Stream via Methanation Reaction at 350°C in the Presence of Ru (0.5%)/Al_2O_3

4.6.2. Effect of Sulfur

It is well known that the presence of even small amounts of sulfur compounds in hydrocarbon feedstocks is detrimental for the activity of the majority of industrial catalysts (e.g., Ni-based catalysts). In most cases (e.g., steam methane reforming), an additional costly stage of feedstock desulfurization is included in the technological scheme in order to avoid rapid deactivation of metal catalysts.

We studied the effect of H_2S on the rate of methane decomposition over carbon catalysts. It was found that the presence of small amounts of H_2S in methane stream does not deactivate the carbon catalyst. The control experiments with Ar-H_2S mixtures demonstrated that H_2S is thermally decomposed over the surface of carbon catalyst (e.g., CB BP2000) at the temperature range of 850-900°C. Figure 4-26 demonstrates the effect of H_2S in the amount of 3 v.% on the rate of methane decomposition over CB(BP2000) catalyst at 870°C. It can be seen that during introduction of H_2S into methane stream the hydrogen concentration in the effluent gas increased

by approx. 2-3 v.% which can be attributed to the contribution of hydrogen produced by thermal decomposition of H_2S.

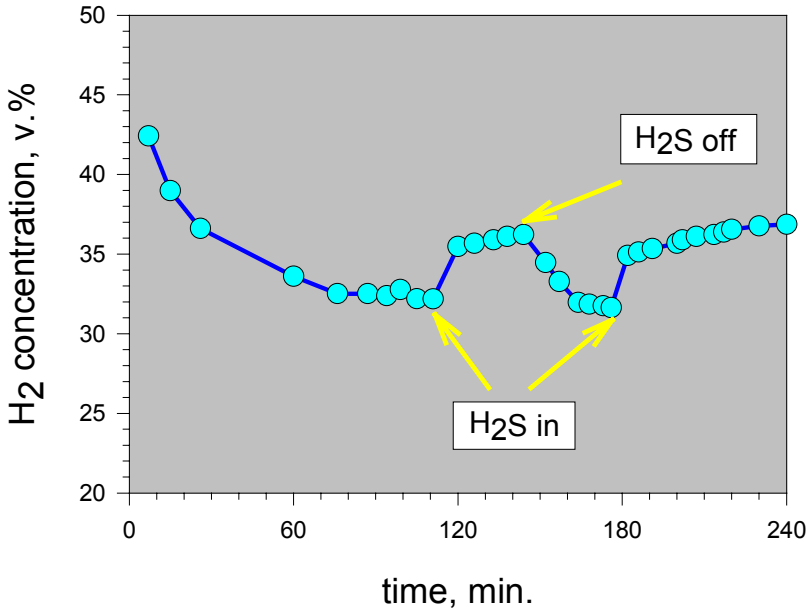

Figure 4-26. Effect of H_2S on Methane Decomposition over CB (BP2000). [H_2S]= 3 v.%, T= 870°C

It is also evident that in the presence of H_2S methane decomposition rate slightly increases which points to a possible accelerating effect of H_2S on methane decomposition reaction. An effect of H_2S on methane decomposition can tentatively be explained in terms of intermediate formation of relatively active $HS^{\bullet}$-radicals which attack methane molecules at elevated temperatures. The following reaction scheme explains the probable role of H_2S:

$$H_2S \rightarrow HS^{\bullet} + H^{\bullet} \qquad (4\text{-}26)$$

$$nHS^{\bullet} \rightarrow S_n + n/2H_2 \qquad (4\text{-}27)$$

$$CH_4 + HS^{\bullet} \rightarrow {}^{\bullet}CH_3 + H_2S \qquad (4\text{-}28)$$

Elemental sulfur (S_n) vapors exit the reactor and condense in a sulfur trap. Unconverted H_2S could be removed from the hydrogen stream by several of-the-shelf technologies, e.g., MEA scrubbing or ZnO polishing:

$$ZnO + H_2S \rightarrow ZnS + H_2O \qquad (4\text{-}29)$$

5. THERMOCATALYTIC REACTOR DEVELOPMENT

The objective of this work was to conduct studies on various conceptual designs for the thermocatalytic reactor for hydrocarbon decomposition. The reactors were designed, fabricated and tested for the simultaneous production of hydrogen and carbon using methane, propane and gasoline as feedstocks.

5 different types of reactors for hydrocarbon decomposition were considered:

- packed bed reactor (PBR)
- tubular reactor (TR)
- free volume reactor (FVR)
- fluid wall reactor (FWR)
- fluidized bed reactor (FBR)

5.1. Packed Bed Reactor

PBR was mainly used for carbon catalysts screening, and studies on the effect of operational parameters (temperature, space velocity) on hydrogen yield, and kinetic measurements. Several examples of PBR test runs are presented in the Table 5-1. In some cases, it was difficult to conduct long run experiments with PBR due to carbon build up within the reactor and potential reactor clogging. It is apparent that the continuous removal of carbon from PBR would be a daunting technical problem, therefore, this type of the reactor is unlikely to be used in large scale hydrogen production units.

5.2. Tubular Reactor

We have conducted a series of experiments on fast pyrolysis of methane using ceramic (alumina) and quartz tubular reactors. The objective was to thermally (homogeneously) decompose methane to hydrogen, carbon and valuable unsaturated and aromatic hydrocarbons. Preliminary testing of the catalytic activity of quartz and alumina toward methane decomposition reaction proved their inertness at temperatures below 1100^{o}C. The tubular reactors with the internal diameters of 3-6 mm and a small reaction zone enabling to achieve the residence times in the range of 1-20 milliseconds, were used in these experiments. Preheated (400^{o}C) methane streams entered the reactor at flow rates in the range of 1-10 l/min and were subjected to pyrolysis at the temperatures of 900-1100^{o}C. The conversion of methane was found to be a function of the temperature and residence time. For example, at the reaction zone temperature of 1100^{o}C and residence times of 1.0, 2.0 and 6.2 ms, methane conversions were 0.1, 2.0 and 16.1%, respectively. Hydrogen and carbon were the main products of pyrolysis accounting for more than 80 w.% of the products. Unsaturated (mostly, C_2) and aromatic (including polynuclear) hydrocarbons were also produced in significant quantities as byproducts of methane pyrolysis. For example, at the reaction zone temperature of 1100^{o}C and the residence time of 6.2 ms the yields of gaseous and liquid products were as follows (mol.%): C_2H_6- 0.9, C_2H_4- 3.3, C_2H_2- 5.8, C_2-C_6- 1.5, polynuclear aromatics (naphthalene, anthracene)- 2.0. Unidentified liquid products of pyrolysis accounted for approximately 5 w.% of methane pyrolysis products. Carbon (coke) was mostly deposited on the reactor wall down-stream of the reaction zone, which indicated that

methane decomposition reaction occurred predominantly homogeneously in gas phase. At higher residence times (seconds and minutes scale), the yields of C_2^+ and polyaromatic hydrocarbons dramatically dropped. These experiments demonstrated that methane decomposition process could be arranged in a homogeneous mode producing not only hydrogen and carbon, but also a variety of very valuable hydrocarbons (ethylene, acetylene, aromatics).

The mechanism of thermal decomposition (pyrolysis) of methane has been extensively studied [24]. Since C - H bonds in methane molecule are significantly stronger than C - H and C - C bonds of the products, secondary and tertiary reactions contribute at the very early stages of the reaction, which obscure the initial processes. It has been shown [24] that the homogeneous dissociation of methane is the only primary source of free radicals and controls the rate of the overall process:

$$CH_4 \rightarrow CH_3^{\bullet} + H^{\bullet} \qquad (5\text{–}1)$$

This reaction is followed by a series of consecutive and parallel reactions with much lower activation energies. After the formation of acetylene (C_2H_2), a sequence of very fast reactions occurs leading to the production of higher unsaturated and aromatic hydrocarbons and finally carbon:

$$C_2H_2 \rightarrow \text{aromatics} \rightarrow \text{polynuclear aromatics} \rightarrow \text{carbon} \qquad (5\text{-}2)$$

This involves simultaneous decomposition and polymerization processes and phase changes from gas to liquid to solid. A detailed mechanism of the final transformations to carbon is rather complex and is not well understood.

These experiments demonstrated that TR could potentially be scaled up for the use in full-scale methane decomposition process, although, it would require the elevated temperatures (above 1000^{o}C) and special surface-treated tubes to prevent carbon deposition in the reaction zone.

5.3. Free Volume Reactor

Free volume reactor is designed to carry out high temperature reactions by contacting a reagent gas with a stream of preheated carrier gas. FVR could be advantageous for the conducting of different dissociation reactions with formation of solid phase products, including methane decomposition reaction. In our work we designed and tested FVR for a continuous production of hydrogen and carbon via methane decomposition. Methane decomposition occurred homogeneously by contacting a hot carrier gas such that carbon was produced in a free volume of the reactor and carried away by the gaseous stream, thus preventing carbon from deposition on the reactor wall. Two options for introducing thermal energy into the reaction zone were considered: by the stream of inert gas (Ar) or hydrogen. Figure 5-1 shows the schematic diagram of FVR used for decomposition of methane and propane. Methane was introduced into the reactor through the inner ceramic tube, and the heat carrier gas entered the space between the inner and outer (quartz) tubes of FVR. We used Ar or hydrogen as heat carrier gases in a ratio 4:1 (by volume) to methane. The heat carrier gas was heated by the electric heater to 1200-

1300°C and entered the reaction zone where it contacted the preheated stream of methane. The results of the FWR testing using hydrogen as a carrier gas are presented in the Table 5-1.

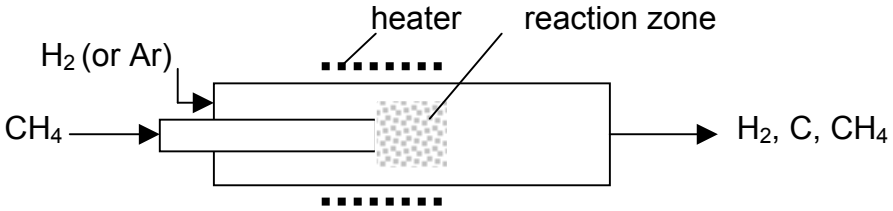

Figure 5-1. Schematic Diagram of Free Volume Reactor

There were some carbon deposits around and, especially, downstream of the reaction zone, which indicated that some portion of methane contacted the hot surface of the outer wall due to a mixing of gases in the reaction zone. This could be prevented if the temperature of a heat carrier gas was higher than that of the wall in the reaction zone. The use of an inert gas as a heat carrier requires a subsequent gas separation stage, which would add to the cost of hydrogen. On the other hand, the use of hydrogen would somewhat reduce the net hydrogen yield.

5.4. Fluid Wall Reactor

The objective of FWR is to carry out the high temperature hydrocarbon decomposition reactions in the layer of a carrier gas heated to the required temperature, thus preventing carbon from deposition on the reactor wall. This can be done by passing a preheated inert gas (or hydrogen) through the porous tubing (which acts as an internal reactor wall) such that it thermally decomposes methane in the reaction zone and carries away produced carbon. Simplified schematic diagram of the FWR is shown on Figure 5-2.

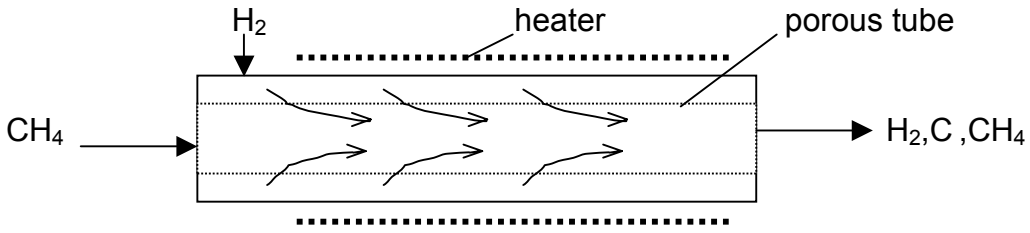

Figure 5-2. Schematic Diagram of Fluid Wall Reactor

We conducted methane decomposition test runs using small size FWR. A flow of hydrogen at positive pressure was introduced into annulus between outer tube (quartz) and the internal porous ceramic tube, and a flow of methane at the atmospheric pressure was introduced into the inner ceramic tube at H_2/CH_4 ratio of 1:3. The outer wall of the reactor was heated by the electric heater to 1100-1300^{o}C. A stream of heated hydrogen permeated through the porous ceramic tube and entered the reaction zone where it contacted a preheated stream of methane. A mixture of hydrogen and unconverted methane after the reactor was metered and analyzed by GC method. Methane conversion was about 10-15%. Carbon was collected in the down stream trap. More experiments will be conducted to optimize the yield of products. These proof-of-concept experiments demonstrated that FWR could potentially be suitable for medium and large scale units for the simultaneous production of hydrogen and carbon from NG and other hydrocarbons.

5.5. Spouted bed reactor

In a spouted bed reactor (SPR) hydrocarbon feedstock enters from the small nozzle at the base of the catalytic bed at high velocity, creating a central dilute phase core (Figure 5-3). The carbon particulates rise inside the core forming a fountain. Hydrocarbon flows mainly inside the core, although some percentage of the flow might be distributed to the peripheral annular region (annulus). We fabricated a small size SBR and tested it for methane decomposition in the presence of carbon black (BP-2000) at the temperature range of 800-1000^{o}C.

Before the actual methane decomposition experiments we ran "cold" experiments to visually determine the optimum gas velocity for carbon particles spouting. It was found that an adequate spouting of carbon black particles by the stream of methane could be achieved at the superficial gas velocity of 2 cm/s and a bed depth to a reactor diameter ratio of 5-6. At higher values of superficial gas velocities and depth to diameter ratios we observed a non-homogeneous fluidization of carbon particles. Applying the above conditions to the methane decomposition experiments (at 900^{o}C) we observed fairly poor conversion of methane (7%). This could be attributed to very short contact time between carbon particles and hydrocarbon within the spouting region. The contact time in the spout was estimated by calculating mean spout diameter according to the following equation [25]:

$$D_s = \frac{0.118 G^{0.48} D_c^{\,0.68}}{\rho_b^{\,0.41}} \qquad (5\text{-}3)$$

where: D_s is a spout diameter (cm), G- methane mass flow rate per unit of reactor cross section (g/sec-cm^2), D_c-reactor diameter (cm), ρ_b- carbon bulk density (g/cm^3)

The calculation yielded the residence time of approximately 0.1 s within the spouting region. Although intense turbulence makes for high coefficients of heat and mass transfer, the effect would be minimal due to very small residence time in the reaction zone (which would be very difficult to control). Thus, very short contact times intrinsic in the operation of SBRs could result in relatively low methane conversion rates. It should be noted that due to inequality of

contact times in the spout and annulus of the SBR the extent of the reaction taking place in these regions would be also unequal, which might present a problem with modeling the reactor.

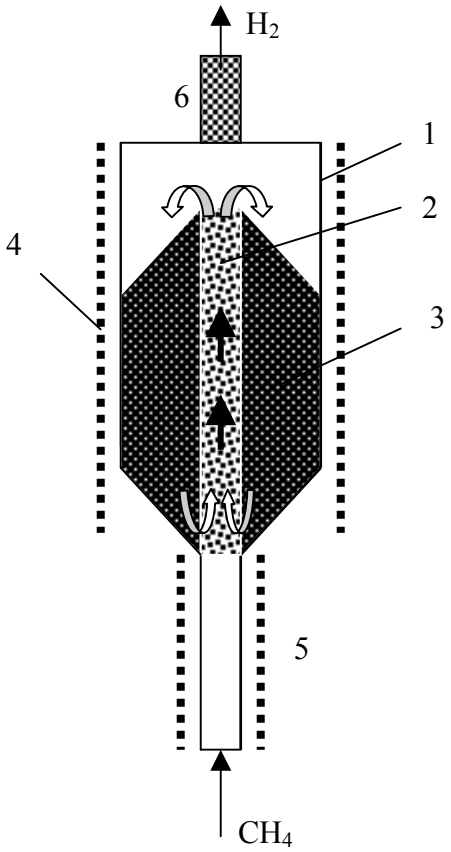

Figure 5-3. Spouted Bed Reactor

1- external wall of the reactor
2- spouting zone
3- catalyst
4-electric heater
5- pre-heater
6- filter

Another potential problem is associated with the size of carbon particles. According to [24], the minimum particle diameter for which spouting appears to be practical is about 1 mm, which by far exceeds the expected range of carbon particle sizes in our process (estimated at 10-100 microns). These considerations weigh heavily against the use of SBR for NG decomposition in a large-scale units.

5.6. Fluidized Bed Reactor

Fluidized bed reactors (FBR) are widely used in chemical, metallurgical and petroleum industries. A fluidized bed system does provide constant flow of solids through the reaction zone, which makes it particularly suitable for the continuous addition and withdrawal of carbon particles from the reactor (similar to fluid catalytic cracking process). In FBR the bed of fine carbon particles behaves as a well-mixed body of liquid giving rise to high particle-to-gas heat and mass transfer rates. During fluidization, carbon particles are allowed to spend a certain time in the reaction zone, which could be easily controlled by adjusting the ratio between the feed rate and the weight of the bed. The bed could also buffer any instabilities which arise during continuous operation.

FBR could be particularly suitable for hydrocarbon decomposition process since it allows to continuously remove carbon from the reactor, similar to fluid catalytic cracking processes. A schematic diagram of FBR used in our experiments is shown in Figure 5-4.

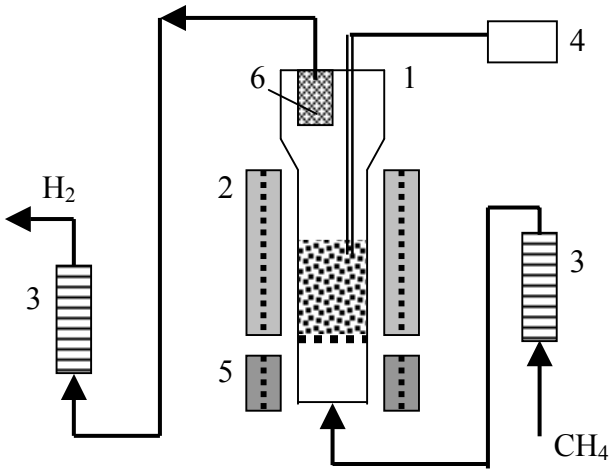

Figure 5-4. Fluidized Bed Reactor

1- fluidized bed reactor
2- electric heater
3- flow meter
4- temperature controller
5- pre-heater
6- filter

Preheated to 400°C a stream of methane (or propane, or methane-propane mixture) entered the FBR from the bottom, and contacted with the fluidized bed of carbon particles (carbon black BP-2000) at 800-950°C in the reaction zone, where pyrolysis of hydrocarbons occurred. Methane minimum flow rate necessary for fluidization of carbon particles was found from the following equation [26]:

$$G = \frac{0.005 d_p{}^2 \varepsilon^3 (\rho_p - \rho_f) \rho_f g}{\psi^2 (1-\varepsilon) \mu} \qquad (5\text{-}4)$$

where: G is the mass flow rate necessary to initiate fluidization, d_p – diameter of the particle (cm), ε- fraction voids, ρ_p- density of particle (g/cm^3), ρ_f- density of methane (g/cm^3), g- acceleration gravity (cm/s^2), ψ- shape factor, μ- viscosity (g/cm.s)

The flow of hydrogen-containing gas exited from the top of the reactor through a ceramic filter and was directed to a gas chromatograph.

FBR reactor was tested using methane, propane, methane-propane mixtures, gasoline vapor and gasoline-methane mixture as feedstocks (Figures 5-5 through 5-7). Because of relatively short residence times (approx. 1 s) in the reaction zone methane decomposition yields were relatively low, whereas, propane and gasoline were almost quantitatively converted into hydrogen-rich gas

using FBR. Figure 5-6 depicts the experimental results of propane and gasoline vapor pyrolysis over CB (BP-2000) catalyst at 850°C using FBR.

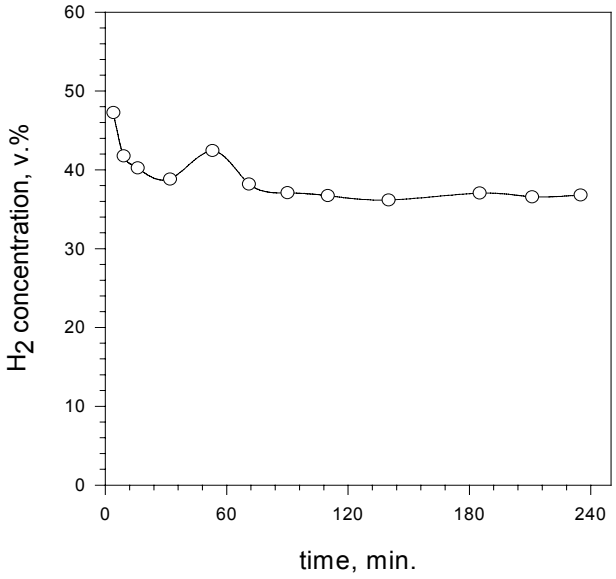

Figure 5-5. Catalytic Decomposition of CH_4 over CB BP2000 at 950°C

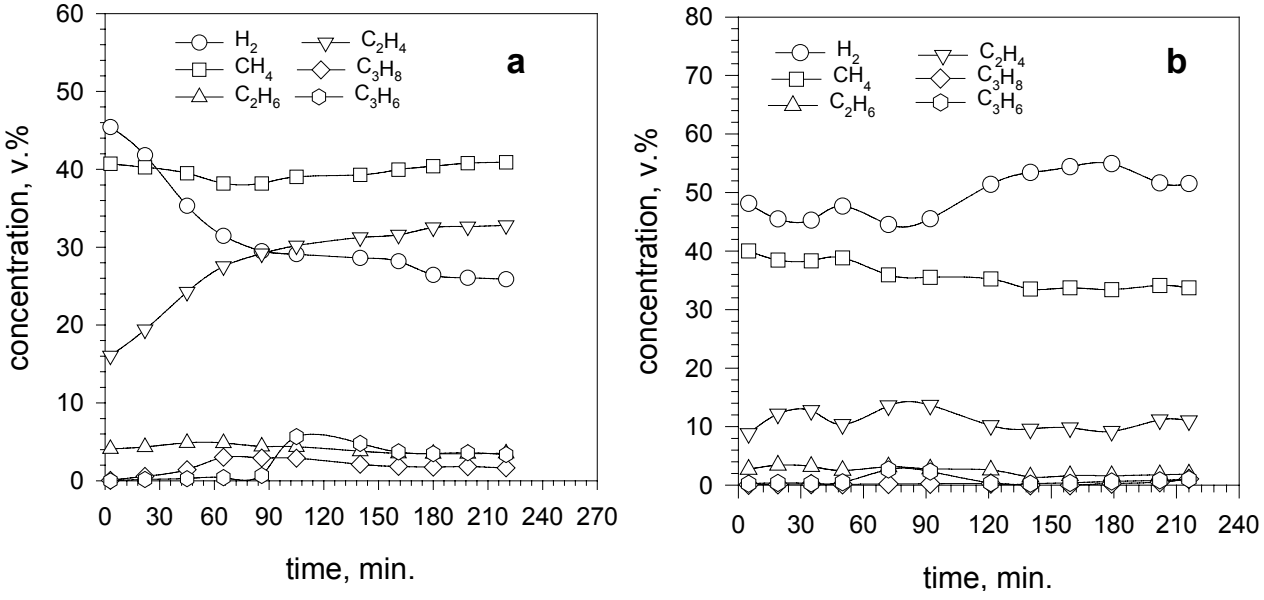

Figure 5-6. Thermocatalytic Pyrolysis of Propane (a) and Gasoline (b) over CB (BP-2000) at 850°C Using FBR

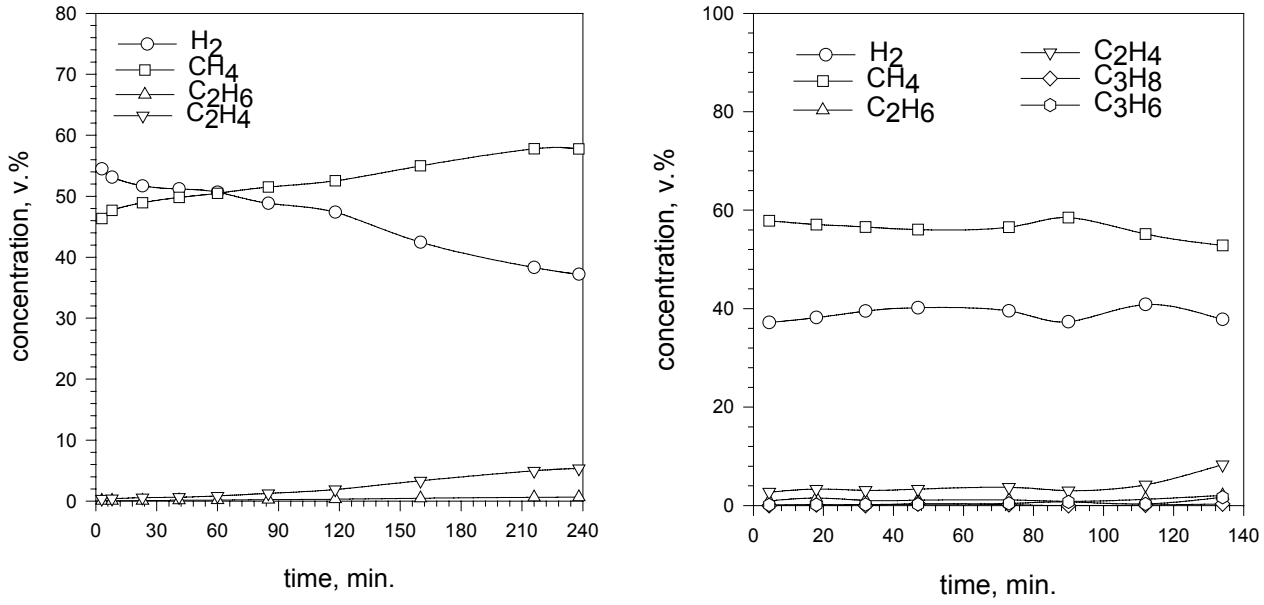

Figure 5-7. Catalytic Pyrolysis of Hydrocarbon Mixtures over BP-2000 Using Fluidized Bed Reactor: CH_4-C_3H_8 (3:1), 20 ml/min, 950°C (left) CH_4 (5 ml/min) – gasoline (1.25 ml/h), 850°C (right)

It is noteworthy that pyrolysis of propane and gasoline in FBR produce more C_2^+ byproducts comparing to PBR. Thermocatalytic pyrolysis of gasoline over CB catalyst lasted more than 3.5 hours during which the gaseous mixture with the average hydrogen concentration of 50 v.% was produced.

Figure 5-7 depict the results of pyrolysis of methane-propane and methane-gasoline mixtures over carbon black BP-2000 at 950 and 850°C, respectively, using fluidized bed reactor. The hydrogen concentration in the effluent gas was in the range of 40-50 v.%. Figures 5-8 depicts the kinetic curves of decomposition of methane, propane and their mixtures (3:1 by volume) over CB catalyst at 850 and 950°C. Propane was almost quantitatively converted into hydrogen-rich gas, whereas, methane decomposition yields were somewhat lower. The propane pyrolysis gas was rich with ethylene and other heavier hydrocarbons. Thus, the experimental results indicated that the gas with the hydrogen concentration in the range of 40-50 v.% could be produced from methane and methane-propane mixtures in a quasi-steady state regime using fluidized bed of BP-2000 particles.

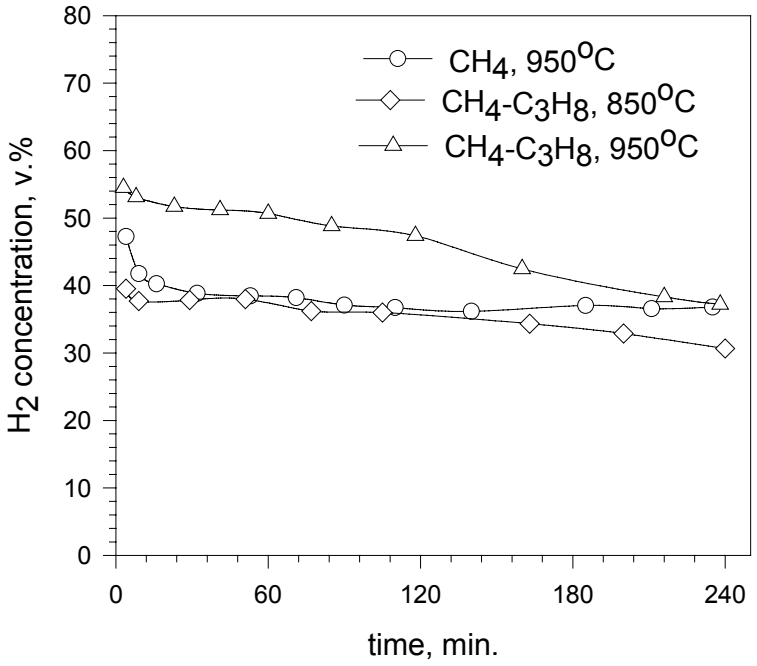

Figure 5-8. Methane and Methane-Propane Decomposition over CB (BP2000) Using Fluidized Bed Reactor

It can be seen from the Figure 5-8, that after 1.5-2 hours hydrocarbon decomposition rates started to drop, which could be explained by the decrease in the catalytic surface area. Indeed, at the end of experiment we observed the accumulation of coarse (0.1-1 mm in diameter) carbon particles in the bottom section of the reaction zone.

5.7. Comparative Assessment of Different Reactors for Hydrocarbon Decomposition

The results of testing of different thermocatalytic reactors for decomposition/pyrolysis of methane, propane and gasoline using carbon catalysts are presented in Table 5-1. Note that the data on the hydrocarbon conversion and the effluent gas composition relate to the average quasi-steady state values.

Table 5-1. Thermocatalytic Reactor Test Results

Hydro-carbon	Catalyst	**Rea-ctor**	T°C	Conver-sion, %	**Gaseous Products, v.%**					
					H_2	CH_4	C_2H_6	C_2H_4 (C_2H_2)	ΣC_3	C_4^+
Methane	CB, BP-2000	PBR	950	30.9	47.2	52.7	0	0.1	0	0
Methane	Acetylene Black	PBR	850	23.3	37.8	61.9	0.1	0.2	0	0
Methane	CB, XC-72	PBR	850	28.0	43.7	56.2	0	0.1	0	0
Methane	CB, BP-2000	FBR	850	9.1	16.7	83.1	0	0.2	0	0
Methane	-	TR	1200	53.8	63.8	27.4	0.1	1.2 (7.5)	0	0
CH_4/H_2 (1:4)	-	FVR	1200		89.3	10.7	0	0	0	0
CH_4/C_3H_8 (3:1)	CB, BP-2000	FBR	850	38.2	50.1	2.1	9.0	0.6	0	
CH_4/C_2H_4 (3:1)	CB, BP-2000	FBR	850		36.2	53.9	2.0	7.9	0	0
Propane	AC, KE	PBR	800	100.0	88.3	11.7	0	0	0	0
Propane	Acetylene Black	PBR	850	100.0	62.1	37.9	0	0	0	0
Propane	CB, BP-2000	FBR	850	98.0	27.0	39.5	1.5	29.4	2.6	0
Gasoline	AC, KE	PBR	800	100.0	49.4	37.6	2.1	9.8	0.6	0.5
Gasoline	CB, BP-2000	FBR	850	100.0	52.0	33.2	2.1	11.1	0.7	0.9
CH_4 /gasoline	CB, BP-2000	FBR	850		40.0	55.5	0.3	3.0	0.5	0.7

AC-activated carbon
CB-carbon black
BP-Black Pearls

5.8. Fabrication and Testing of 1 kW Thermocatalytic Reactor

5.8.1. Description of Experimental Set-up

A bench-scale thermocatalytic reactor (TCR) for CO/CO_2-free production of hydrogen-rich gases was designed, fabricated and tested at the Florida Solar Energy Center. The TCR employed a carbon-based catalyst; its design is proprietary (a U.S. Patent Application No. 60/203370 has been filed before U.S. PTO). Figure 5-9 depicts a simplified schematic diagram of the experimental set-up for testing TCR coupled with PEM fuel cell. The set-up consists of a TCR, a series of flow meters (rotameters) for measuring flow rates of a hydrocarbon feedstock (or fuel gas), an inert gas (Ar) and air, a series of valves, a PEM fuel cell, and a testing and analytical (GC) equipment. The photo of the experimental set-up assembled at FSEC is shown in Figure 5-10. The flow rate of hydrocarbon gas (methane or propane) varied in the range of 0.5-5 l/min. Ar was used to purge a reactor and PEM fuel cell before introducing a fuel gas. The temperature in the TCR was maintained at 800-900^{o}C, at the atmospheric pressure.

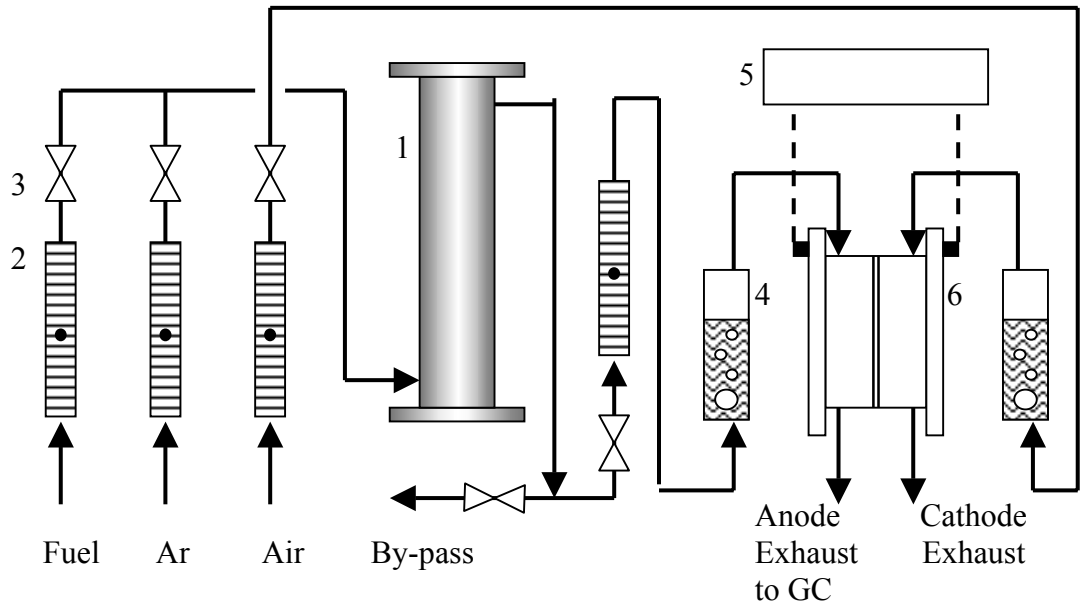

Figure 5-9. Schematic Diagram of the Experimental Set-up with TCR and PEM Fuel Cell. TCR, 2- Flow meters, 3- Valves, 4- Humidifiers, 5- Electrical load with meters, 6- PEM fuel cell

A flow of hydrocarbon gas (e.g., methane or propane) enters TCR from the bottom section and is decomposed over the surface of a carbon-based catalyst producing hydrogen-rich gas which exits TCR via a ceramic filter. The concentration of hydrogen in the hydrogen-containing gas (HCG) depends on the feedstock, the reactor temperature and the residence time. Propane

Figure 5-10. Experimental Set-up with TCR, PEM Fuel Cell, Fuel Tank and Testing Equipment

produces HCG with the concentration of hydrogen up to 70-80 v.%, the balance being methane and traces of C_2+ (depending on the flow rate). In case of methane, hydrogen content of the pyrolysis gas was somewhat lower (40-60 v.%, the balance-unconverted methane). No carbon oxides were detected in the pyrolysis gases. Since hydrogen gas was free of carbon monoxide (CO) and other reactive impurities, it could be directly fed to a PEM fuel cell.

The results of the hydrogen generator testing (without connecting it to a fuel cell) are presented in Figure 5-11. In the first series of experiments propane was introduced into the hydrogen

generator at different flow rates. Figure 5-11 (left) demonstrates the distribution of propane pyrolysis products as a function of the effluent gas flow rate. Hydrogen concentration in the pyrolysis gas reached almost 80 v.% at lower flow rates, and it dropped to approximately 70 v.% as the effluent gas flow rate increased from 1.2 to 5.1 L/min. The balance was methane with the traces of ethane. No appreciable amounts of carbon oxides or other reactive gases were detected in the pyrolysis gas.

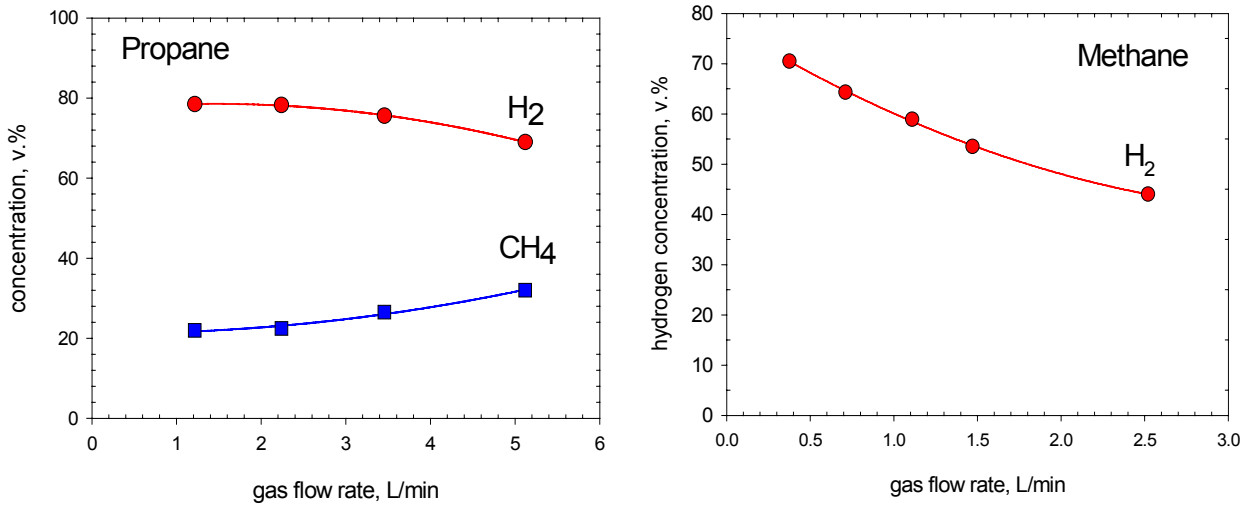

Figure 5-11. Production of Hydrogen-rich Gas from Propane (left) and Methane (right) Using 1 kW Thermocatalytic Reactor

As expected, methane produced the gas with somewhat lower concentration of hydrogen (Figure 16, right). At low flow rates the concentration of hydrogen in methane decomposition gas was 70 v.%, however, it dropped to 45 v.% at high flow rates (2.5 L/min) of the effluent gas. Again, no carbon oxides were detected in the gaseous stream exiting the hydrogen generator.

5.8.2. Testing of TCR Coupled with PEM Fuel Cell

A single cell PEM fuel cell was used in this series of experiments. Since the power range of the PEM fuel cell was much lower compared to the output of TCR, only a small portion of the TCR effluent gas (in the range of 100-500 mL/min) was directed to an anode compartment of PEM fuel cell (via a bubble humidifier). A flow of air (0.5-2.5 L/min) was introduced into the cathode compartment of the fuel cell. PEM fuel cell and both humidifiers were maintained at 80^{o}C. The exhaust gases from anode and cathode compartments of PEM fuel cell passed through condensers, where most of the moisture was condensed, and the flow rates of both exhaust gases were measured. The anode exhaust gas was directed to a GC analyzer where H_2 concentration was quantified. PEM fuel cell electrodes were connected to an electrical resistance load equipped with the meters for measuring cell potential and electrical current. The cell potential *vs* current curves were plotted for the TCR-produced hydrogen-containing gases with the average hydrogen concentrations of 43, 60 and 79 v.% (balance- methane) (Figure 5-12).

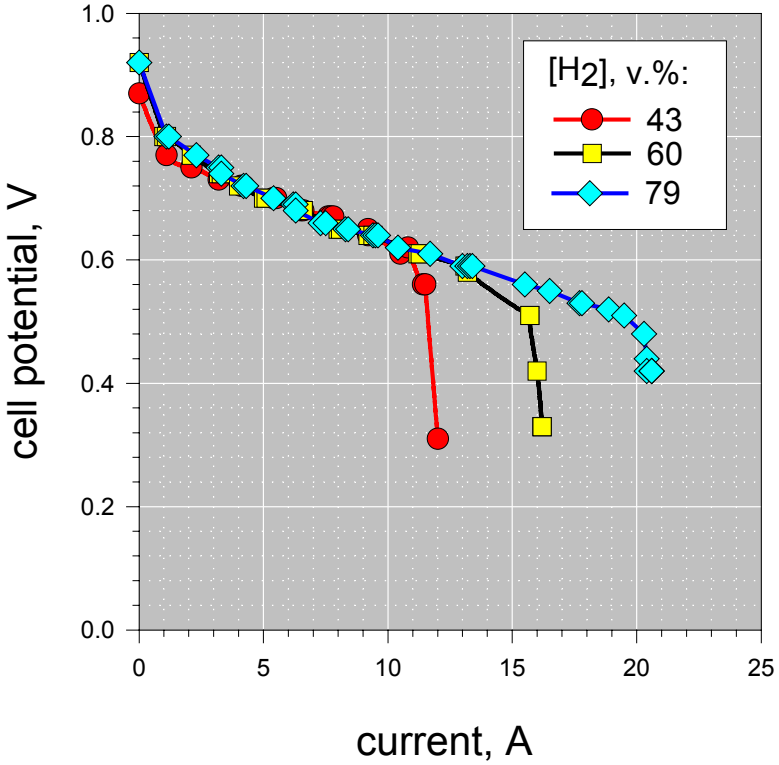

Figure 5-12. Testing of TCR Coupled with PEM Fuel Cell (Single Cell). Cell potential *vs* current curves for PEM fuel cell

The plots "cell potential vs current" are typical of PEM fuel cell curves with activation, ohmic and concentration polarization regions. It can be seen that the dissimilarity in the behavior of different *i-v* plots showed up most vividly in the concentration polarization region.

We also monitored the concentrations of hydrogen in the fuel cell anode exhaust gas (Figure 5-13). It was demonstrated that the rate of hydrogen consumption in PEM fuel cell was a function of hydrogen concentration in the pyrolyzate gas and the fuel gas throughput. At low feed flowrates (e.g., 100-200 mL/min) almost all the hydrogen was consumed in the fuel cell, regardless of the original hydrogen concentration in the feed gas. At relatively high flowrates (e.g., 500 mL/min), however, a significant portion (almost half) of hydrogen exited the anode compartment of the fuel cell unconverted. The presence of methane in the feed gas in the whole range of its concentrations (20-60 v.%) did not adversely affect the performance of the fuel cell.

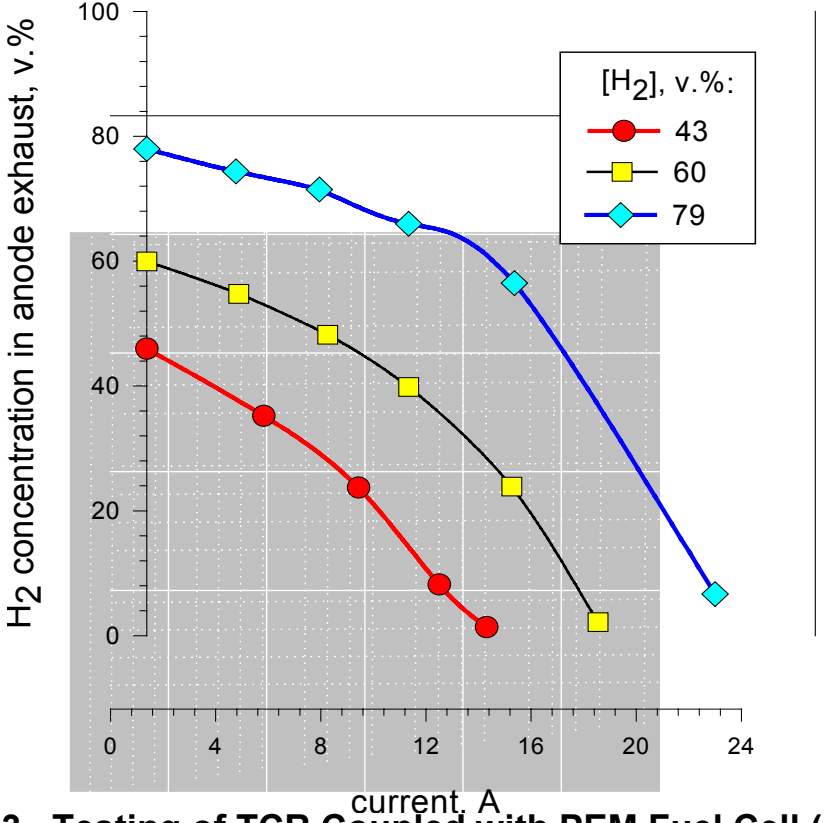

Figure 5-13. Testing of TCR Coupled with PEM Fuel Cell (Single Cell). The Effect of Electrical Load on H_2 Concentration in the Anode Exhaust Gas

In summary, the experimental results indicated that hydrogen-methane mixtures of different ratios can be used as fuels for PEM fuel cell. The curves "voltage vs current" are typical of PEM fuel cell "S"-shape curves with activation, ohmic and concentration polarization regions. The concentration of hydrogen in hydrogen-containing gas (HCG) in the range of 40-100 v.% does not noticeably affect the PEM cell potential, however, it greatly influences the current: higher H_2 concentration, the higher is the current. It was found also that the concentration of hydrogen in the anode exhaust gas is a function of the fuel gas flow rate and H_2 concentration in the fuel gas. For example, at relatively low flow rates of HCG hydrogen concentration in the exhaust gas could drop almost to zero (the balance methane). The same is true for the flow rate of the anode exhaust gas: it significantly drops at low inlet flow rate and low initial hydrogen concentration in HCG. Humidification of hydrogen fuel gas and air significantly improves the performance of the PEM fuel cell.

5.9. Testing of 3 kW Thermocatalytic Reactor Using Commercial Hydrocarbon Fuels

5.9.1. Results of Testing of 3 kW TCR

We designed and fabricated 3 kW thermocatalytic reactor (TCR) (see Figure 5-14). To eliminate the effect of the reactor material on the methane decomposition rate the reactor was made of mullite ($3Al_2O_3$-$2SiO_2$) that can withstand temperatures up to 1700°C. The outside diameter of the TCR is 2 inches. The reactor was heated externally and internally using type K thermocouples and Dwyer temperature controller with the data acquisition system. The reactor temperature was maintained at 850°C and atmospheric pressure.

Figure 5-14. Experimental Set-up with 3 kW Thermocatalytic Reactor

We tested 3 kW thermocatalytic reactor (TCR) using pipeline natural gas and commercial propane as feedstocks. Tables 5-2 and 5-3 show the composition of pipeline natural gas and commercial propane, respectively.

Table 5-2. Composition of Pipeline Natural Gas Used in the Experiments

Components	N_2	CH_4	C_2H_6	C_3H_8	C_4+	CO_2	CH_3SH
Volume, %	0.9	93.1	4.1	0.7	0.3	0.9	4 ppm

Table 5-3. Composition of Commercial Propane

Components	N_2	CH_4	C_2H_6	C_3H_8	C_4+	CO_2
Volume, %	0.5	0.2	5.9	93.1	0.2	0.1

A flow of preheated hydrocarbon gas (e.g., methane or propane) enters TCR from the bottom section and is decomposed over the surface of a carbon-based catalyst producing hydrogen-rich gas which exits TCR via a ceramic filter. The concentration of hydrogen in the hydrogen-containing gas (HCG) depends on the feedstock, the reactor temperature and the residence time.

Propane produces HCG with the concentration of hydrogen up to 70 v.%, the balance being methane and traces of C_2+ (depending on the flow rate). In case of methane, hydrogen content of the pyrolysis gas was somewhat lower (40-50 v.%, the balance-unconverted methane).

The composition of the effluent gas of catalytic pyrolysis of natural gas and propane is presented in Table 5-4.

Table 5-4. Composition of Hydrogen-rich Gas Produced from Commercial Hydrocarbon Fuels

Feedstock	Composition of gaseous products, v.%					
	H_2	CH_4	C_2H_6	C_2H_4	CO	CO_2
Pipeline Natural Gas	45.5	53.6	0.0	0.0	0.7	0.1
Commercial Propane	61.8	30.4	2.1	5.1	0.1	0.0

5.9.2. Gas Conditioning

In this task we improved the purity of hydrogen gas by removing reactive contaminants such as unsaturated hydrocarbons (olefins). Olefins (particularly, ethylene) are minor side products of methane and, especially, propane decomposition reactions. Ethylene could potentially deactivate the catalytic components of fuel cells. The purification can be accomplished by means of low-temperature catalytic hydrogenation reactions that converted the potentially harmful impurities into benign products. Particularly, we found that ethylene in the amount of 2-10 v.% in H_2-CH_4 gaseous mixtures (4:1 by volume) was quantitatively converted into ethane in the presence of Ni/Al_2O_3 catalyst (obtained from ICI Catalco) according to the following equation:

$$C_2H_4 + H_2 \rightarrow C_2H_6 \qquad (5\text{-}5)$$

The optimal temperature range for the reaction was found to be 120-220^{o}C. At higher temperatures the contribution of undesirable side reactions of ethylene decomposition was significant:

$$C_2H_4 \rightarrow 2C + 2H_2 \qquad (5\text{-}6)$$

The similar effect was achieved with the hydrogenation of other unsaturated hydrocarbons, e.g., propylene.

5.9.3. Effect of Impurities in Commercial Hydrocarbon Fuels

The presence of the traces of oxidants (e.g., air and moisture) commonly present in industrial hydrocarbon fuels may potentially result in contamination of hydrogen with carbon oxides (CO and CO_2). The presence of CO/CO_2 impurities in hydrogen gas in many cases might be undesirable (e.g., CO even in trace quantities deactivates PEM fuel cell). It was found that the presence of small amounts of moisture in the methane stream not only wasn't detrimental to the catalyst activity, but it actually improved the process sustainability. For example, in the presence of 2.4 v.% of water vapor in the feedstock the methane decomposition rate remained at 35 mmol/min-g level for almost 9 hours, whereas, it dropped to 18 mmol/min-g when moisture-free methane was used in the experiment. It should be noted, however, that the presence of moisture in the feedstock resulted in the contamination of hydrogen with small amounts (< 1 v.%) of carbon oxides produced, most likely, via steam gasification of carbon at the elevated temperatures (850^{o}C) of the process.

The Table 5-5 demonstrates the effect of moisture on the composition of the pyrolysis gas produced by decomposition of methane over a number of carbon catalysts.

Table 5-5. Effect of Moisture on the Composition of Pyrolysis Gas Produced by Decomposition of Methane at 850^{o}C

Carbon catalyst	[H_2O], v.%	Composition of gaseous products, vol.%			
		H_2	CH_4	CO	CO_2
AC (lignite)	0	36.1	63.9	0	0
AC (lignite)	2.2	39.7	59.7	0.6	0
AC (petroleum coke)	2.2	40.2	59.5	0.3	0
Carbon Black (BP2000)	2.4	42.1	57.7	0.1	0.1
After methanation	2.4	42.1	57.9	5 ppm	9 ppm

We conducted a series of experiments on the removal of small quantities of carbon oxides from hydrogen gas via methanation reactions. The experiments indicated that carbon oxides could be practically removed from the hydrogen-methane stream with the aid of a methanator using an alumina-supported Ru-catalyst at 350^{o}C. It was found that CO concentration dropped from 2500 ppmv (before) to approx. 3 ppmv (after methanator). Correspondingly, CO_2 concentration dropped from 1000 to 10 ppmv as a result of methanation reaction.

We determined the effect of sulfur compounds (e.g., hydrogen sulfide, H_2S) potentially present in commercial hydrocarbon fuels on the carbon catalyst activity and long term stability. The significance of this task relates to the fact that the presence of even small amounts of sulfur compounds in hydrocarbon feedstocks is detrimental for the activity of the majority of industrial catalysts (e.g., Ni-based catalysts). In most cases (e.g., steam methane reforming), an additional costly stage of feedstock desulfurization is included in the technological scheme in order to avoid rapid deactivation of metal catalysts.

It was found that the presence of small amounts of H_2S (≤3 v.%) in methane stream does not deactivate the carbon catalyst. Particularly, we observed that during introduction of H_2S into methane stream the hydrogen concentration in the effluent gas increased by approx. 2 v.% which can be attributed to the contribution of hydrogen produced by thermal decomposition of H_2S. Indeed, the control experiments with Ar-H_2S mixtures demonstrated that H_2S could be partially thermally decomposed over the surface of carbon catalyst (e.g., CB BP2000) at the temperature range of 850-900^oC:

$$H_2S \rightarrow H_2 + 1/2S_2 \qquad (5\text{-}7)$$

In the presence of CO_2 (that is an oxidant) H_2S is converted with high yield (95%) into the mixture of compounds comprising hydrogen, CO, water, elemental sulfur and minor amounts of carbonyl sulfide:

$$H_2S + CO_2 \rightarrow H_2, S_2, CO, H_2O, (COS) \qquad (5\text{-}8)$$

The effect of H_2S on methane decomposition can tentatively be explained in terms of intermediate formation of relatively active $HS^{\bullet}$-radicals which attack methane molecules at elevated temperatures.

6. STRUCTURAL AND SURFACE CHARACTERIZATION OF CARBON PRODUCTS

6.1. X-ray Diffraction (XRD) Studies of Carbon Catalysts

We conducted X-ray Diffraction (XRD) studies of the original carbon catalysts and carbon samples produced during hydrocarbon (methane or propane) decomposition. Figure 6-1 depicts the sample holder geometry.

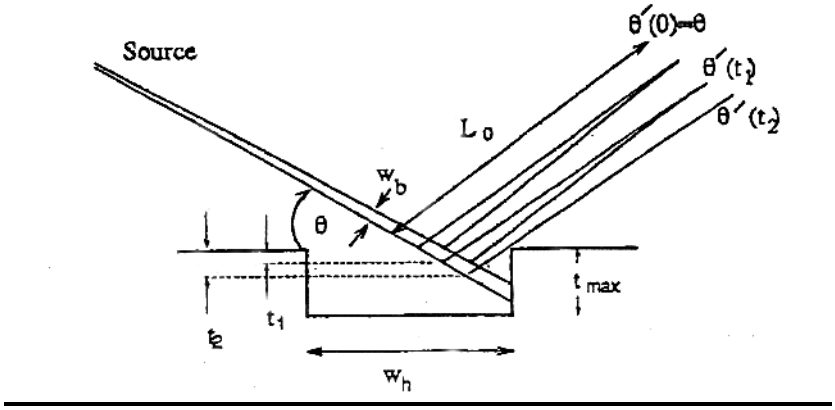

Figure 6-1. XRD Sample Holder Geometry

On this Figure t_{max} is sample holder depth, w_h- holder width, w_b- beam width, L_o-goniometer radius. Typical parameters for the diffraction scans are detailed below.

- D/MAX 2200T/PC ULTIMA+ Theta/Theta Goniometer, 185 mm radius, 6^o take-off angle
- Configuration for standard diffraction for phase identification:
- continuously variable divergence slit (computer controlled)
- continuously variable anti-scatter slit
- 0.30 mm receiving slit
- 0.8 mm monochromator receiving slit
- curved crystal graphite monochromator
- scintillation counter
- source: Cu anode X-ray tube
- generator settings: 50kV/40 mA

Carbon black BP-2000 with the surface area of 1500 m^2/g and activated carbon Darco KBB (produced from hardwood) with the same surface area were used in these studies. Figure 6-2 depicts XRD spectrum of the original carbon black (BP-2000) sample used in the experiments. Figure 6-3 demonstrates XRD spectrum of the carbon sample produced by propane pyrolysis at 850^oC. It was found that the original sample had one- or, possibly, some two-dimensional ordering, whereas, sample produced from propane had ordering in the "columnar" or stacking (003) direction. The following diagram illustrates this concept:

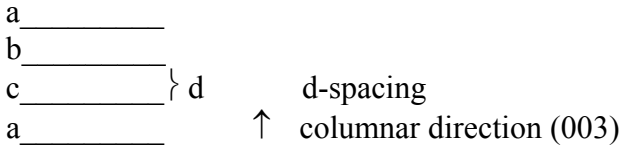

where, a, b, and c are alternating arrangements of carbon ring plates. The d-spacing (lattice spacing) or spacing between plates is practically uniform, so that the (003) columnar reflection is clearly present. Thus, carbon produced during propane pyrolysis clearly has a typical graphite a-b-c-a type stacking of the carbon ring plates.

The actual d-spacing (d =3.4948 Å) of this (003) peak is larger than that of the standard graphite structure (d = 3.3480 Å), which indicates that the plates are slightly further apart in the columnar stacking direction. This reflection is almost absent in the original carbon black sample which indicates that the plates are not stacked in a columnar arrangement, but, instead, are randomly oriented with respect to each other. The other two crystalline diffraction peaks in carbon sample produced by propane decomposition (43.5 and 46.2$^{o}2\theta$) also result from the three dimensional ordering, and result from the regular arrangement of spacings in various directions with respect to the columnar direction. The peaks 62.2 and 67. 2$^{o}2\theta$ are due to scattering rather than to crystalline diffraction. The peak at 62.2 is due to C – C atomic distance for atoms which are out-of-plane, and the peak at 67.2 results from the C – C atomic distance for the in-plane carbon atoms.

The size of graphite crystallite produced by propane decomposition was estimated at 23 Angstrom (Figure 6-4). The following is a profile fitting results:

2-Theta	25.549 (0.018)
d(A)	3.4836 (0.0047)
Height	2150 (11)
Area	277158 (1727)
Shape	0.870
Skew	0.491
FWHM Breadth	5.156
XS(A)	23 (1)

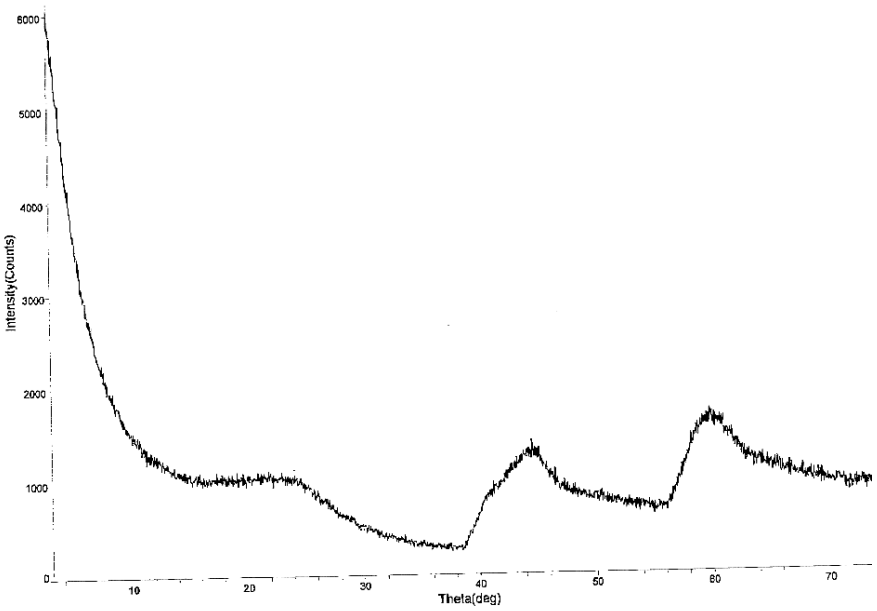

Figure 6-2. XRD Spectrum of Carbon Black BP-2000

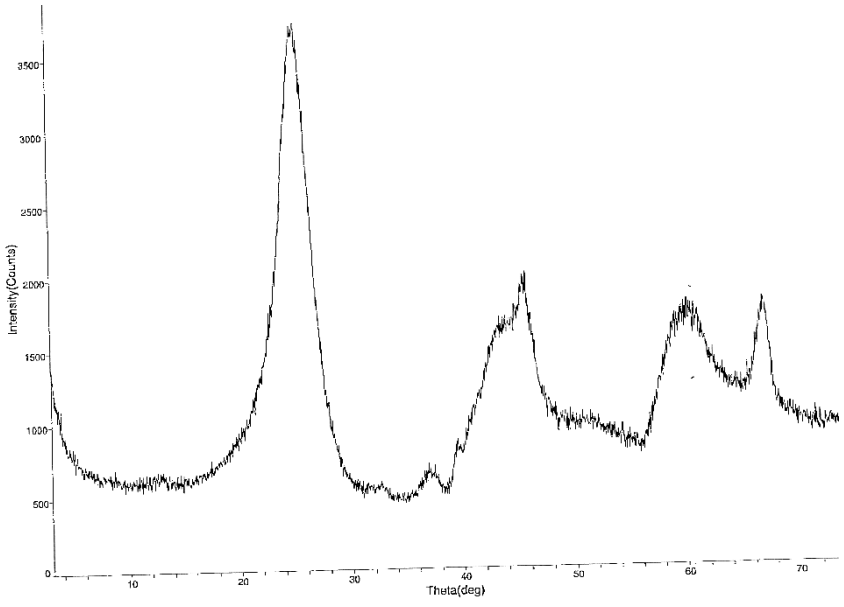

Figure 6-3. XRD Spectrum of Carbon Produced by Propane Pyrolysis over Alumina

Figures 6-5 and 6-6 show XRD spectra of carbon samples produced by decomposition of ethylene over carbon black BP-2000.

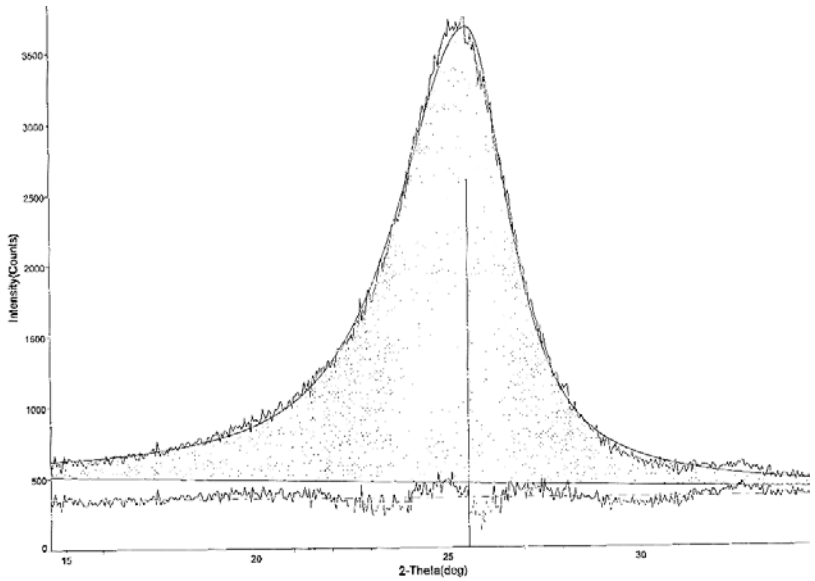

Figure 6-4. XRD Spectrum Profile Fitting for Carbon Produced by Propane Pyrolysis

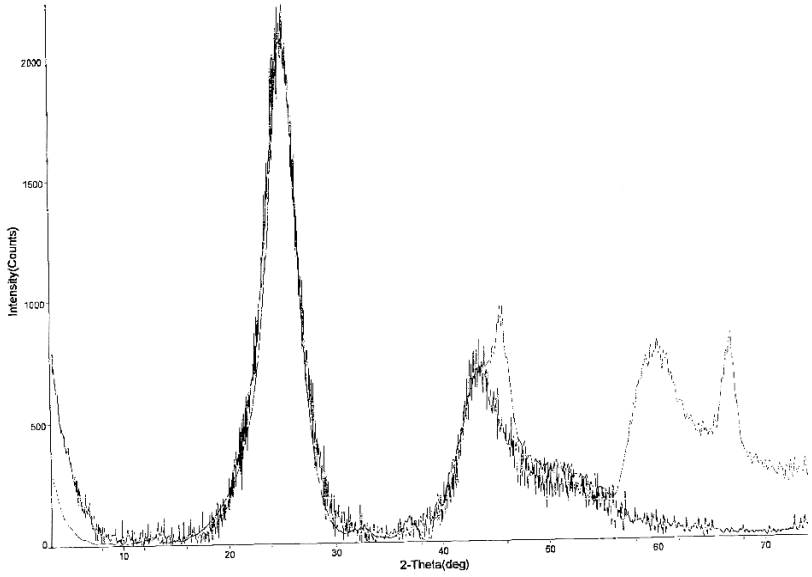

Figure 6-5. XRD Spectrum of Carbon Produced by Ethylene Pyrolysis over Carbon Black (BP-2000)

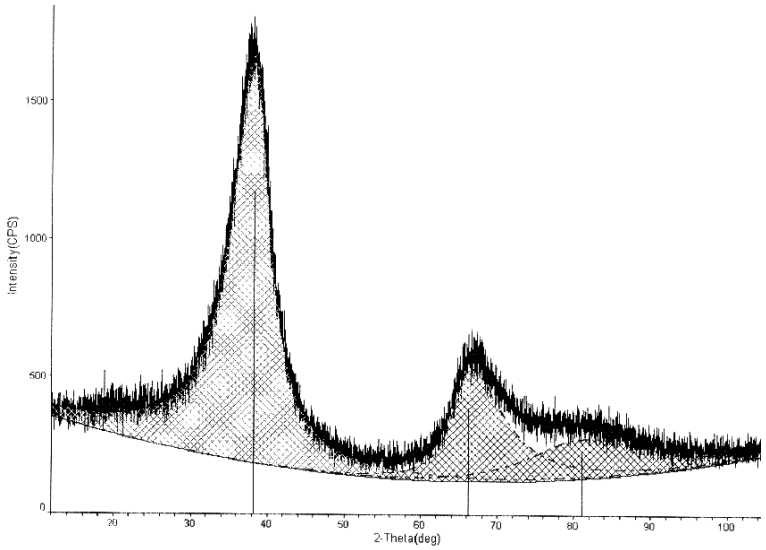

Figure 6-6. XRD Spectrum Profile Fitting for Carbon Produced by Ethylene Pyrolysis

XRD spectrum of the sample of activated carbon (Darco KBB) also indicated the lack of clear three dimensional ordering. Thus, XRD studies confirmed that carbon species produced by decomposition of alkanes (methane and propane) at 850^{o}C predominantly have an ordered (graphite-like) structure. This fact explains the gradual drop in the activity of AC and other carbon catalysts during methane and propane pyrolysis. Figure 6-7 combines XRD spectra of the original carbon black (BP2000) sample and two different samples of carbon black (fine and coarse carbon particles) after exposure of CB to propane at 850^{o}C.

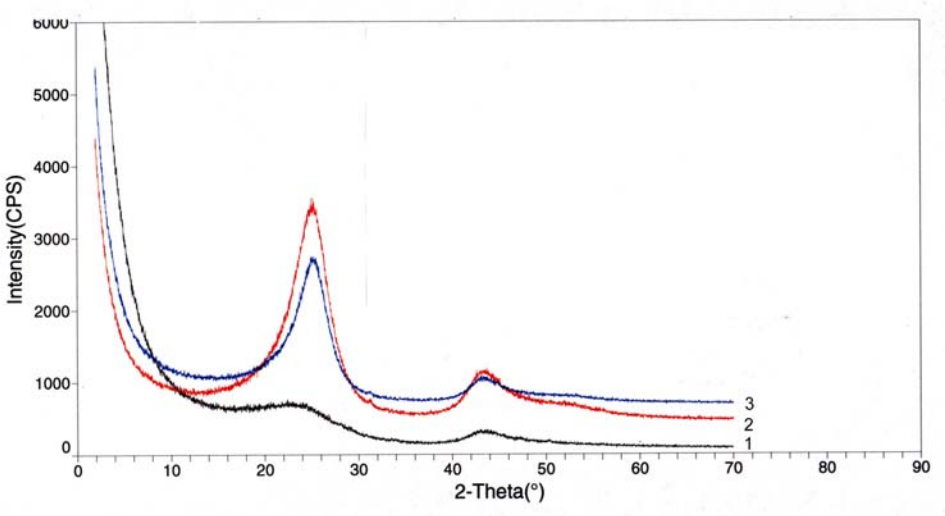

Figure 6-7. XRD Spectra of Carbon Samples. 1- original CB (BP2000), 2 and 3- samples of CB after exposure to C_3H_8 at 850^{o}C (fine and coarse carbon particles, respectively)

In agreement with our earlier findings, the original carbon sample had one- or two-dimensional ordering, whereas, samples produced from hydrocarbon decomposition exhibited an order in the stacking (003) direction. The d-spacing (lattice spacing) is practically uniform, so that the (003) columnar reflection is clearly present. The value of spacing between plates (d=3.49Å) is consistent with an ordered graphite-like or a turbostratic structure.

6.2. X-Ray Photoelectron Spectroscopic Studies of Carbon Samples

The results of X-Ray Photoelectron Spectroscopic (XPS) studies of different carbon samples are shown in Figures 6-8 through 6-18.

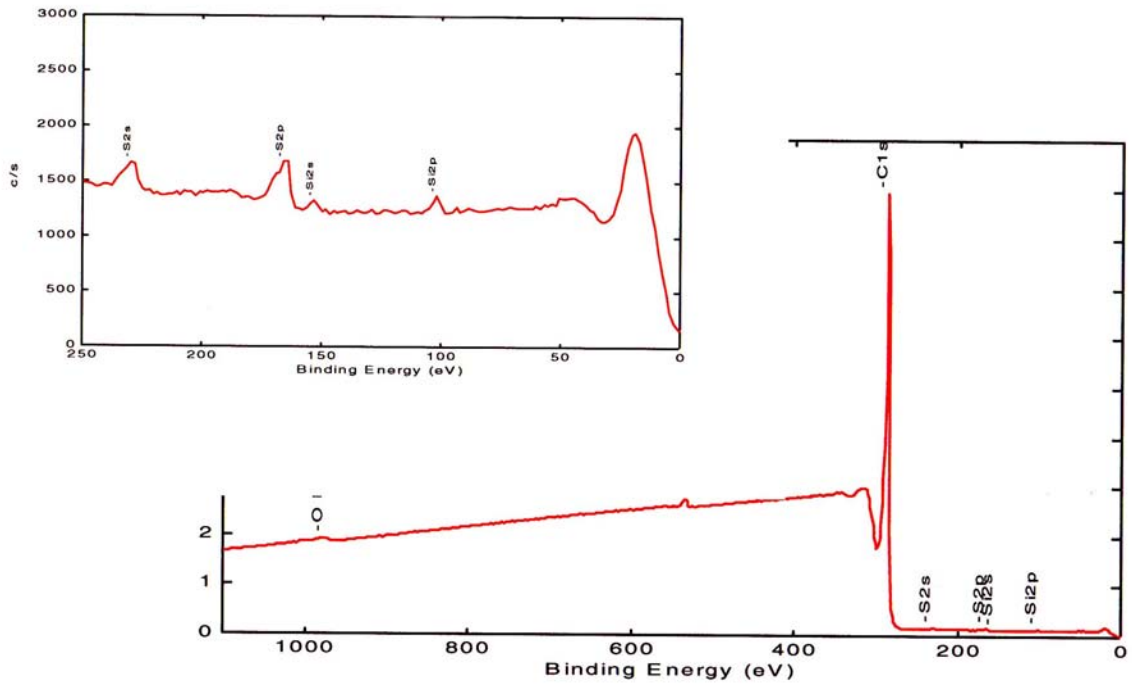

Figure 6-8. XPS Survey Scan of Original Carbon Black (BP2000) Sample

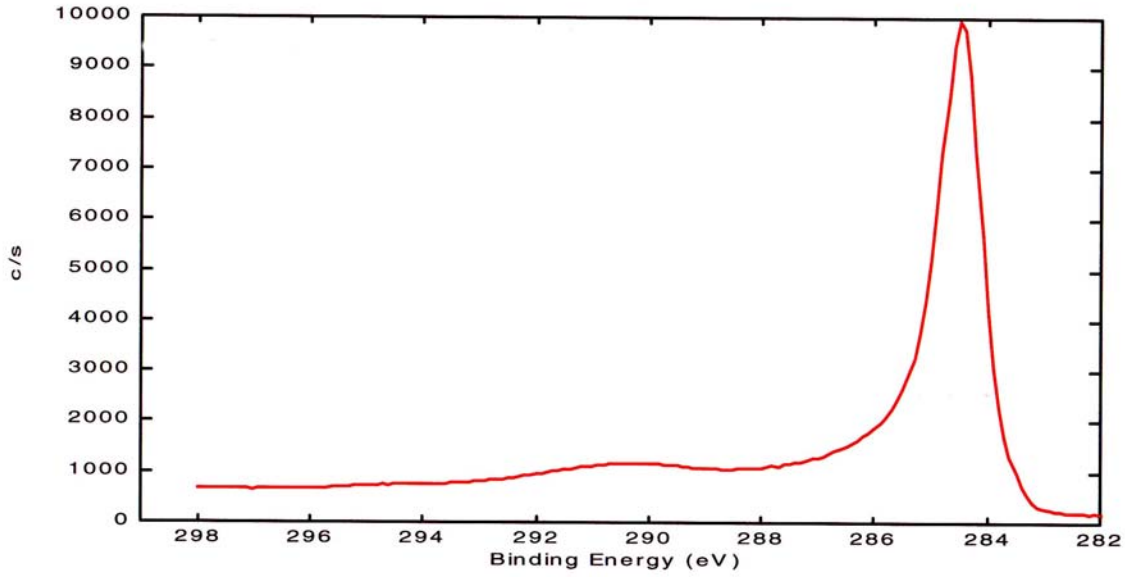

Figure 6-9. XPS Spectrum of the Original Carbon Black (BP2000) Sample

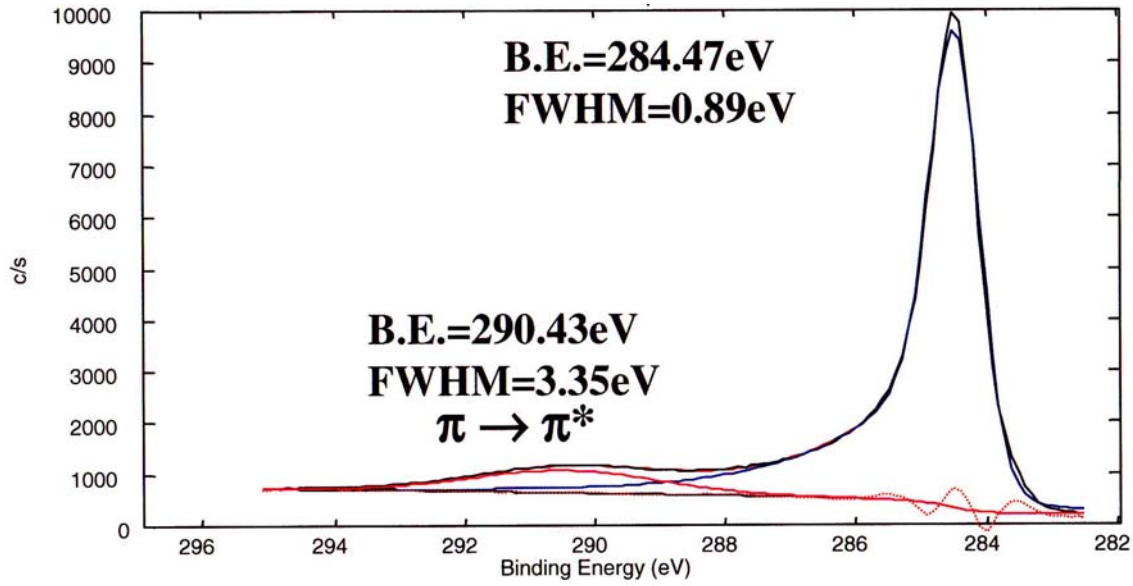

Figure 6-10. Peak Fitting of C1s Region for Original CB (BP2000) Carbon Samples.

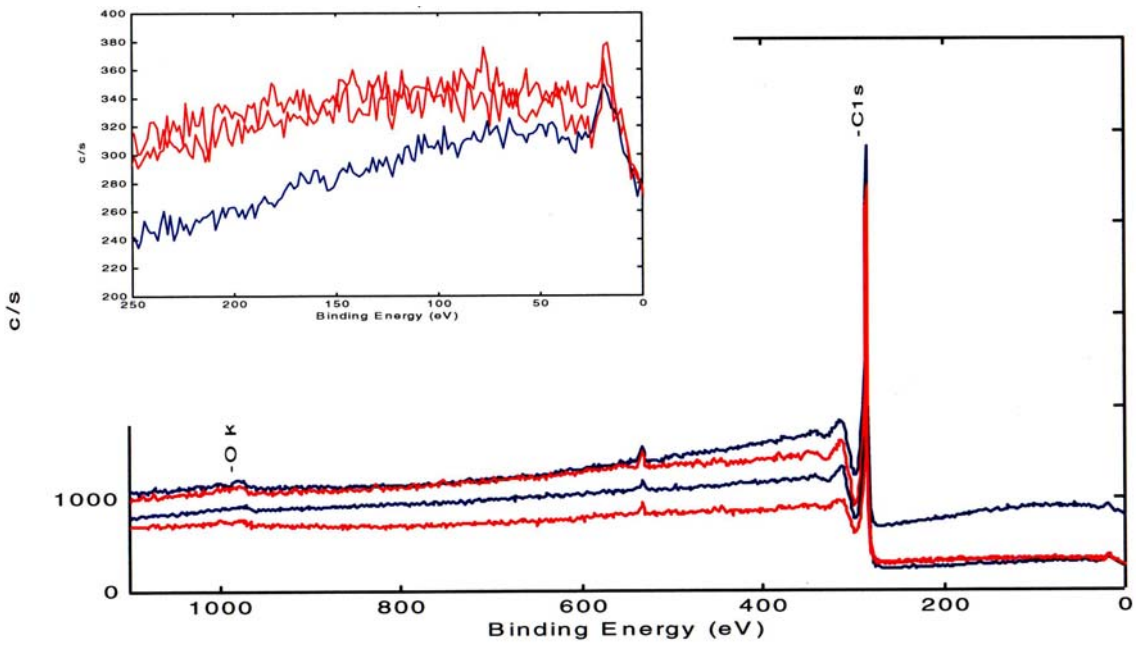

Figure 6-11. XPS Survey Scan of Carbon Samples Produced by Propane Pyrolysis over CP (BP2000). Blue- Coarse Particles, Red- Fine Particles

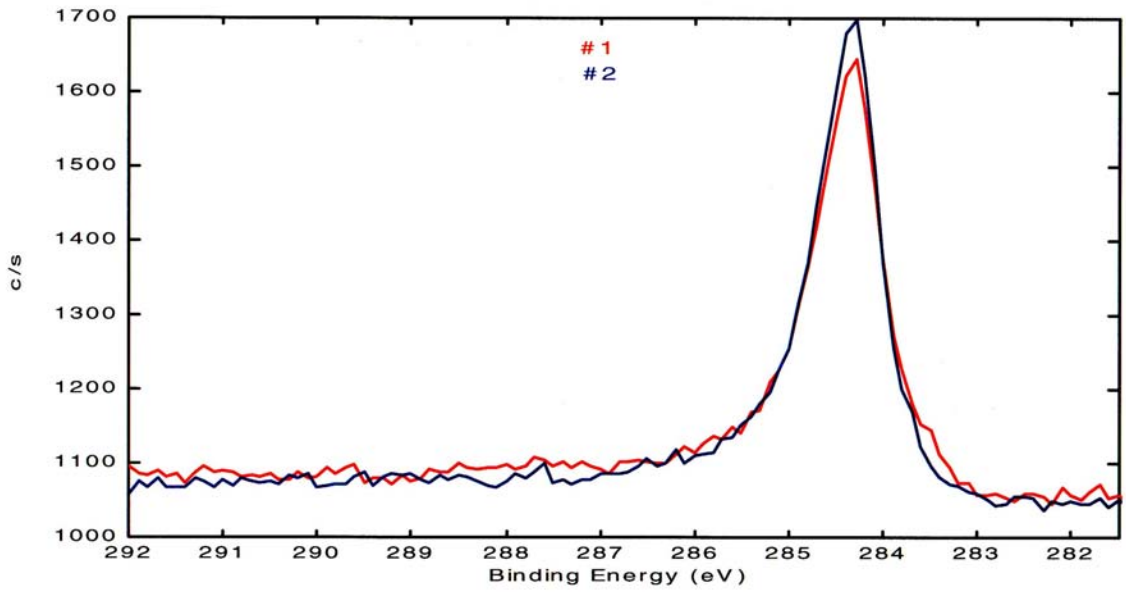

Figure 6-12. XPS Spectra of the Carbon Samples (Coarse Powder Samples #1 and #2) Produced by Propane Pyrolysis over Carbon Black (BP2000)

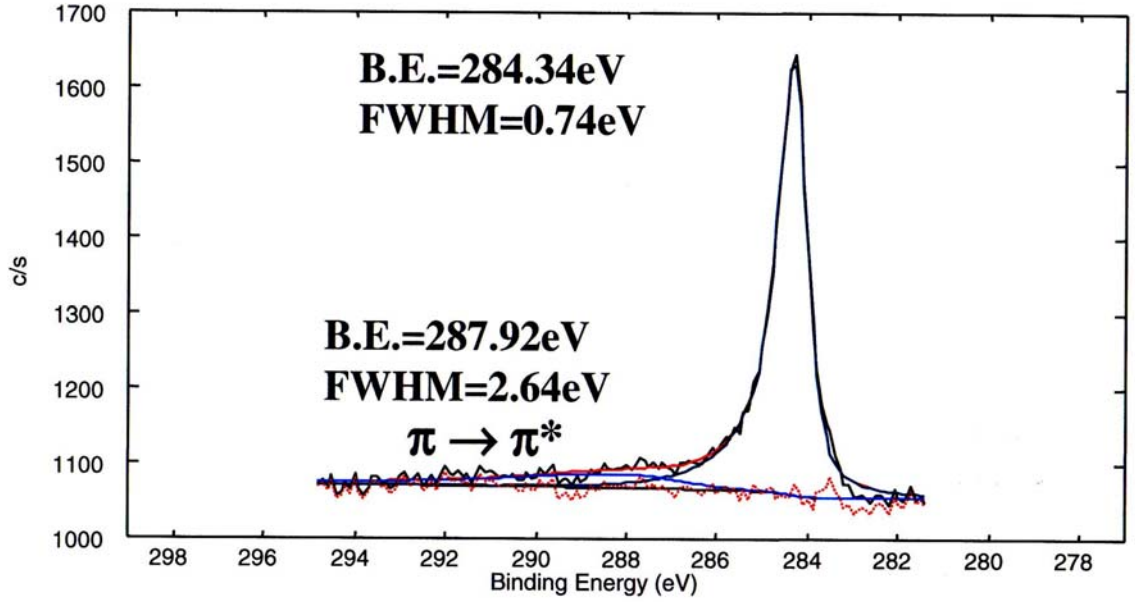

Figure 6-13. Peak Fitting of C1s Region for the Coarse Carbon Sample #1

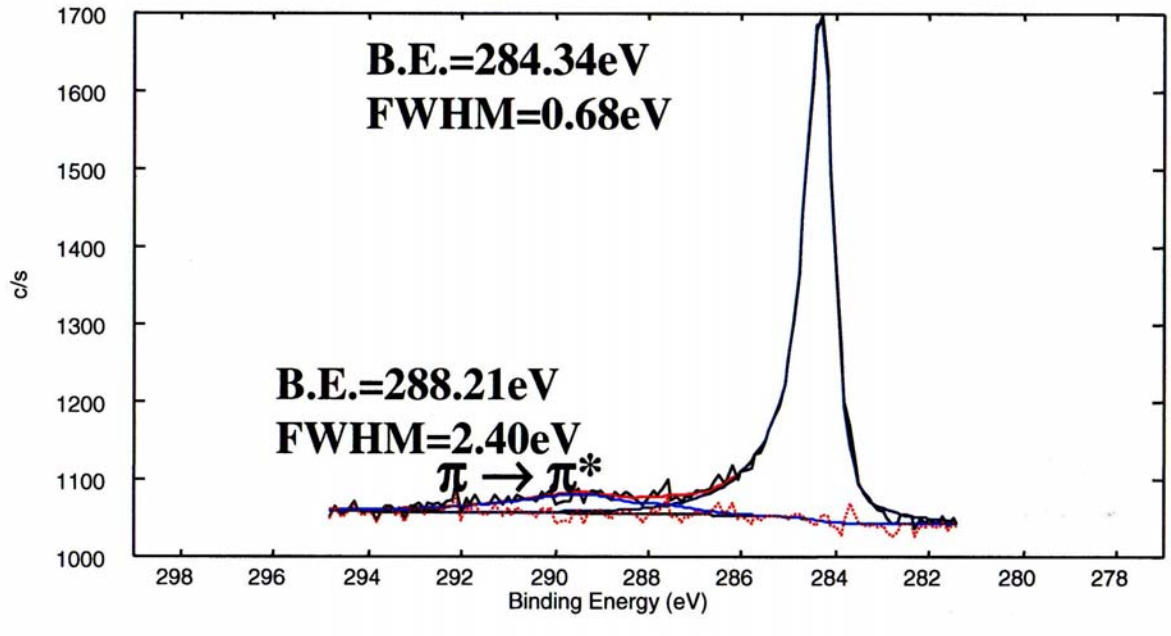

Figure 6-14. Peak Fitting of C1s Region for the Coarse Carbon Sample #2

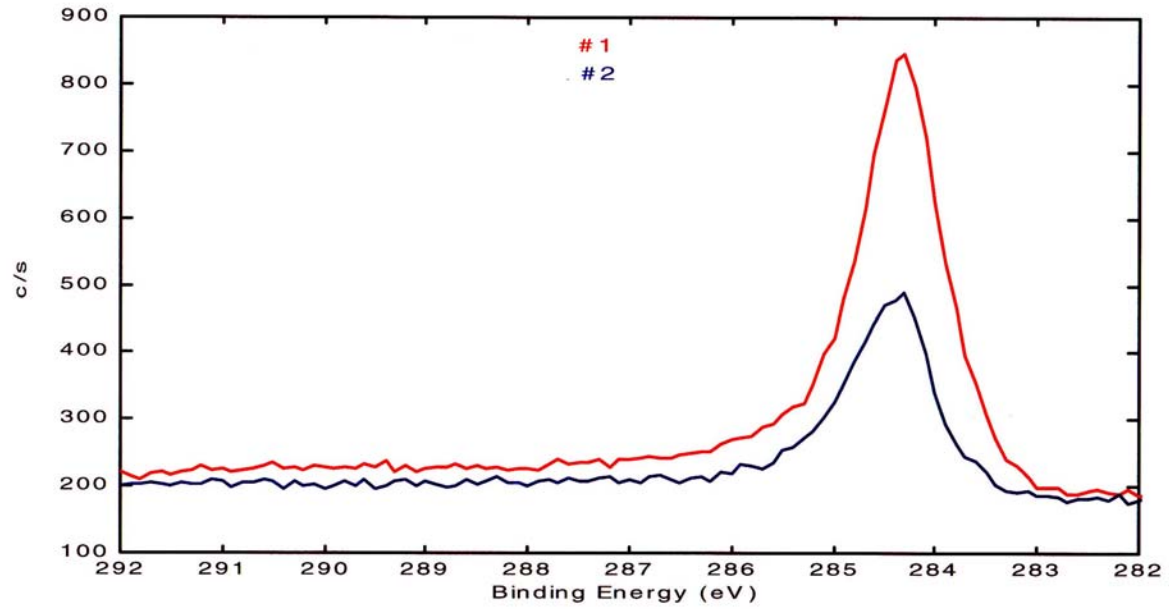

Figure 6-15. XPS Spectra of the Carbon Samples (Fine Powder Samples #1 and #2) Produced by Propane Pyrolysis over Carbon Black (BP2000)

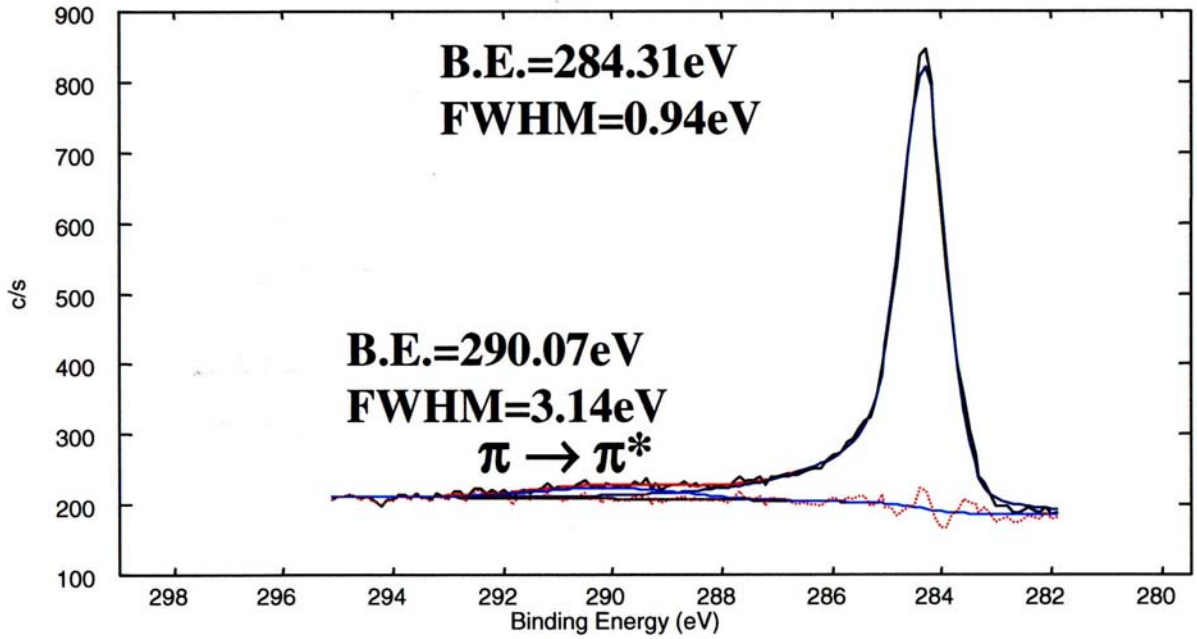

Figure 6-16. Peak Fitting of C1s Region for the Fine Carbon Particles (Sample #1)

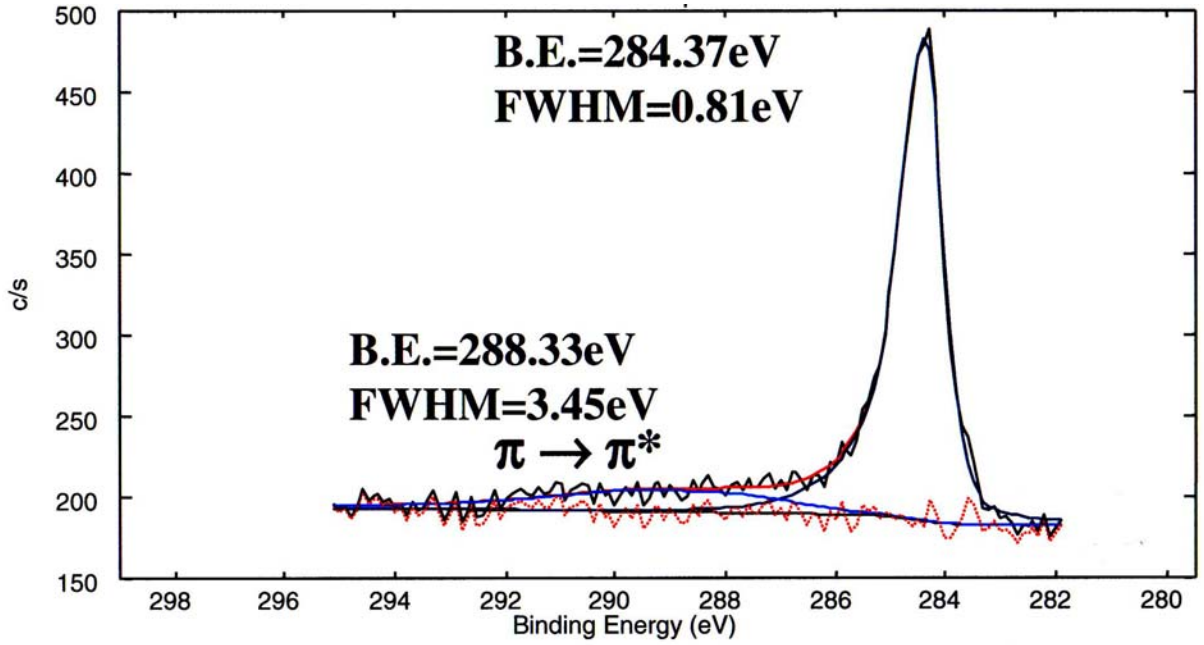

Figure 6-17. Peak Fitting of C1s Region for the Fine Carbon Particles (Sample #2)

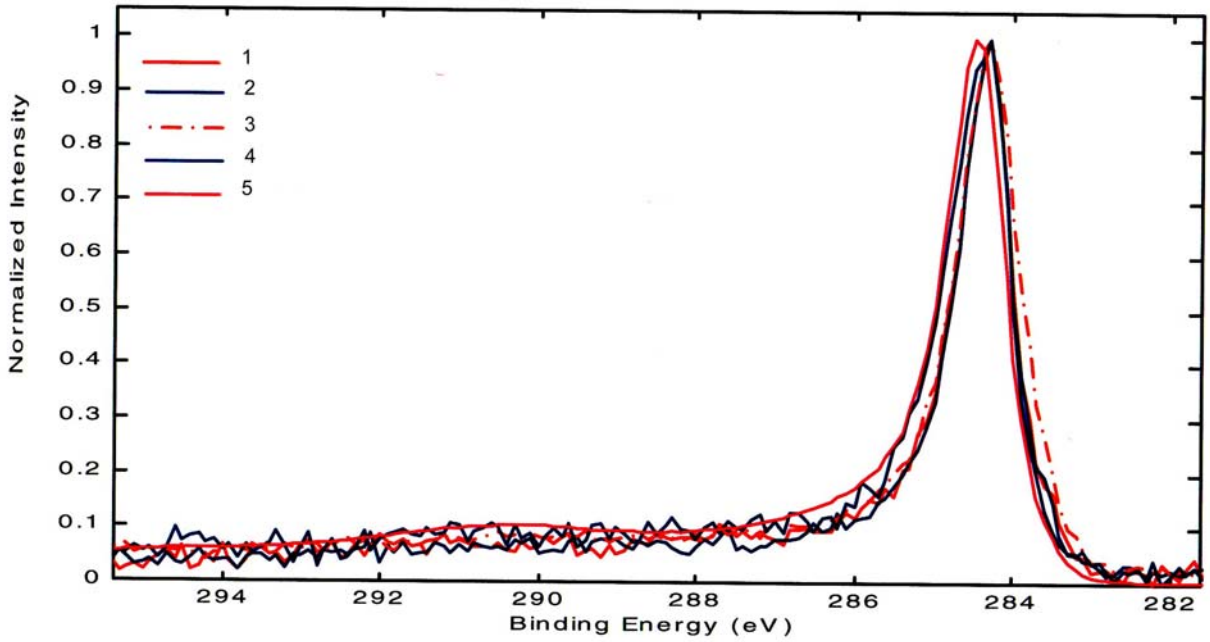

Figure 6-18. XPS Spectra of Different Carbon Samples (Coarse and Fine Particles, Samples #1 through # 5). Overlay of All C1s Regions

The original carbon black (BP2000) showed trace amounts of silicone, sulfur and oxygen on its surface. Surface atomic concentrations are as follows (%): carbon- 98.6, oxygen- 1.0, sulfur- 0.2 and silicon- 0.1. Sulfur could result from the sulfur-containing aromatized petroleum fractions used in production of carbon black by the Furnace Black process. It can be seen from Figure 16 that only trace amounts of oxygen are present on the surface of carbon particles produced by decomposition of propane over CB catalyst at 850^{o}C

It is clear from XPS spectra that there does not appear any distinction by XPS on the nature of original carbon and fine or coarse carbon particles produced by propane decomposition over CB (BP2000) catalyst. The carbon peak can be fit assuming the presence of graphitic-type carbon. It should be noted, however, that XPS is not very sensitive to the degree of the aromaticity of carbon (e.g., it can not differentiate between sp^3, sp^2 and sp carbon). The carbon in all the samples can be fit well assuming only one type of carbon.

6.3. Scanning Electron Microscopic Studies of Carbon Samples

We conducted Scanning Electron Microscope (SEM) studies of the surface of carbon catalysts. Average particle size of powdered activated carbons was 40-100 μm. Carbon black particles were significantly smaller in size and varied in the range of 0.1 – 1 μm. Figure 6-19 depicts SEM micrographs of CB (BP-2000) catalyst before exposure to hydrocarbons at different magnifications.

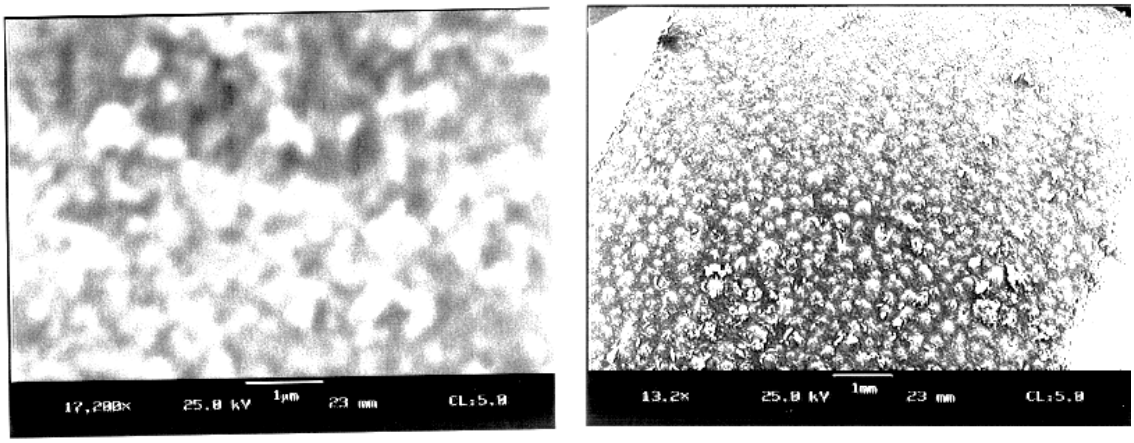

Figure 6-19. SEM Micrograph of Carbon Black (BP-2000)

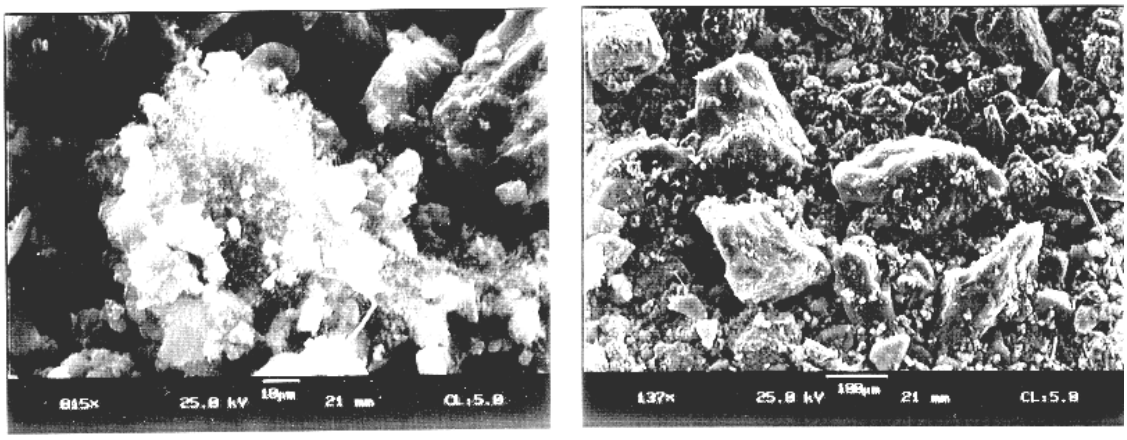

Figure 6-20. SEM Micrograph of Carbon Produced by Decomposition of CH_4/C_3H_8 Mixture over Carbon Black (BP-2000)

Figures 6-19 and 6-20 demonstrate SEM micrographs of original CB BP-2000 and carbon produced by decomposition of CH_4/C_3H_8 gaseous mixture over the surface of carbon black BP-2000, respectively.

Prolonged (3-4 hours) exposure of carbon catalyst (CB BP-2000) to a hydrocarbon stream at elevated temperatures (800-900^{o}C) resulted in formation of spherical carbon particles with the dimensions in the range of 0.5-1.5 mm (Fig. 6-21). This corresponds to more than thousand-

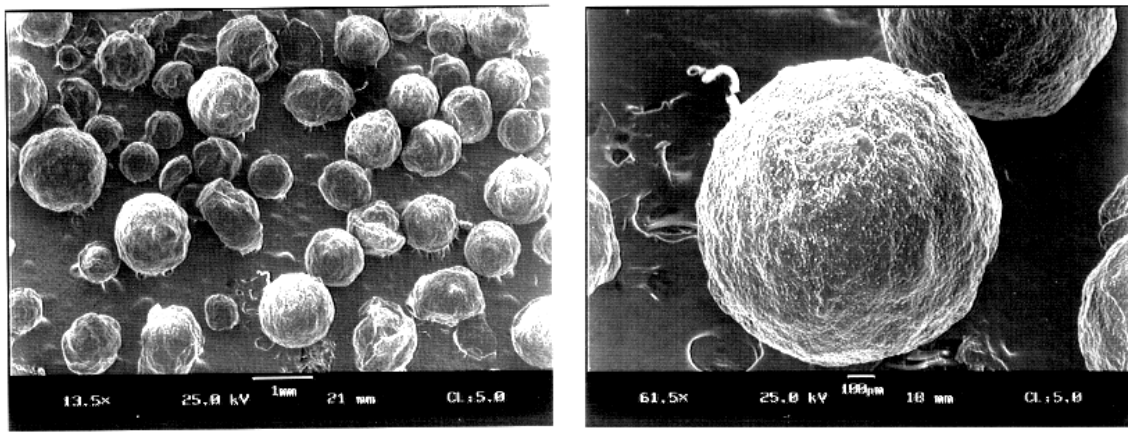

Figure 6-21. SEM Micrograph of Spherical Carbon Particles Produced by Decomposition of C_3H_8 over Carbon Black (BP-2000)

fold increase in particles mean diameter. On the other hand, the amount (weight) of carbon in the reactor increased only 6 times as a result of propane pyrolysis. This implies that a great deal of the agglomeration of carbon particles occurred during the process. Surface area calculations indicate that propane pyrolysis over CB catalyst would result in the reduction of the total geometrical surface of carbon particles by two orders of magnitude. This would have led to a drastic decrease in propane pyrolysis rate due to a significant reduction in the catalytic surface, which did not happen. The reason for that is that the actual surface area of each particle was much higher than its geometrical surface due to the presence of clusters of carbon particles about 3-10 μm in diameter on the surface of the larger carbon particles (not shown on the micrograph). It can be seen from the Figure 6-21 that a crashed spherical particle (at the bottom) has a distinct layered structure. XRD analysis of the spherical carbon particles revealed that they exhibited an ordered graphite-like (turbostratic) structure similar to that of the above-described micron-size carbon particles.

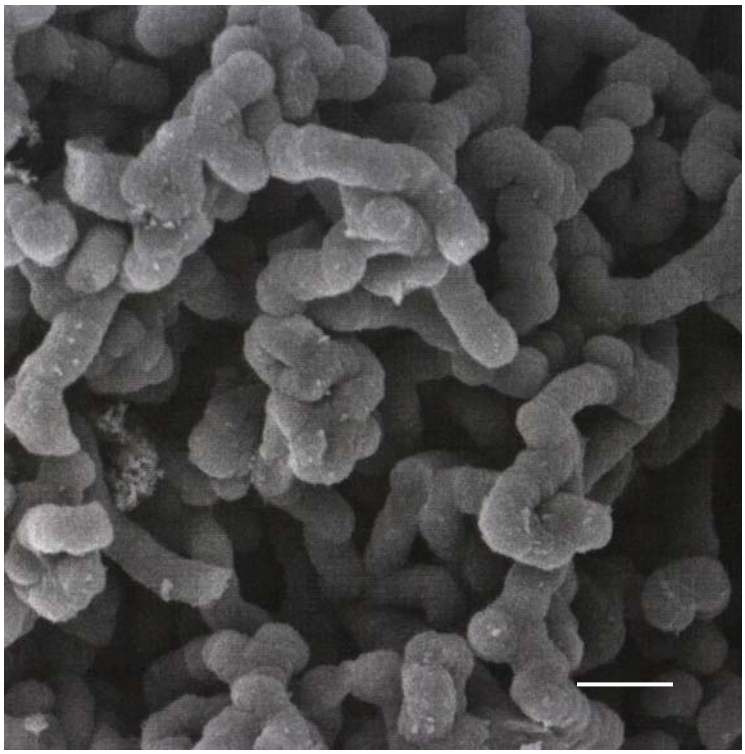

Figure 6-22. SEM Micrographs of Carbon Filaments Produced by Catalytic Decomposition of Propane. Average Filament Diameter - 1 μm)

It was found that the clusters of relatively thick carbon filaments are present on the surface of some spherical particles (not all of them). The carbon filaments have the diameter of approximately 1 micron, and are of the "octopus" type, with branches spreading out occasionally from the "main" filament (Figure 6-22). The common size of carbon nodules and filaments suggests that the nodules could be precursors to the filaments. It is apparent that carbon

filaments arise when the available surface area is small, and the filaments growth is the only way to maintain a higher carbon deposition rate.

6.4. Carbon Particle Size and Distribution Measurements

Carbon particle sizing was performed using ACCUSIZER 770/SPOS Single Particle Optical Sizer. The ACCUSIZER 770 uses the method of single-particle optical sensing (SPOS) to quickly count and size a large number of particles, one at a time, thus constructing the true particle size distribution (PSD). The ACCUSIZER uses autodilution, which automatically dilutes the starting sample to the optimum concentration. SPOS is a measurement based on the population of particles. Figures 6-23 and 6-24 show the results of acetylene black and graphite particles size and distribution measurements using. For example, it is clear from Figure 6-23 that mean particle size for acetylene black sample is 0.77 μm (measured by SPOS method). The total number of particles in the sample was 1099992, dilution: 5.52. The carbon particle size measured by Dynamic light scattering method (DLS) was in the range of 330-470 nm (or 0.33-0.47 μm). This does not agree with the size of acetylene black particles (0.042 μm) reported in the product specification, which indicates that the carbon particle aggregation most likely occurred during sample preparation and particle size measurements.

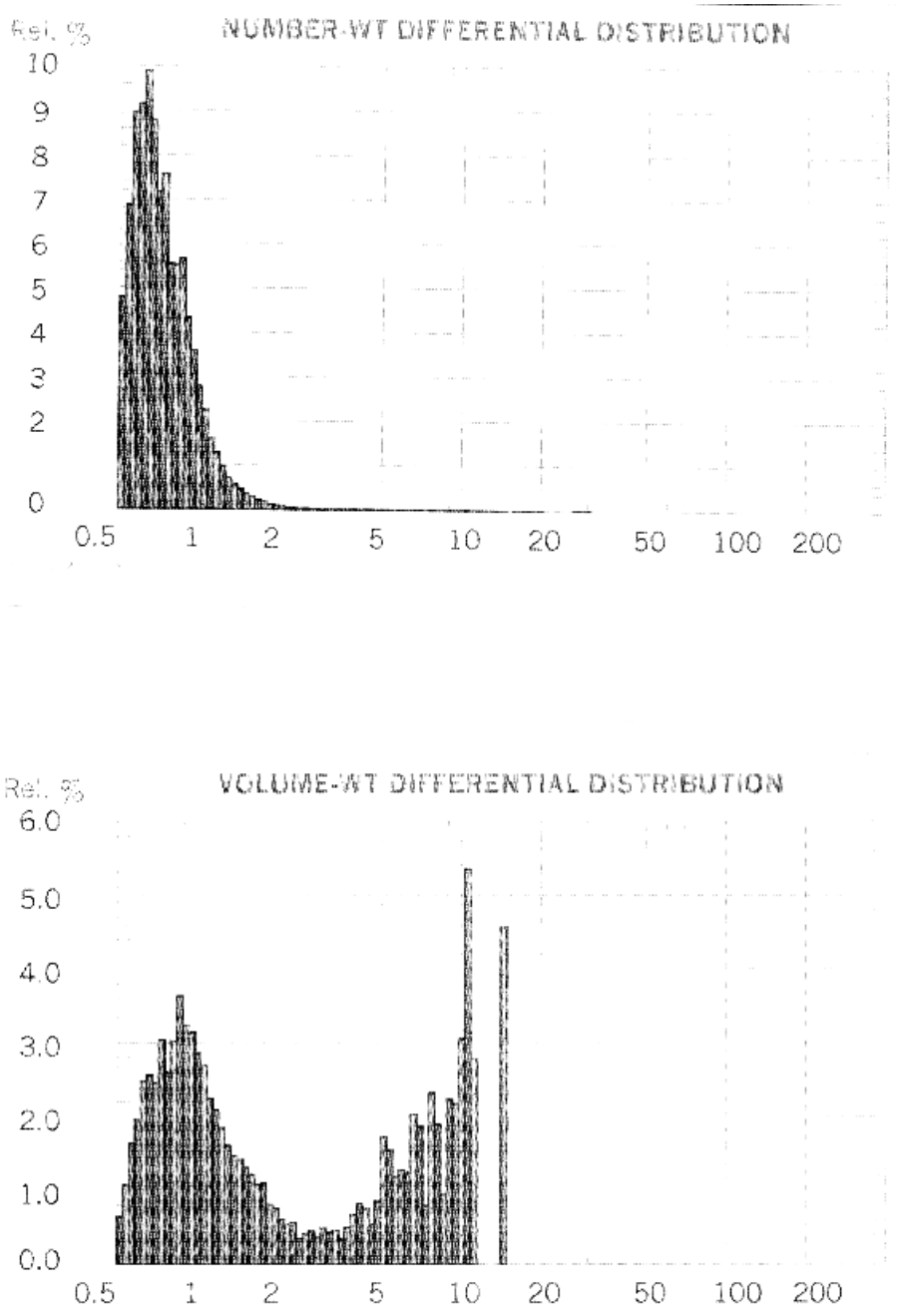

Figure 6-23. Acetylene Black Particle Size Measurements Using Model 770 Accusizer

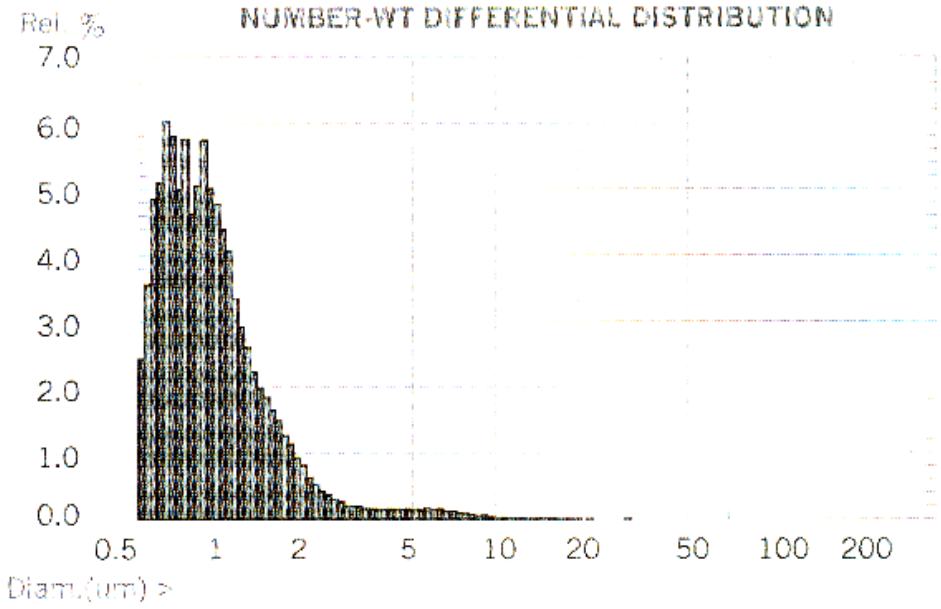

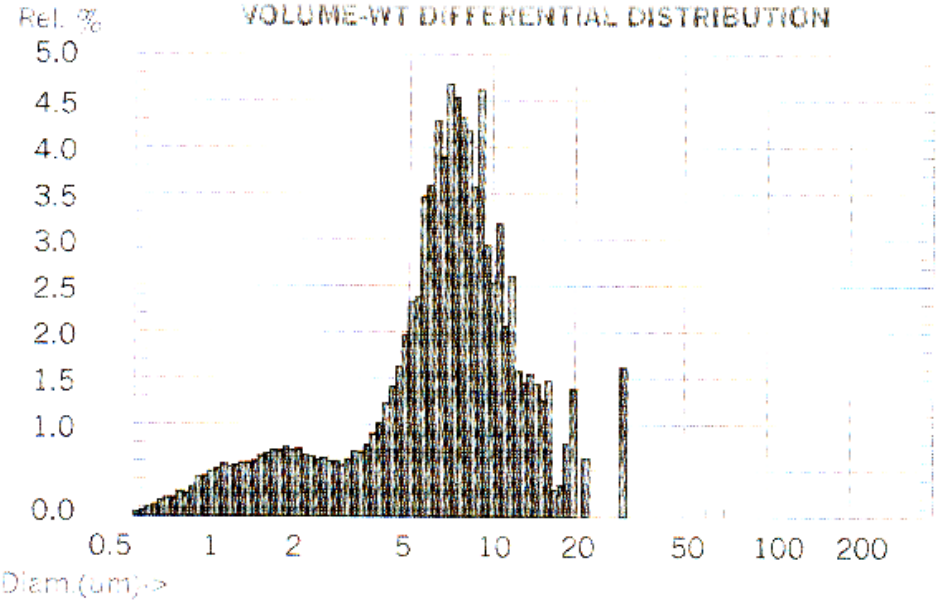

Figure 6-24. Graphite Particle Size Measurements Using Model 770 Accusizer

6.5. AAS Analysis of Carbon Samples for the Presence of Transition Metals

Carbon samples were tested for the presence of transition metals that are known to be catalytically active in decomposition of methane, e.g., Ni, Fe, Co and Cu. The Table 6-1 depicts the results of Atomic Absorption Spectrometric (AAS) analysis of two carbon samples used in our methane decomposition experiments.

Table 6-1. AAS Analysis of Carbon Samples for the Presence of Transition Metals

Carbon samples	Units	Metals			
		Ni	Fe	Cu	Co
Sample 1 (CB BP2000)	mg/kg	1.5	13.2	1.0	1.0
Sample 2	mg/kg	1.0	17.5	1.6	1.0

It is evident that although metals are present at ppm levels in the carbon sample, the catalytic activity of carbon catalysts toward methane decomposition can not be solely attributed to the catalytic action of these metals.

7. TECHNO-ECONOMIC EVALUATION OF HYDROGEN PRODUCTION BY THERMOCATALYTIC DECOMPOSITION OF NG

7.1. Techno-economic Analysis of Thermocatalytic Process

Techno-economic analysis of thermocatalytic decomposition of natural gas was conducted by NREL, based on the experimental data input provided by FSEC. Courtesy of NREL, here we present the selected results of the analysis related to one particular process design which included a fluidized bed catalytic reactor and a fluidized bed heater with carbon particles circulating between these two apparatuses (similar to the schematic presented in Figure 7-1).

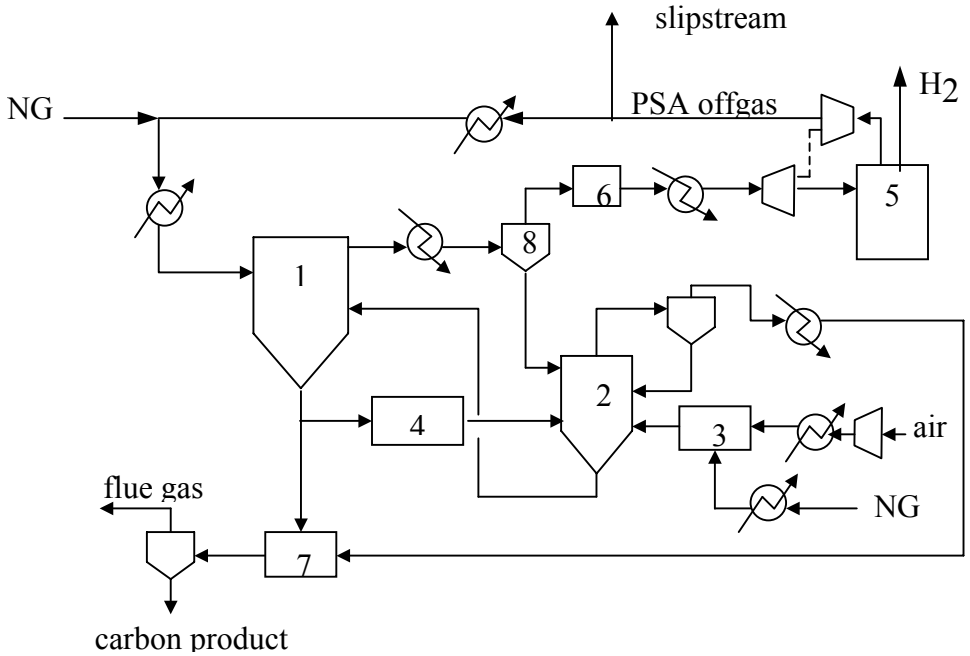

Figure 7-1. Simplified Schematic Diagram of the Process for Production of Hydrogen and Carbon via Thermocatalytic Decomposition of NG. 1- FBR (pyrolyzer), 2- FBR (heater), 3- Combustor, 4- Grinder, 5- PSA, 6- Filter, 7- Quencher, 8- Cyclones

Process heat is provided by combusting part of NG and carbon. PSA unit was assumed for the production of high purity hydrogen (>99 v.%). Three plant sizes were analyzed (in MMscfd): small- 6, medium- 20 and large- 60. The analysis assumed the internal rate of return of 15%. Figure 7-2 demonstrates hydrogen selling price as a function of natural gas selling price for three hydrogen plants (assuming carbon selling price of $300/t).

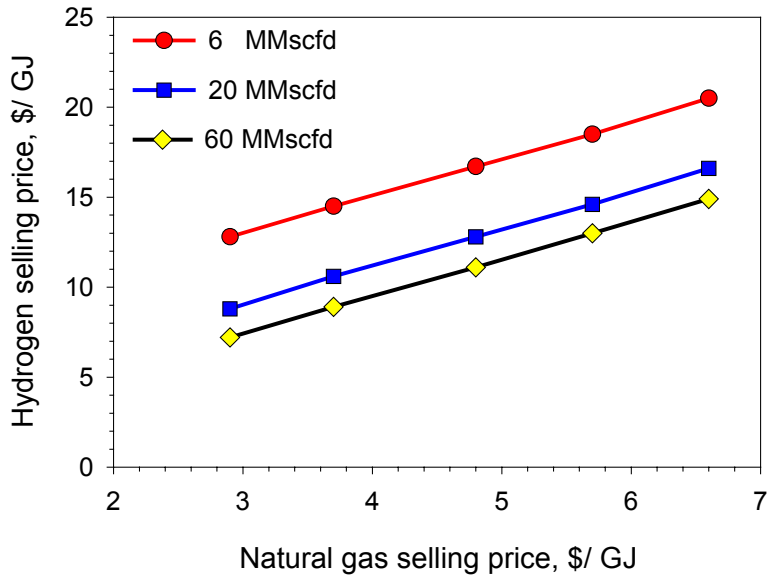

Figure 7-2. Hydrogen Selling Price vs Natural Gas Selling Price

At natural gas prices ranging from $2.9 to 6.6 per GJ, hydrogen selling price varied in the range of $7.2-14.9 /GJ, for a large plant, and $12.8 – 20.5/ GJ, for a small plant. It should be noted that hydrogen selling prices would be further reduced if a carbon credit for avoided CO_2 emissions were applied.

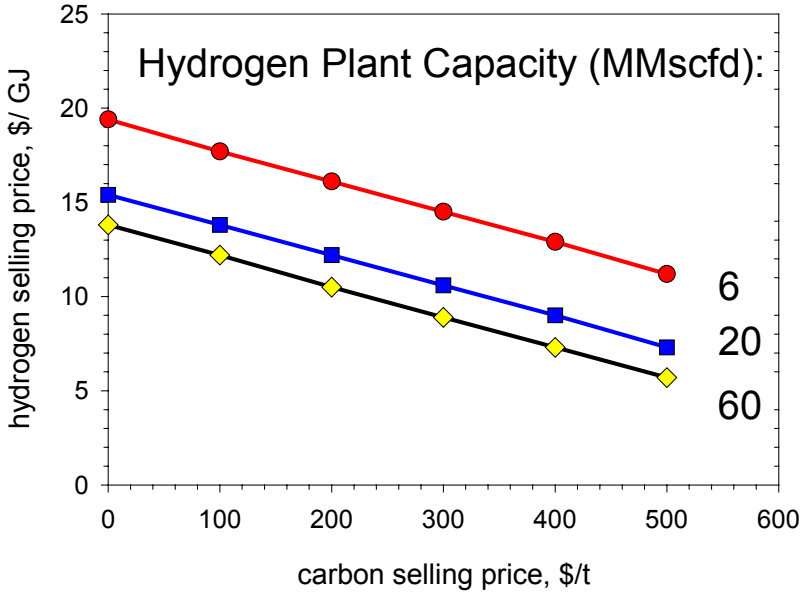

Figure 7-3. Hydrogen Selling Price vs Carbon Selling Price

The sensitivity analysis on the effect of carbon selling price on the hydrogen selling price was also conducted. Figure 7-3 shows the plots: hydrogen selling price vs carbon selling price for a small, a medium and a large hydrogen plants at NG selling price of $3.72 per GJ. It is evident that carbon credit significantly reduces the cost of hydrogen production. Particularly, at carbon selling prices ranging from $0 to 500 per metric ton, the plant gate hydrogen selling price varies from $13.8 to 5.7 /GJ, for a large plant, and from $19.4 to 11.2/ GJ, for a small plant.

7.2. Comparative Assessment of TCD and SMR Processes

We have conducted a comparative economic assessment of TCD (with and without carbon credit) and SMR (with and without CO_2 sequestration) processes (Figure 7-4).

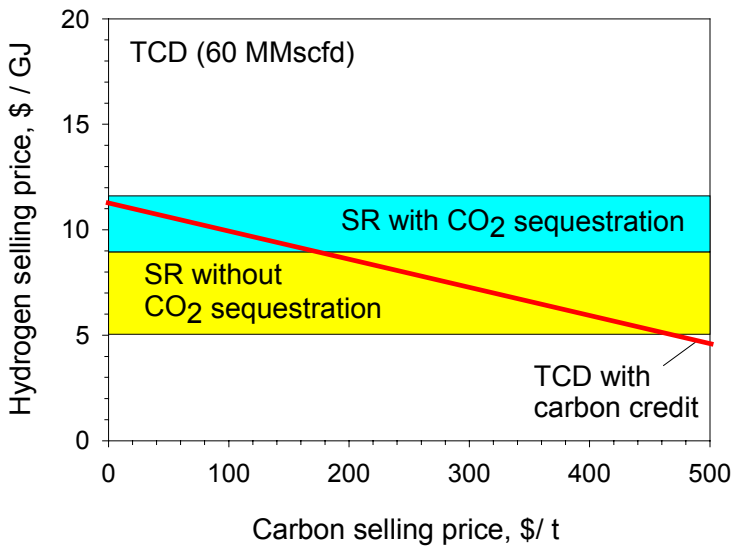

Figure 7-4. Comparative Economic Assessment of TCD and SMR

The comparison is based on a large capacity hydrogen plant and NG selling price of about $3 /GJ. The cost of hydrogen production by a large SMR plant was estimated at $5-9/GJ [27]. It was assumed that the total cost of hydrogen production by SR plant coupled with CO_2 sequestration would increase by 25-30% [7]. For the purpose of this comparative assessment, sequestration of CO_2 from TCD process is not considered (it was assumed that upon the optimization of TCD process, CO_2 emissions from it would be minimal compared that to SMR). It is evident from the Figure 7-4 that the cost of hydrogen production by TCD process becomes comparable with that of SR process (without CO_2 sequestration), if carbon is sold at the price range of approximately $160 - 460 per ton. However, if strict environmental restrictions on CO_2

emissions will be imposed in future, and CO_2 sequestration from SR process would become mandatory, hydrogen selling prices for SMR and TCD will be comparable, even without carbon credit.

According to Steinberg, the overall net energy efficiencies of TCD and SMR processes become close (58 and 60%, respectively) after accounting for 15% energy loss due to CO_2 sequestration [28]. Thus, both the overall energy efficiencies and hydrogen yields for TCD and SMR (after CO_2 sequestration) become fairly close. One should consider, however, that TCD process produces a valuable byproduct carbon, whereas, in SMR process 40% of the energy is lost irreversibly due to high reaction endothermicity and CO_2 sequestration stage. Carbon byproduct could potentially be sold, thus reducing hydrogen production cost. Figure 7-5 demonstrates comparative assessment of net hydrogen yields for SMR and TD (or thermocatalytic decomposition, TCD) processes.

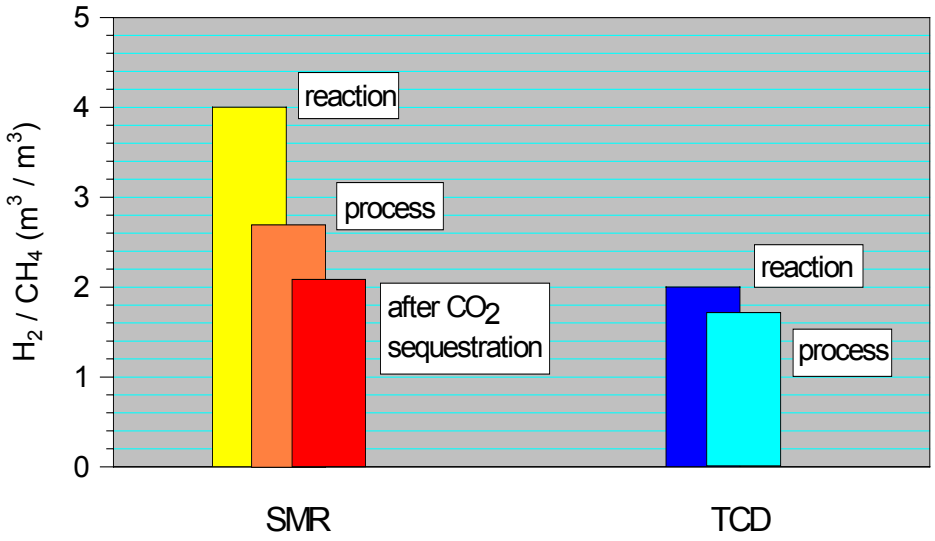

Figure 7-5. Comparative Assessment of Net Hydrogen Yields for SMR and TCD Processes.

7.3. Evaluation of Application Areas for Carbon Products

Since carbon credit markedly affects the economics of the TCD process, a great deal of consideration was given to the characterization of carbon-product and estimation of its market value. This work was conducted in cooperation with the Universal Oil Products (UOP) (Des Plaines, IL). UOP has conducted SEM, XRD and XPS analysis of carbon produced by catalytic pyrolysis of propane and methane over carbon black catalyst. In general, the results of XRD analysis conducted by UOP were in an agreement with the results of the prior analysis of carbon samples, conducted by AMIA Laboratories (Rigaku). It was inferred that carbon produced by TCD process revealed a graphite-like structure. It was also concluded that carbon produced in the process could be suitable for the production of electrodes in the aluminum and ferro-alloy industries. Currently, aluminum industry produces annually close to 4 mln ton of aluminum,

with carbon (coke) consumption rate of 0.4-0.5 kg of carbon per kg of Al [29]. Thus, aluminum industry could be very important market for sulfur- and metal-free carbon produced in TCD process with the selling prices of $300 per ton and higher.

Although metallurgical and tire industries provide very important markets for the carbon products, it is realized that much larger markets should eventually be developed in order to economically justify the large scale production of hydrogen via methane decomposition. Therefore we place a strong emphasis on the development of new application areas for the carbon products. Our experimental results indicated that depending on the operational parameters of hydrocarbon decomposition process several valuable forms of carbon could be obtained, e.g., pyrolytic graphite, spherical carbon particles, carbon filaments and others. The selling prices for these modifications of carbon are well above $1/kg.

We conducted a collaborative effort with MER Corporation (Tucson, AZ) on identifying new application areas, e.g., batteries, for carbon products produced by thermocatalytic decomposition of hydrocarbons (methane and propane). We produced the carbon samples with the turbostratic structure (d-spacing =3.49Å) and MER tested them in lithium-ion batteries. The results are summarized in Table 7-1.

Table 7-1. The Results of Testing of Carbon Samples in Lithium-ion Batteries*

	Discharge capacity	Charge capacity	Irreversible capacity
1st cycle	410	73	462
2nd cycle	383	167	296
3rd cycle	201	167	47
4th cycle	190	168	30

* Courtesy of MER Corp.

The results show that the reversible capacity of the battery is somewhat lower compared to best commercial carbon samples. Two factors that can potentially improve reversibility characteristics of the carbon samples include: (i) larger d-spacing in turbostratic carbon samples and (ii) lower surface area. We agreed with MER that we will produce the carbon samples with the desired characteristics and send them to MER for further testing in lithium-ion batteries.

We have a collaborative effort with the Lawrence Livermore National Laboratory on testing carbon samples as a fuel for a direct carbon fuel cell (based on molten carbonate fuel cell). We have produced several samples of carbon with the turbostratic structure and sent them to LLNL for the testing. The evaluation of novel application areas for carbon products is in progress.

8. REACTOR MODELING AND PROCESS SCALING-UP STUDIES

In cooperation with Reaction Engineering International (REI) we conducted studies on the modeling and scaling-up of the fluidized bed thermocatalytic reactor for thermocatalytic decomposition of natural gas. In particular, a flow model of fluidized bed reactors, including diffusional dispersion of reaction products within the bed, and reaction product mixing was used to calculate the performance. These models capture most of the chemistry and physics occurring within the fluidized bed reactor.

8.1. Energy Balance and Kinetics Constraints

A fluidized bed reactor was modeled for the production of hydrogen and carbon via thermocatalytic decomposition (TCD) of natural gas (methane) with the capacity of 220 t/day.

The heat put requirements for the process are:

$$CH_4 = C + 2H_2 \qquad \Delta H = +\ 89750\ \text{J/mol} \quad (\text{at } 850°C) \qquad (8\text{-}1)$$
$$\Delta H = +\ 89989\ \text{J/mol} \quad (\text{at } 900°C)$$

A preheated methane stream at 500°C of 220 ton/day (144.4 mol/s) enters the fluidized bed reactor of catalytically active carbon particles, where the feedstock decomposes at a temperature of 850 to 900°C and a pressure of 200 kPa. Methane conversion in the reactor is 33-43%, which corresponds to hydrogen concentration of 50-60 vol.% in the effluent gas balanced with unconverted methane and other minor species.

Energy Balance Constraint

The catalytic decomposition of methane is an endothermic reaction. The heat of reaction is provided by the incoming carbon particles. Energy is also required to heat up the incoming methane stream from 500°C to the bed temperature. Assume that methane conversion is 38% and the initial temperatures of methane stream and carbon particles are 500°C and 900°C, respectively. Then, total energy input can be calculated as

$$\begin{aligned}\text{Energy required} &= m_m x \Delta H + m_m C_{pm}(T_{bed} - T_{in,m}) \\ &= 144.4 \times 38\% \times 89750 + 144.4 \times 70.0 \times (850 - 500) = 8.463 \times 10^6\ \text{W} = 8463\ \text{kW}\end{aligned} \qquad (8\text{-}2)$$

$$\begin{aligned}\text{Carbon flow rate} &= \frac{\text{Energy required}}{C_{pc}(T_{in,c} - T_{bed})} = \frac{8.463 \times 10^6}{22.5 \times (900 - 850)} = 7523\ \text{mol/s} \\ &= 90.3\ \text{kg/s} = 8597\ \text{ton/day}\end{aligned} \qquad (8\text{-}3)$$

The carbon circulation rate appears to be too high; it will be shown later that with this circulation rate the bed material will be replaced every 35 s. A high circulation rate will increase the operational difficulty and cost. Thus, it is desirable to reduce the carbon circulation. One possibility is to increase the incoming stream temperatures. Assume that the methane stream and

carbon particles are heated to 600°C and 1100°C, respectively, before entering the fluidized bed. The carbon flow rate is then

$$\text{Carbon flow rate} = \frac{\text{Energy required}}{C_{pc}(T_{in,c} - T_{bed})} = \frac{144.4 \times 38\% \times 89750 + 144.4 \times 70.0 \times (850 - 600)}{22.5 \times (1100 - 850)} \quad (8\text{-}4)$$
$$= 1324\,\text{mol/s} = 15.9\,\text{kg/s}$$

Kinetics Constraint

One of the advantages of a fluidized bed is its excellent mixing characteristic. As a first approximation, we assume that the fluidized bed is a well-stirred reactor. Thus,

$$m_m(C_{m,in} - C_{m,out}) = k_o \exp(-\frac{E}{RT_{bed}})C_{m,out}^{0.5}V \quad (8\text{-}5)$$

where V is the reactor volume. The activation energy of the reaction is 201 kJ/mol (for activated carbon) and k_o, the pre-exponential factor, can be determined as follows.

Since the initial methane decomposition rate is 1.6 mmol/min-g(cat) (an average of 1.2 – 2.0 mmol/min-g(cat)) at 850ºC with 100% methane at atmospheric pressure, assuming a 0.50^{th}-order reaction (for activated carbon), we have,

$$kp_m^{0.5} = k_o \exp(-\frac{E}{RT})p_m^{0.5} = k_o \exp(-\frac{201 \times 10^3}{8.314 \times 1123.15})(1.01325 \times 10^5)^{0.5} = 1.6 \quad (8\text{-}6)$$

thus, k_o = 186.8 mol/s·g(cat)·$Pa^{0.5}$. Assume again a bed voidage of 0.50 and a carbon density of 1800 kg/m^3, k_o can be converted to 1.6812×10^8 mol/ s·m^3 bed·$Pa^{0.5}$.

From Equation (8-6), we can estimate the residence time of methane in the reactor as,

$$\tau = \frac{V}{m_m} = \frac{C_{m,in} - C_{m,out}}{k_o \exp(-\frac{E}{RT_{bed}})p_{m,out}^{0.5}} = \frac{\frac{P_{bed}}{RT_{bed}} - \frac{p_m}{RT_{bed}}}{k_o \exp(-\frac{E}{RT_{bed}})p_{m,out}^{0.5}} \quad (8\text{-}7)$$
$$= \frac{\frac{200 \times 10^3}{8.314 \times 1123.15} - \frac{0.45 \times 200 \times 10^3}{8.314 \times 1123.15}}{1.6812 \times 10^8 \exp(-\frac{201 \times 10^3}{8.314 \times 1123.15})(0.45 \times 200 \times 10^3)^{0.5}} = 0.52\,\text{s}$$

The reactor volume is then given by

$$\text{Bed volume} = (\text{volumetric flow rate of methane}) \times (\text{residence time}) = m_m \tau$$
$$= 144.4 \times 0.0224 \times \frac{1123.15}{273.15} \times \frac{1.01325 \times 10^5}{2.0 \times 10^5} \times 0.52 = 3.5\,\text{m}^3 \quad (8\text{-}8)$$

Particle inventory in the fluidized bed is

$$\text{Bed mass} = \rho_p (1 - \varepsilon) V = 1800 \times (1 - 0.50) \times 3.5 = 3150\,\text{kg} \quad (8\text{-}9)$$

The residence time of carbon particles can be calculated as

$$\tau_c = \frac{\text{Bed mass}}{\text{Carbon circulation rate}} = \frac{3150}{90.3} = 35\,\text{s} \quad (8\text{-}10)$$

If the carbon circulation rate is 15.9 kg/s, the particle residence time is 198 s.

8.2. Model Development

As the gas velocity increases, a fluidized bed of solid particles may undergo several flow regimes: the bubbling regime, the slugging regime (occurs only in the reactors with small diameters), the turbulent regime, fast fluidization and pneumatic transport. Extensive research work has been reported in the literature on the prediction of flow regime transition. Initially, the fluidized bed to be modeled was assumed to be in the bubbling regime. A three-phase countercurrent back-mixing model was developed to describe methane decomposition in this regime. Detailed model equations are given in the Appendix; a computer code was then developed. For the case under consideration, the transition velocity from the bubbling regime to the turbulent regime is about 1.0 m/s based on an empirical correlation obtained using experimental data from fluidized beds under elevated pressure and high temperature. Calculations show that the cross-sectional area of the bed has to be greater than 10.5 m^2 in order for the bed to be in the bubbling regime. Given this large cross-sectional area, it might be difficult to construct the reactor. Thus, a second model was also developed which is suitable for the turbulent regime. This model is also given in the Appendix and has been implemented into the computer code.

Models used to describe bubbling fluidized beds can be generally classified into two categories: two-phase models and three-phase models. Much of the earlier work employed two-phase models, which do not describe solids circulations in the fluidized bed, and hence, could not predict a recycle peak in the tracer concentration in solids mixing experiments. Three-phase models assume that the fluidized bed consists of three phases, namely, the bubble phase, the wake (plus cloud) phase and the dense phase. Gas in the bubble phase moves upward in plug flow; the wake phase moves in plug flow along with the bubbles and in the dense phase the gas may move upward or downward depending on the superficial gas velocity in the fluidized bed. A three-phase model with solids circulation is the preferred model for bubbling fluidized beds. Therefore, this model has been implemented into a computer code. Figure 8-1 shows a schematic diagram of three-phase bubbling phase fluidized bed.

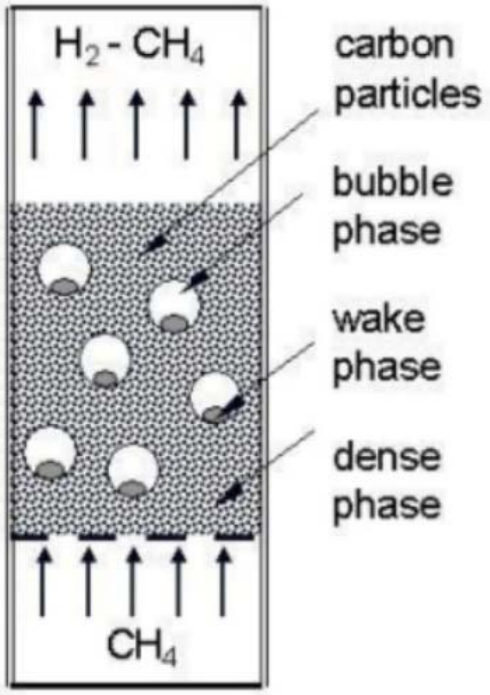

Figure 8-1. Schematic Diagram of Three-phase Bubbling Phase Fluidized Bed

Figure 8-2 shows methane conversion as a function of bed height in a bubbling fluidized bed. The cross-sectional area of the bed was assumed to be 14 m^2, so that the bed is in the bubbling regime. Two expanded bed heights and two bed temperatures were used in the calculations. As can be seen from the figure, the bed temperature has a significant effect on methane conversion. Note that methane conversion decreases as the distance above the gas distributor increases near the top of the bed; this is due to back-mixing of the gas in the dense phase. Examination of each methane concentration profile along the distance above the gas distributor reveals that it passes through a minimum at a position within the bed. Methane conversion as a function of expanded bed height is shown in Figure 8-3. If the bed temperature is 850°C, to achieve 38% methane conversion, the expanded bed height should be 0.85 m; if the bed temperature is 900°C, the expanded bed height should be 0.35 m. If the fluidized bed is in the turbulent regime, we assume that the cross-sectional area of the bed is 3.5 m^2. Figures 8-4 and 8-5 show the effects of bed temperature and expanded bed height on methane conversion. For this case, if the bed temperature is 850°C, 38% methane conversion requires an expanded bed height of 1.5 m. On the other hand, if the bed temperature is 900°C, the expanded bed height should be 0.65 m.

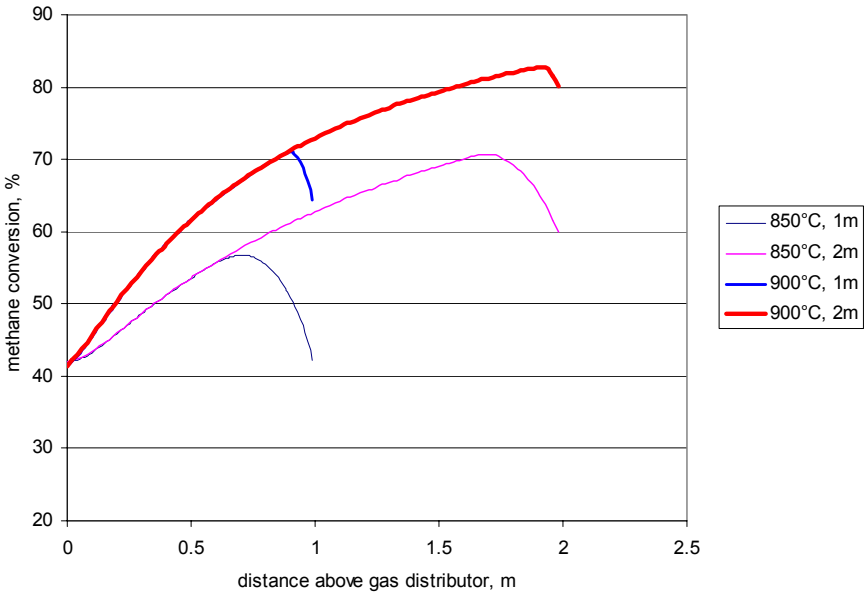

Figure 8-2. Methane Conversion as a Function of Distance Above Gas Distributor (A: 14 m^2, bubbling regime).

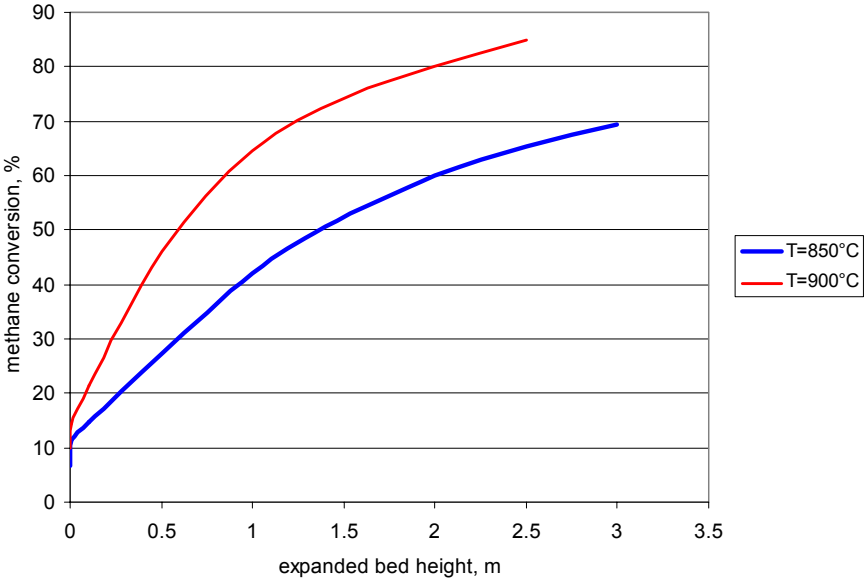

Figure 8-3. Methane Conversion as a Function of Expanded Bed Height (A: 14 m^2, bubbling regime).

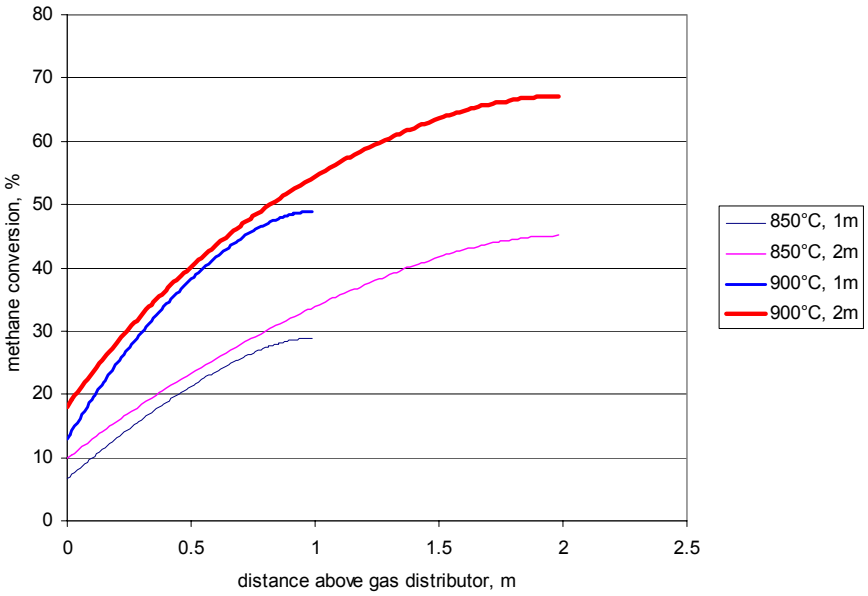

Figure 8-4. Methane Conversion as a Function of Distance Above Gas Distributor (A: 3.5 m^2, turbulent regime).

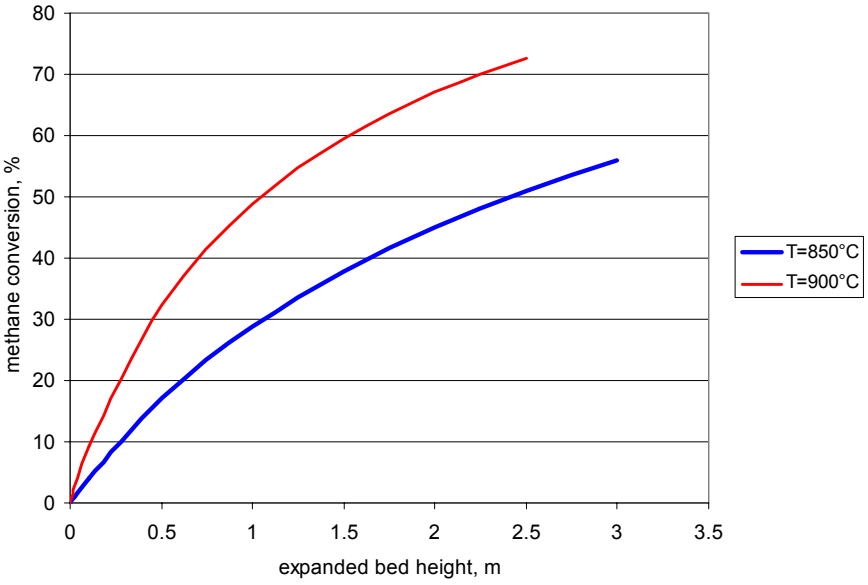

Figure 8-5. Methane Conversion as a Function of Expanded Bed Height (A: 3.5 m^2, turbulent regime).

8.3. Computer Code and Model Outputs

For the turbulent bed model, the model outputs are:

- Methane and hydrogen concentrations as functions of distance above the gas distributor
- Methane conversion as a function of distance above the gas distributor
- Methane and hydrogen concentrations in the effluent gas, methane conversion, carbon flow rate, carbon residence time, average bed voidage, elutriation rate and change in carbon particle size.

For the bubbling bed model, in addition to the above outputs, the model also delivers:

- Bubble properties as functions of distance above the gas distributor
- Methane and hydrogen concentrations in the bubble phase, the wake phase and the dense phase as functions of distance above the gas distributor

Figure 8-6 depicts the comparison of the experimental and predicted data using the above-described model. It is evident that the data are in fairly good agreement.

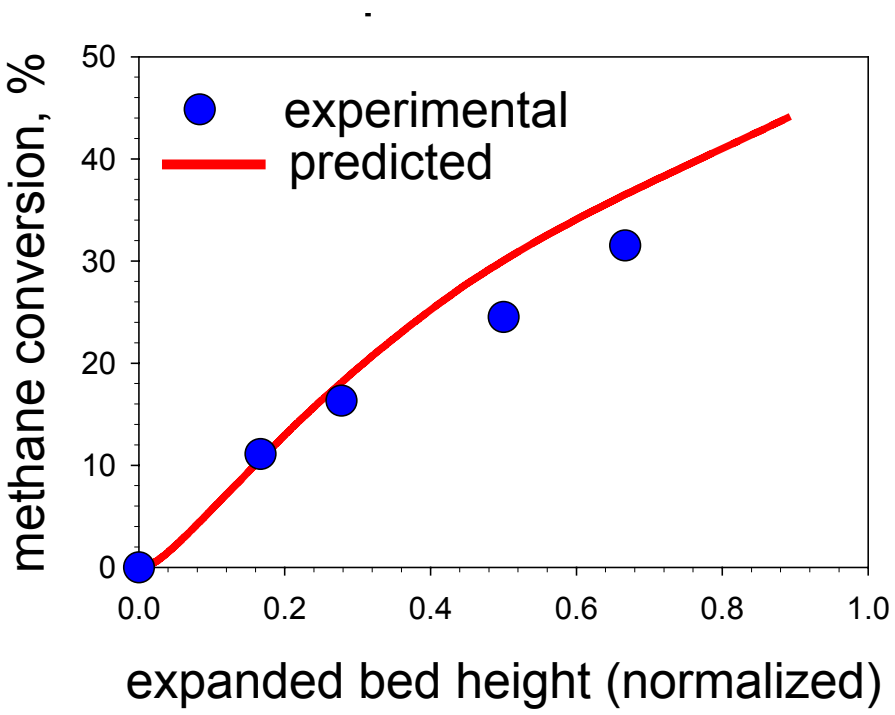

Figure 8-6. Comparison of Experimental and Simulation Data

Appendix: Model Details

1. Conservation Equations for the Three-Phase Bubbling Fluidized Bed Model

A. Overall Balances

$$u_0 = u_b f_b + f_b f_w \varepsilon_{mf} u_b + [1 - f_b(1+f_w)] u_{g,e} \varepsilon_{mf} \tag{8-11}$$

$$-u_b f_b f_w = u_{s,e}[1 - f_b(1+f_w)] \tag{8-12}$$

$$u_{g,e} = u_{s,e} + u_{mf} / \varepsilon_{mf} \tag{8-13}$$

$$u_0 = \frac{[f_b + (1-f_b)\varepsilon_{mf}] u_{0,inlet} \sum_{i=1}^{n} \frac{p_{i,inlet} M_i}{R T_{g,inlet}}}{f_b \sum_{i=1}^{n} \frac{p_{i,b} M_i}{R T_{g,b}} + f_b f_w \varepsilon_{mf} \sum_{i=1}^{n} \frac{p_{i,w} M_i}{R T_{bed}} + (1 - f_b(1+f_w)) \varepsilon_{mf} \sum_{i=1}^{n} \frac{p_{i,e} M_i}{R T_{bed}}} \tag{8-14}$$

B. Species balances

1. Gaseous species in the bed

a) Bubble phase

$$\frac{\partial (u_b f_b C_{i,b})}{\partial z} - (\lambda_1 C_{i,b} + \lambda_2 C_{i,w}) \frac{\partial (u_b f_b)}{\partial z} + f_b K_{bw} (C_{i,b} - C_{i,w}) = 0 \tag{8-15}$$

b) Wake phase

$$\begin{aligned} &\frac{\partial [u_b f_b f_w \varepsilon_{mf} C_{i,w}]}{\partial z} + (\lambda_1 C_{i,b} + \lambda_2 C_{i,w}) \frac{\partial (u_b f_b)}{\partial z} \\ &+ (\lambda_3 C_{i,w} + \lambda_4 C_{i,e}) \left[\frac{\partial u_0}{\partial z} - \varepsilon_{mf} \frac{\partial [u_b f_b f_w]}{\partial z} - \frac{\partial (u_b f_b)}{\partial z} \right] \\ &+ f_b K_{bw} [C_{i,w} - C_{i,b}] + f_b K_{we} [C_{i,w} - C_{i,e}] + R_w = 0 \end{aligned} \tag{8-16}$$

c) Emulsion phase

$$\begin{aligned} &\frac{\partial [\{1 - f_b(1+f_w)\} \varepsilon_{mf} u_{g,e} C_{i,e}]}{\partial z} - (\lambda_3 C_{i,w} + \lambda_4 C_{i,e}) \left[\frac{\partial u_0}{\partial z} - \varepsilon_{mf} \frac{\partial [u_b f_b f_w]}{\partial z} - \frac{\partial (u_b f_b)}{\partial z} \right] \\ &+ f_b K_{we} [C_{i,e} - C_{i,w}] + R_e = 0 \end{aligned} \tag{8-17}$$

2. Gaseous species in the freeboard

$$\frac{\partial(u_0 C_{i,f})}{\partial z} = 0 \tag{8-18}$$

Exchange coefficients

The mass transfer coefficient between the bubble phase and the wake phase is

$$K_{bw} = 5.85(D_g^{0.5} g^{0.25} / d_b^{1.25}) + 4.5 u_{mf} / d_b \tag{8-19}$$

The mass exchange coefficient between the wake and emulsion phases is taken as

$$K_{we} = 6.77(0.71\sqrt{g d_b}\, D_g \varepsilon_{mf} / d_b^3)^{1/2} \tag{8-20}$$

2. Conservation Equations for the Turbulent Fluidized Bed Model

$$\frac{d}{dz}\left(D_z \frac{dC}{dz}\right) - \frac{d(u_0 C)}{dz} - R_t = 0 \tag{8-21}$$

where D_z is the axial gas dispersion coefficient and can be estimated from the following correlation

$$Pe_g = \frac{u_0 H_t}{D_z} = 3.47 Ar^{0.149}\, Re^{0.0234}\, Sc^{-0.231} \left(\frac{H_t}{D_t}\right)^{0.285} \tag{8-22}$$

Peclet number could be correlated in terms of the operating conditions as

$$Pe_g = \frac{u_0 H_t}{\varepsilon D_z} = 7.0 \times 10^{-2} Ar^{0.32} \left(\frac{D_t}{d_p}\right)^{0.4} \tag{8-23}$$

The correlation has also been implemented in the computer code, allowing the user to choose different correlations. The boundary conditions are

$$u_0 (C_i - C_{i,in}) = D_z \frac{dC_i}{dz} \qquad \text{at } z = 0 \tag{8-24}$$

$$D_z \frac{dC_i}{dz} = 0 \qquad \text{at } z = H_t \tag{8-25}$$

Nomenclature

A	cross-sectional area of the bed, m^2
C	gas species concentration, mol/m^3
C_{pc}	carbon specific heat, J/mol/K
C_{pm}	methane specific heat, J/mol/K
D_t	reactor diameter, m
D_z	axial gas dispersion coefficient, m^2/s
E	activation energy, J/mol
g	gravitational acceleration, m/s^2
H_t	expanded bed height, m
k_o	pre-exponential factor, $mol/s/m^3$ bed/$Pa^{0.5}$
m_m	mole flow rate of methane, mol/s
M_i	gas species molecular weight, kg/mol
P_{bed}	pressure in the bed, Pa
p_i	gas species partial pressure, Pa
p_m	methane partial pressure, Pa
R	universal gas constant, J/mol/K
R_w, R_e, R_t	reaction rate in the wake phase, the dense phase, the turbulent regime, $mol/m^3/s$
T_{bed}	fluidized bed temperature, °C or K
$T_{in,c}$	carbon inlet temperature, °C or K
$T_{in,m}$	methane inlet temperature, °C or K
V	reactor volume, m^3
x	methane conversion
ε	bed voidage
μ	gas viscosity, Pa·s
ρ_g	gas density, kg/m^3
ρ_p	carbon density, kg/m^3
τ	gas residence time, s
τ_c	particle residence time, s
ΔH	heat of reaction, J/mol

9. CONCLUSION

Thermocatalytic decomposition of NG (or other hydrocarbon fuels) as a viable technological approach to the production of hydrogen and solid carbon is discussed in this report. Decomposition (or pyrolysis) of hydrocarbons occurs in the presence of catalytically active carbon particles at moderate temperatures (<900^{o}C) in an air/water-free environment, which eliminates the concurrent production of carbon oxides. This results in the following advantages: (1) no CO/CO_2 byproducts are generated during hydrocarbon decomposition stage, (2) no expensive catalysts are used in the process, (3) several valuable forms of carbon can be produced in the process depending on the process conditions (e.g., turbostratic carbon, pyrolytic graphite, spherical carbon particles, carbon filaments etc.), (4) CO_2 emissions could be drastically reduced (compared to conventional processes).

Factors affecting carbon catalyst activity and stability and process sustainability were investigated. The means for improving the catalyst long-term stability and process sustainability were determined (U.S. Patent No. 6,670,058 B2). It was determined that the process sustainability could be improved using two approaches: (i) the in-situ generation of catalytically active carbon species produced by co-decomposition of methane and unsaturated and/or aromatic hydrocarbons, and (ii) reactivation of carbon catalysts via surface treatment with activating agents, e.g., steam and/or CO_2. Several types of reactors, including, spouted and fluidized bed reactors were evaluated for hydrocarbon decomposition process. A fluidized bed reactor was selected as the most suitable for the efficient decomposition of methane and propane with the production of hydrogen-rich gas and simultaneous withdrawal of carbon from the reactor. It was found that a wide range of hydrocarbon fuels, including methane, propane and gasoline could be efficiently converted into a gas with hydrogen concentration of 40-60 v.%, with the balance being predominantly methane.

A bench-scale 1 kW_{th} and 3 kW_{th} thermocatalytic reactors (TCR) for CO/CO_2-free production of hydrogen-rich gas was designed, fabricated and operated using methane or propane as feedstocks. The effect of moisture and sulfur compounds present in commercial hydrocarbon fuels on the process efficiency and the catalyst activity and stability was determined. It was found that the presence of small amounts of moisture and H_2S were not detrimental to the process efficiency. However moisture resulted in contamination of hydrogen with CO and CO_2 (that were removed from the product gas via methanation reaction down to ppm level). It was demonstrated that the resulting hydrogen gas could be directly fed to PEM fuel cell.

Carbon products of the process were analyzed by a number of material characterization techniques, including XRD, SEM, AES, XPS, EDS, DR- FTIR. The market value of the carbon products of the process were evaluated. Studies on the modeling and scaling up of the fluidized bed reactor for thermocatalytic decomposition of natural gas were conducted. Techno-economic analysis of hydrogen and carbon production by thermocatalytic decomposition of natural gas was conducted in cooperation with NREL. It was determined that hydrogen could be produced at a selling price of $7-21/GJ depending on the cost of natural gas and carbon selling price.

Acknowledgements

This work was supported by the U.S. Department of Energy Hydrogen Program under the contract No. DE-FC36-99GO10456. The author thanks FIT graduate student Franklyn Smith for the help with the experimental work and interpretation of data. The author also acknowledges the contribution of the Universal Oil Products, National Renewable Energy Laboratory, AMIA Laboratories, CREOL and Materials Characterization Facility of the University of Central Florida, MER Corporation, Reaction Engineering International.

10. REFERENCES

1. B. Cromatry, *Proceedings of the 9th World Hydrogen Energy Conference;* Paris, France, pp 13-22, 1992
2. J. Ogden, T. Kreutz, M. Steinbugler, A. Cox, J. White, *Proc. 1996 DOE Hydrogen Program Review*, 1, 125-184
3. N. Mayersohn, *Popular Science,* 66, 67-71, 1993
4. M. Steinberg, and H. Cheng, Modern and prospective technologies for hydrogen production from fossil fuels, *Proceedings of the 7th World Hydrogen Energy Conference,* Moscow, 699 (1988)
5. S. Lynum, R. Hildrum, K. Hox, and J. Hugdabl, Kvarner based technologies for environmentally friendly energy and hydrogen production, *Proc. 12th World Hydrogen Energy Conference,* Buenos Aires, 697 (1998)
6. L. Fulcheri, and Y. Schwob, From methane to hydrogen, carbon black and water. *Int. J. Hydrogen Energy, 20: 197 (*1995**)**
7. J. Pohlenz, N. Scott, Method for hydrogen production by catalytic decomposition of a gaseous hydrocarbon stream, *U. S. Patent No 3,284,161* (UOP) (1966)
8. B. Kim, J. Zupan, L. Hillebrand, and J. Clifford, Continuous catalytic decomposition of methane, *NASA Contractor Report, NASA CR-1662*, NASA, Washington D.C.(1970)
9. M. Callahan, Hydrocarbon fuel conditioner for a 1.5 kW fuel cell power plant. *Proceedings of 26th Power Sources Symposium,* Red Bank, N.J, 181 (1974)
10. M. Pourier, C. Sapundzhiev, Catalytic decomposition of natural gas to hydrogen for fuel cell applications, *Int. J. Hydrogen Energy, 22:429* (1997)
11. K. Ledjeff-Hey, T. Kailk, J. Roes, Catalytic cracking of propane for hydrogen production for fuel cells, *Fuel Cell Seminar*, Palm Springs (1998)
12. T. Koerts, M. Deelen, R. van Santen, Hydrocarbon formation from methane by a low-temperature two-step reaction sequence, *J. Catalysis*, 138: 101 (1992)
13. F. Solymosi, A. Erdohelyi, A. Csereyi, A. Felvegi, Decomposition of CH_4 over supported Pd catalysts *J. Catalysis,* 147: 272 (1994)
14. M. Calahan, Thermo-catalytic hydrogen generation from hydrocarbon fuels. *From Electrocatalysis to Fuel Cells.* G.Sanstede, ed., Battelle Seattle Research Center (1972)
15. N. Muradov, How to produce hydrogen from fossil fuels without CO_2 emission, *Energy and Environmental Progress*, *Hydrogen Energy and Power Generation*, N. Veziroglu, ed., Nova Science, NY, 93 (1991)
16. N. Muradov, Hydrogen production by catalytic cracking of natural gas*, Proc. 11th World Hydrogen Energy Conference;* Stuttgart, Germany, 697 (1996)

17. A. Pyatenko, M. Nizhegorodova, V. Lipovich, V. Popov, Investigation of the process of catalytic decomposition of methane on d-metals, *Khimiya Tverdogo Topliva*, 23: 682 (1989)
18. J. Rostrup-Nielsen, Equilibria of decomposition reactions of carbon monooxide and methane over nickel catalyst, *J. Catalysis,* 27: 343 (1972)
19. A. Steinfeld, V. Kirilov, G. Kuvshinov, Y. Mogilnikh, A. Reller, Production of filamentous carbon and hydrogen by solar thermal catalytic cracking of methane, *Chem. Eng. Sci.* 52: 3399 (1997)
20. E. Shustorovich, The bond-order conservation approach to chemisorption and heterogeneous catalysis: applications and implications, *Advances in Catalysys*, 37:101 (1990)
21. A. Frennet, Chemisorption and exchange with deuterium of methane on metals, *Catal. Rev.- Sci. Eng.,* 10: 37 (1974)
22. R. Diefendorf. *J. Chem. Physics,* 57, 3, 815 (1960)
23. A. Tesner, *The Kinetics of Carbon Black Production;* VINITI: Moscow (1987)
24. C. Chen, M. Back, R. Back, Mechanism of the thermal decomposition of methane, *Symp. Industrial and Laboratory Pyrolysis,* (1976)
25. K. Mathur, N. Epstein. Spouted Beds. Acad. Press, 1974
26. Fluidization. D. Othmer editor. Reinhold Publ., NY, 1956
27. J. Ogden, M. Steinbugler, and T. Kreutz. "Hydrogen as a Fuel for Fuel Cell Vehicles: a Technical and Economic Comparison." In *Proceedings of the Annual U.S. Hydrogen Meeting,* 469. Alexandria, VA: NHA, 1997.
28. M.Steinberg, "Fossil Fuel Decarbonization Technology for Mitigating Global Warming." *Intern. J. Hydrogen Energy,* 24: 771, 1999.
29. *Kirk-Othmer Encyclopedia of Chemical Technology*. V. 4. New York: John Wiley & Sons, 1978